



TOPICAL REVIEW

OPEN ACCESS

Hydrogen storage in complex hydrides: past activities and new trends

RECEIVED

23 December 2021

REVISED

13 April 2022

ACCEPTED FOR PUBLICATION

30 May 2022

PUBLISHED

23 June 2022

Original content from this work may be used under the terms of the [Creative Commons Attribution 4.0 licence](https://creativecommons.org/licenses/by/4.0/).

Any further distribution of this work must maintain attribution to the author(s) and the title of the work, journal citation and DOI.



Erika Michela Dematteis¹ , Mads B Amdisen² , Tom Autrey³ , Jussara Barale¹ , Mark E Bowden³ , Craig E Buckley⁴ , Young Whan Cho⁵ , Stefano Deledda⁶, Martin Dornheim⁷ , Petra de Jongh⁸ , Jakob B Grinderslev² , Gökhan Gizer⁷ , Valerio Gulino^{1,8} , Bjørn C Hauback⁶ , Michael Heere⁹ , Tae Wook Heo¹⁰ , Terry D Humphries⁴ , Torben R Jensen² , Shin Young Kang¹⁰ , Young-Su Lee⁵ , Hai-Wen Li¹¹ , Sichi Li¹⁰ , Kasper T Møller¹² , Peter Ngene⁸ , Shin-ichi Orimo^{13,14} , Mark Paskevicius⁴ , Marek Polanski¹⁵ , Shigeyuki Takagi¹³ , Liwen Wan¹⁰ , Brandon C Wood¹⁰ , Michael Hirscher¹⁶ and Marcello Baricco^{1,*}

¹ Department of Chemistry, NIS and INSTM, University of Turin, Via Pietro Giuria 7, 10125 Torino, Italy

² Interdisciplinary Nanoscience Center (iNANO) and Department of Chemistry, Aarhus University, DK-8000 Aarhus C, Denmark

³ Physical and Computational Sciences Directorate, Pacific Northwest National Laboratory, Richland, WA 99352, United States of America

⁴ Department of Physics and Astronomy, Fuels and Energy Technology Institute, Curtin University, GPO Box U1987, Perth, WA 6845, Australia

⁵ Center for Energy Materials Research, Korea Institute of Science and Technology, 5 Hwarang-ro 14-gil, Seongbuk-gu, Seoul 02792, Republic of Korea

⁶ Department for Hydrogen Technology, Institute for Energy Technology, PO Box 40, NO-2027 Kjeller, Norway

⁷ Institute of Hydrogen Technology, Helmholtz-Zentrum Hereon, Max-Planck-Straße 1, Geesthacht 21502, Germany

⁸ Materials Chemistry and Catalysis, Debye Institute for Nanomaterials Science, Utrecht University, Universiteitsweg 99, 3584 CG Utrecht, The Netherlands

⁹ Technische Universität Braunschweig, Institute of Internal Combustion Engines, Hermann-Blenk-Straße 42, 38108 Braunschweig, Germany

¹⁰ Laboratory for Energy Applications for the Future (LEAF), Lawrence Livermore National Laboratory, 7000 East Avenue, Livermore, CA 94550, United States of America

¹¹ Hefei General Machinery Research Institute, No. 888, Changjiang West Road, Hefei 230031, People's Republic of China

¹² Department of Biological and Chemical Engineering, Aarhus University, Aabogade 40, Aarhus DK-8200, Denmark

¹³ Institute for Materials Research, Tohoku University, Sendai 980-8577, Japan

¹⁴ Advanced Institute for Materials Research (WPI-AIMR), Tohoku University, Sendai 980-8577, Japan

¹⁵ Department of Functional Materials and Hydrogen Technology, Military University of Technology, 00-908 Warsaw, Poland

¹⁶ Max Planck Institute for Intelligent Systems, Heisenbergstrasse 3, 70569 Stuttgart, Germany

* Author to whom any correspondence should be addressed.

E-mail: marcello.baricco@unito.it

Keywords: complex hydrides, amides, amines, borohydrides, alanates, reactive hydride composites, borates

Abstract

Intense literature and research efforts have focussed on the exploration of complex hydrides for energy storage applications over the past decades. A focus was dedicated to the determination of their thermodynamic and hydrogen storage properties, due to their high gravimetric and volumetric hydrogen storage capacities, but their application has been limited because of harsh working conditions for reversible hydrogen release and uptake. The present review aims at appraising the recent advances on different complex hydride systems, coming from the proficient collaborative activities in the past years from the research groups led by the experts of the Task 40 'Energy Storage and Conversion Based on Hydrogen' of the Hydrogen Technology Collaboration Programme of the International Energy Agency. An overview of materials design, synthesis, tailoring and modelling approaches, hydrogen release and uptake mechanisms and thermodynamic aspects are reviewed to define new trends and suggest new possible applications for these highly tuneable materials.

Contents

1. Introduction	3
2. Systems	4
2.1. Alanates	4
2.2. Borohydrides	6
2.2.1. Synthesis	6
2.2.2. Structural properties	6
2.2.3. Derivatives of metal borohydrides with neutral molecules	9
2.2.4. Anion substitutions	10
2.2.5. Cation substitutions	11
2.2.6. Thermal properties and reactivity	13
2.3. Borates	15
2.4. Ammines	17
2.5. Amides and imides	21
2.6. Transition metals complex hydrides	23
2.7. RHCs	24
3. New trends and properties	25
4. Outlooks and conclusions	27
Data availability statement	29
Acknowledgments	29
References	30

1. Introduction

The shift towards 'green' and sustainable energy production, storage, and use requires efficient and widespread development of renewable energy technologies to tackle climate change and implement a sustainable energy and ecological transition. Many technological energy solutions have been investigated and developed in the past decades, one of those includes hydrogen technology and hydrogen storage materials to boost energy storage and distribution of intermittent renewables.

Hydrogen, as a promising energy carrier, forms covalent bonds to non-metallic elements in the periodic table, some metalloids, such as boron and silicon, most of the late *d*-metals, but also light elements characterised as 'weak' metals, such as beryllium and aluminium [1]. Complex hydrides include many classes of materials suitable for solid-state hydrogen storage with high gravimetric and volumetric hydrogen capacities, that allow hydrogen storage in compact and light-weight tanks [2]. This review focuses on complex hydride systems based on a select elements, i.e. nitrogen, boron, aluminium, and some transition metals (e.g. manganese, iron, cobalt and nickel). Many reviews have considered these systems recently, and the vivid research activities underline the interest in looking into structural, thermal and reactivity properties of these compounds, towards the developments of new materials. For this reason, the present review aims at collecting possible paper of interest and resuming in a concise way the relevant research of the last 20 years, focusing on hydrogen storage properties in complex hydrides, and suggesting new trends and possible future research directions beside hydrogen storage.

Non-metals and metalloid elements tend to form molecular compounds with hydrogen and the lighter ones are gaseous under ambient conditions [1]. Most of these gaseous compounds are toxic, reactive, or otherwise harmful and the only exceptions appear to be water (H₂O) and methane (CH₄). Nitrogen can react with hydrogen and form ammonia (NH₃), which is a thermodynamically stable molecule (i.e. free energy of formation, $\Delta G_f^\circ \ll 0$). Boron has a rich chemistry with hydrogen and forms a diversity of boranes, but all are thermodynamically unstable ($\Delta G^\circ > 0$). The electron deficient molecule, monoborane (BH₃), dimerises readily to form diborane (B₂H₆) even at low partial pressures. Diborane has the characteristic three-centre-two-electron bonds also observed in solid polymeric alane (AlH₃), which is also thermodynamically unstable. However, alane and borane react similarly with an ionic metal hydride, e.g. lithium hydride LiH, via an additional reaction to form thermodynamically stable tetrahydridoalane and tetrahydridoborate, i.e. LiAlH₄ and LiBH₄, respectively. In contrast, ammonia reacts with a similar ionic metal hydride, e.g. LiH, via an elimination reaction to form lithium amide (LiNH₂) and hydrogen. Thus, for the complex hydrides the hydrido ion (H⁻) acts as a ligand and forms homoleptic complexes, tetrahydridoaluminate ion (AlH₄⁻) or tetrahydridoborate ion (BH₄⁻), which are often briefly denoted alane and borohydride, respectively, as well as nitrogen-based complex ions, amide (NH₂⁻) and imide (NH₂²⁻). Ammine coordination complexes can be formed as well by neutral coordination of the complex anion. Alkali or alkaline earth metals can act as counter ions (cations) and stabilise these complex ions to form stable ionic solids [3].

The late transition metals, e.g. Mn, Fe, Co, and Ni, generally have a low affinity to hydrogen, but they do react with hydrogen when alloyed or mixed with a metal with a higher affinity, such as magnesium. Distinct to the metallic hydrides, they only exist with fixed stoichiometry, e.g. Mg₂FeH₆, Mg₂CoH₅, and Mg₂NiH₄ [4–7]. The structural analysis of these solids reveal that they also consist of a homoleptic coordination complex with the hydrido anion (H⁻) as a ligand, forming octahedral [FeH₆]⁴⁻, square-pyramidal [CoH₅]⁴⁻, and tetrahedral [NiH₄]⁴⁻ groups [8, 9].

Complex hydrides have relatively high hydrogen content, see table 1, which have provided significant interest in their properties and possible uses. Magnesium iron hydride is remarkable with an extreme volumetric hydrogen density of $\rho_V \sim 150 \text{ g H}_2 \text{ l}^{-1}$, which is over twice that of liquid hydrogen, i.e. $\rho_V = 71 \text{ g H}_2 \text{ l}^{-1}$, and magnesium nickel hydride is one complex hydride, out of very few, to store hydrogen reversibly at moderate conditions [10–12].

The decomposition of the family of complex hydrides, MAH_x, can in general be illustrated by the intermediate formation of a neutral hydride by the central atom in the complex, AH_y, and an ionic hydride by the counter metal cation, MH_z, in the solid [3]. As mentioned above, the neutral counter part to the complex hydride (AH_y) is usually thermodynamically unstable, in particular at elevated temperatures, and will immediately decompose. In case the neutral counter part is a gas, it may be released from the solid hydrogen storage material during decomposition, e.g. ammonia appears to be an intermediate for the amide-imide system and it may be released from the solid state [41]. Similarly, lithium borohydride may release diborane when decomposed in vacuum or reacted with an additive such as silicon dioxide [42]. Thus, the family of complex hydrides has significantly more complex mechanisms for release and uptake of hydrogen as compared to metallic and ionic hydrides, and most of them remain not fully understood.

Table 1. Properties of selected complex metal hydrides. M : molecular weight, ρ : density, ρ_m : gravimetric hydrogen density, ρ_v : volumetric hydrogen density, ΔH_{dec} : decomposition enthalpy, T_{dec} : reported decomposition temperature.

	M (g mol ⁻¹)	ρ (g ml ⁻¹)	ρ_m (wt% H ₂)	ρ_v (g H ₂ l ⁻¹)	ΔH_{dec} (kJ mol ⁻¹)	T_{dec} ^a (°C)	References
LiBH ₄	21.78	0.66	18.4	122	69	~400	[13]
NaBH ₄	37.83	1.07	10.8	116	108	~500	[14]
Mg(BH ₄) ₂	53.99	0.79	14.8	117	120	~350	[15, 16]
LiAlH ₄	37.95	0.92	10.6	97	10	~150	[17, 18]
Li ₃ AlH ₆	53.85	1.02	11.2	114	25	~200	[19–21]
NaAlH ₄	54.00	1.28	7.3	93	33	~230	[22, 23]
Na ₃ AlH ₆	102.00	1.45	5.9	86	49	~275	[24]
LiNH ₂	22.96	1.17	8.8	103	66 ^b	~250	[25, 26]
Mg ₂ FeH ₆	110.50	2.74	5.5	150	98	~400	[4, 10, 27–30]
Mg ₂ CoH ₅	112.58	2.89	4.5	126	86	~360	[6, 31–36]
Mg ₂ NiH ₄	111.34	2.70	3.6	98	64	~325	[7, 37–40]

^a Decomposition temperatures strongly depend on the physical conditions for the measurement and the published data scatters significantly.

^b Decomposition of LiNH₂ to NH₃ and H₂.

Basic research activities have demonstrated that the dehydrogenated states of a complex hydride usually has relatively high stability and hydrogen uptake only occurs at extreme conditions [43]. Further investigations are needed to fully describe and model those systems and to explore possible real applications at the prototype scale [44, 45]. Therefore, materials containing complex ions were identified as possible hydrogen storage materials until the late nineties, where titanium was found to catalyse the release and uptake of hydrogen in NaAlH₄ [46]. Possible strategies of tailoring properties of complex hydrides include anion or cation substitutions, nanoconfinement, or the design of proper mixtures, either forming eutectics or so called reactive hydride composites (RHCs).

The present review examines the latest advancements (mainly in recent times, but also including relevant investigation over the last 20 years) in complex hydride systems (section 2), to define their synthesis, structural properties, thermodynamics, and characteristics of their reactivity to fully model systems as a function of composition towards a rational design of promising new materials for real applications. The main classes discussed include alanates (section 2.1), borohydrides (section 2.2), boranes (section 2.3), amines (section 2.4), amides and imides (section 2.5), transition metals complex hydrides (section 2.6), and RHCs (section 2.7).

Trends in properties and new applications are discussed in section 3, especially underlining the intense outputs of research groups and collaborative projects of the International Energy Agency Hydrogen Technology Collaboration Program Task 40 experts.

2. Systems

2.1. Alanates

Aluminium is the most abundant metal in the crust of the earth. Therefore, hydrides based on aluminium are attractive for future large-scale applications such as energy storage. Alane (AlH₃) is among the most promising candidate materials for hydrogen storage, owing to its high hydrogen capacities, $\rho_m = 10.1$ wt% H₂ and $\rho_v = 149$ g H₂ l⁻¹, and it has been proposed both as a possible fuel for rockets and for mobile propulsion [47, 48]. Alane readily forms metal alanates by addition reactions with more stable hydrides. In the mid-nineties, the discovery of reversible hydrogen release and uptake for titanium-catalysed sodium tetrahydridoaluminate (NaAlH₄) provided a paradigm shift for the research field covering solid-state hydrogen storage [48, 49].

Another research direction is the decomposition of alanates in the presence of aluminium sulphides, e.g. the system 6KAlH₄–Al₂S₃, which release 71% of the theoretical hydrogen content below 300 °C, i.e. at 65 °C lower than for pure KAlH₄, via several unknown compounds [50]. The NaAlH₄–Al₂S₃ system releases 4.9 wt% of H₂ starting at $T < 100$ °C without the need for a catalyst, via complex decomposition processes that involve multiple new sulphur-containing hydride compounds. The system shows partial H₂ reversibility, without the need for a catalyst, with a reversible capacity of ~1.6 wt% H₂ over 15 cycles in the temperature range of 200 °C–300 °C. This absorption capacity is limited by the need for high H₂ pressures (>280 bar) to drive the absorption process at the high temperatures required for reasonable absorption kinetics. The large number of new phases discovered in this system suggests that destabilization of complex hydrides with metal sulphides is a novel research avenue for hydrogen storage materials [51].

Nanoconfinement represents another promising strategy for promoting (de)hydrogenation kinetics and reversibility that has been the subject of intense recent investigations. Nanoconfinement of NaAlH₄ in carbon scaffolds significantly reduces the hydrogen release temperatures due to a promoting effect of the scaffold, which is independent of maximum pore size (D_{\max}), and a nano-size effect observed for pores in the range $7 \leq D_{\max} \leq 39$ nm [52]. Carbon dioxide activation of carbon aerogels increases both pore volume and surface area, and increasing CO₂-activation tends to facilitate the infiltration process [53]. Synergetic effects between nanoconfinement and a catalytic effect from a TiCl₃ functionalized carbon aerogel scaffold have been achieved, with onset of hydrogen release at $T_{\text{onset}} = 33$ °C and maximum release at 125 °C [54, 55]. It has also been shown that NaAlH₄ nanoconfined in carbon scaffolds can be a potential anode material for batteries [56]. The decomposition of NaAlH₄ at 450 °C forms Al and Na, where the Na can be removed under vacuum leaving a porous aluminium scaffold [57]. The specific surface area of the obtained scaffold was determined to be 7.9 ± 0.1 and 6.0 ± 0.5 m² g⁻¹ by the Brunauer–Emmet–Teller method and from small-angle x-ray scattering measurements, respectively. This aluminium scaffold has been used to nano-confine various complex metal hydrides, allowing for a decrease in decomposition temperature between 150 °C and 250 °C from that of the bulk [58]. NaAlH₄ has also been melt infiltrated into these Al scaffolds, resulting in a reduced decomposition temperature, in fact hydrogen release is observed from 100 °C [59].

In addition to NaAlH₄, nanoconfinement has also proven a successful strategy for other aluminum-based hydrides. One example is LiAlH₄, which has often been overlooked, despite its high gravimetric capacity, due to its intrinsic metastability. The bulk material releases hydrogen in three steps, the first of which (the conversion to Li₃AlH₆) is weakly exothermic by -10 kJ mol⁻¹ H₂. However, recent work combining synthesis, computational modeling, and advanced characterization to demonstrate that metastable LiAlH₄ can be thermodynamically stabilized by nanoconfinement inside the pores of nitrogen-functionalized CMK-3 carbons [60], making the hydrogen uptake and release reversible. The theoretical investigation uncovered two critical factors to achieve full reversibility of the nanoconfined system. First, by computing cluster structures and energies of related Li–Al–H compounds, the authors discovered that the undesired Li₃AlH₆ phase hindering full reversibility is significantly destabilized upon nanosizing. This is consistent with the lack of any indication of Li₃AlH₆ in the experimental data. Second, electronic structure calculations and *ab-initio* molecular dynamics simulations revealed that the nitrogen sites change the density of states of CMK-3 in the vicinity of the Fermi level, effectively acting as solvation sites for lithium ions and stabilizing the fully hydrogenated LiAlH₄ phase. This enables LiAlH₄ regeneration under 1000 bar H₂, which was previously assumed to be infeasible. On the other hand, it has been achieved at 100 bar via the formation of solvent adducts [61–63].

Another recent study demonstrated reversible dehydrogenation of metastable alane (AlH₃) through a similar nanoconfinement approach [64]. Analogous to the first stage of LiAlH₄ decomposition, hydrogen release from AlH₃ is exothermic. As a result, extraordinary pressures (of the kbar-range) are required for full rehydrogenation [65]. The authors discovered this rehydrogenation becomes feasible by stabilizing molecular AlH₃ within the nanopores of a bipyridine-functionalized covalent triazine framework (AlH₃@CTF-bipy). Density functional theory was used to compute geometric and electronic structures, energies, and spectroscopic features of standalone versus confined AlH₃ nanoclusters. The calculations illuminated a surprising and non-intuitive mechanism: dissociative AlH₃ binding to bipyridine sites accompanied by single-electron transfer forms AlH₂ groups on nanopore surfaces, that serve as nucleation sites for AlH₃ cluster formation. This proposed mechanism was fully validated by nuclear magnetic resonance (NMR) and electron paramagnetic resonance (EPR) experiments. Through first-principles thermodynamic models, the authors predicted that these nucleated AlH₃ clusters are much more stable than bulk AlH₃, consistent with rehydrogenation experiments of AlH₃@CTF-bipy at pressures more than tenfold lower than the bulk (700 bar vs >7000 bar).

In general, the hydrogen storage performance of complex hydrides is not only controlled by intrinsic properties, but it can also be severely affected by potential contaminants introduced during synthesis and preparation. Along these lines, White *et al* [66] explored the effect of native surface oxidation on the kinetics of hydrogen release from Ti-catalysed NaAlH₄ [66]. They used near-ambient-pressure *in-situ* x-ray photoelectron spectroscopy (XPS) to track the dynamical evolution of various intermediates in the surface oxide region. Providing unbiased interpretation of spectroscopy results for interfaces is notoriously challenging because bulk-like species are rarely formed, and it is difficult to find reference spectra for phase-pure compounds. Accordingly, the authors combined the experiments with direct simulation of XPS signatures of key chemical species identified in complex structure models. They determined that surface oxides can impede diffusion in the later stages of the reaction, but can actually aid formation of chemical intermediates. First-principles simulations further revealed that hydrogen release is facilitated by activating the hydridic-protic H···H interaction through the appearance of surface oxygen. As such, the authors

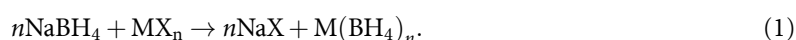
concluded that, whereas bulk oxide layers can slow reversible (de)hydrogenation of NaAlH₄, atomically thin surface oxide or hydroxide layers could actually be beneficial. This work highlights the need to revisit ‘well-known’ properties, while emphasizing the importance of controlling the dynamical behaviour of their surfaces to achieve kinetic improvements.

2.2. Borohydrides

The past few decades have revealed a multitude of novel metal borohydrides, M(BH₄)_n, and this class of materials is further expanded by a variety of bi-metallic and some tri-metallic compounds [3, 67]. Thus, metal borohydrides have extremely rich compositional chemistry and fascinating structural flexibility [68]. The structural features provide a range of physical properties within diverse fields, e.g. hydrogen storage, solid-state batteries, and optical and magnetic properties, demonstrating several possible applications for this class of materials [3, 49, 69–71], as described in section 3. The evaluation of the thermodynamics of pure borohydrides has been implemented in the past to evaluate the possible interaction among different compounds in binary and higher mixtures [43–45, 72–74]. Experimental and theoretical approaches can be combined during thermodynamic assessments by the calculation of phase diagrams (CALPHAD) method as evidenced in the development of complex hydride databases [75]. Chemical manipulation of the materials has further provided several classes of derivatives, e.g. anion and cation substituted compounds and introduction of neutral molecules, which open up new routes for rational materials design and thus tailoring of desired properties [76]. Mixtures of borohydrides to form reactive hydride composited have been reported and tested in some lab-scale prototype tank for hydrogen storage [77–79].

2.2.1. Synthesis

Sodium borohydride (NaBH₄) is a versatile reducing agent used in a number of industrial processes. The commercial production is based on a synthetic route developed by Brown and Schlesinger in the 1950s [80]. Mechano-chemistry is the typical synthesis method of novel metal borohydrides, which can be formed through a metathesis reaction between LiBH₄ or NaBH₄ and a metal halide, MX_n. The approach often yields the monometallic borohydride and the lithium or sodium halide salt [81–88]:



The stability of the metal halide salt is believed to be the driving force for forming the monometallic borohydride. Contrarily, the heavier alkali metal borohydrides, MBH₄ (M = K, Rb, Cs), often provide bimetallic borohydrides [3, 68]. The metal halide is an unwanted by-product and the mechano-chemical synthesis may lead to a reaction between the metal halide and the metal borohydride, which forms either a solid solution or a mixed metal borohydride-halide compound [3, 68, 89–93]. Hence, additional purification steps are required to obtain a single-phase metal borohydride sample. High purity grade metal borohydrides for research purposes are available from mainstream chemical suppliers at the lab-scale. Applicative-oriented projects, however, have demonstrated their scale up to reach the kilogram-level. Some research laboratories, such as Aarhus University (Denmark) and KatChem (Czech Republic), successfully up scaled the production of novel borohydrides, by either ball milling and/or wet chemistry methods [94].

Pristine metal borohydrides are successfully prepared by solvent based methods, which may also provide specific structural polymorphs depending on the reaction conditions [95]. Specifically, the reaction between an ionic or polar-covalent metal hydride and a borane (BH₃) donating neutral complex, e.g. dimethyl sulphide borane, (CH₃)₂S·BH₃, in an anhydrous solvent follows a nucleophilic addition/hydride-transfer mechanism to form the M(BH₄)_n. Subsequent purification and/or de-solvation of the metal borohydride may be necessary, providing a high purity product and some degree of polymorphic control [95].

Solid-gas or solid-liquid reactions are efficient in reacting metal borohydrides with a variety of neutral molecules, e.g. NH₃, THF, DMS etc, to produce a compound where the metal is fully coordinated by the neutral molecules, which act as a ligand, via a lone pair [95–97]. Thus, there is limited or no control of the composition of the reaction product, but this may be modified by subsequent heat treatment or by mechano-chemical treatment with appropriate ratios of the pristine metal borohydride [96, 98–100].

Interestingly, mechano-chemistry has also devised a new approach to access pure, crystalline compositions of metal borohydrides that cannot be prepared by any other synthesis method, e.g. most di- and tri-metallic borohydrides [70, 101–108].

2.2.2. Structural properties

The structural diversity of metal borohydrides is closely related to the BH₄[−] group acting as a flexible ligand. The complex ligand can coordinate via a corner (B–H, κ¹), an edge (B–H₂, κ²), or a face (B–H₃, κ³) to a metal, or act as a counter anion in the anionic compound. The latter usually occurs if the metal is fully

coordinated by stronger ligands, e.g. NH_3 [96, 109, 110]. Cations with high charge density, i.e. charge (q) over volume (V), q/V , and relatively high Pauling electronegativity, χ_P , are polarising and they have a tendency for directionality in the bonding and formation of (polar-) covalent bonds. Zirconium borohydride is a solid consisting of isolated, neutral, molecular $\text{Zr}(\text{BH}_4)_4$ complexes and thus has a low sublimation temperature, $T_{\text{sub}} = 29^\circ\text{C}$, due to the lack of an interconnecting network [111]. Titanium borohydride also forms a molecular borohydride, $\text{Ti}(\text{BH}_4)_3$, but it is much more reactive, $T_{\text{dec}} \sim 0^\circ\text{C}$, which is attributed to the electron configuration, d^1 . Transition metals with d -electron configurations, d^0 , d^5 , or d^{10} form metal borohydrides stable at ambient conditions [112]. Transition metal borohydrides, $\text{TM}(\text{BH}_4)_2$, $\text{TM} = \text{Cr}^{2+}$ (d^4), Fe^{2+} (d^6), and Co^{2+} (d^7) are only stable in solution ($T < -30^\circ\text{C}$), but can be stabilised by neutral molecules, such as ammonia, which coordinate to the metal and prevent redox reactions with the borohydride complex [113].

Alkaline earth and d-block metals with moderate charge density and Pauling electronegativity, e.g. divalent metals, M^{2+} , mainly form framework structures. These compounds typically contain borohydride complexes bridging two or three metals, which provide a high degree of structural flexibility. This is highlighted by the many polymorphs and an amorphous phase observed for magnesium borohydride, $\text{Mg}(\text{BH}_4)_2$. Next to its five known and two yet unsolved polymorphic crystal structures, the amorphous phase of $\text{Mg}(\text{BH}_4)_2$ has been experimentally revisited recently in a detailed study [15, 114, 115]. The amorphous phase can be formed in three different ways [116–118]: (a) reactive ball milling of MgB_2 in H_2 atmosphere, (b) mechano-chemically induced polymorphic transition, and (c) by a pressure collapse. A recent study utilised the product of synthesis (b) and investigated it by total scattering and pair distribution function (PDF) analysis, which is possible as hydrogen (H) has an oxidation state of -1 , and, as such, it is characterized by an electron density. The local ordering, up to 5.1 \AA , resembles the ordering in γ - $\text{Mg}(\text{BH}_4)_2$ with $\text{Mg}-\text{BH}_4-\text{Mg}$ building blocks. Up to 12.3 \AA , the PDF suggests that the interpenetrating channels known from the γ -phase are somewhat present, although with a loss of its functional porosity, whereas above 12.3 \AA , a featureless PDF pattern was found, confirming the amorphous nature of this phase [114, 115, 117].

Metals with even lower charge density and Pauling electronegativity have increasingly ionic interactions in the solid state, i.e. increasing degree of charge transfer from the metal to the BH_4^- complex [119]. This is illustrated by the alkaline earth metal borohydrides, where $\text{Be}(\text{BH}_4)_2$ forms a polymeric, partly covalent structure, while $\text{Ba}(\text{BH}_4)_2$ is more ionic. The dominating ionic bonding becomes clearer for the heavier alkali metal borohydrides, MBH_4 , $\text{M} = \text{Na}, \text{K}, \text{Rb}, \text{and Cs}$, which form rock salt (NaCl) type solids. The most hydrogen dense solid material, ammonium borohydride, NH_4BH_4 , is isostructural to this series, revealing pronounced ionic bonding in this compound [120]. This contrasts the bonding in the more stable ammonia borane, NH_3BH_3 , which is a Lewis acid-base pair adduct with a covalent N–B bond.

Among the rare-earth metal (RE) borohydrides, the majority form trivalent $\text{RE}(\text{BH}_4)_3$, but due to a stable $+2$ oxidation state of $\text{RE}^{2+} = \text{Sm}, \text{Eu}, \text{Yb}$, they usually form divalent $\text{RE}(\text{BH}_4)_2$ directly or during heating by reduction from RE^{3+} to RE^{2+} [88, 91, 95, 97, 121]. The crystal structures of the divalent $\text{RE}(\text{BH}_4)_2$ are isostructural to the alkaline earth metal borohydrides with similar ionic radii, i.e. $\text{RE}(\text{BH}_4)_2$ ($\text{RE}^{2+} = \text{Sm}, \text{Eu}$) are isostructural to $\text{Sr}(\text{BH}_4)_2$ and $\text{Yb}(\text{BH}_4)_2$ is isostructural with the different polymorphs of $\text{Ca}(\text{BH}_4)_2$ [88, 91, 95, 97, 121]. The trivalent $\text{RE}(\text{BH}_4)_3$ can crystallize in three different structures, α -, β -, and r- $\text{RE}(\text{BH}_4)_3$, with space group symmetry $Pa-3$, $Fm-3m$, and $R-3c$, respectively. They are all related to the rhenium oxide (ReO_3) structure type, where β - $\text{RE}(\text{BH}_4)_3$ is the ideal ReO_3 structure, while α - and r- $\text{RE}(\text{BH}_4)_3$ are obtained by tilting of the $[\text{RE}(\text{BH}_4)_6]$ octahedra, as shown in figure 1(a). $\text{La}(\text{BH}_4)_3$ is the only compound which only crystallizes in the r- $\text{RE}(\text{BH}_4)_3$ structure, while the intermediate sized $\text{RE}^{3+} = \text{Ce}, \text{Pr}$ are the only compounds that can crystallize in both the α -, β -, and r- $\text{RE}(\text{BH}_4)_3$ polymorph [97, 122–124]. The smaller $\text{RE}^{3+} = \text{Nd}-\text{Lu}$ crystallize in either the α - or β - $\text{RE}(\text{BH}_4)_3$ polymorph, where the synthesis conditions allow for some polymorphic control [97, 125]. The volume of the $\text{RE}(\text{BH}_4)_3$ correlates linearly with the volume of the RE-ions, and the volume increases in the order r- < α - < β - $\text{RE}(\text{BH}_4)_3$, as shown in figure 1(b).

Thus, the bonding of mono-metallic borohydrides spans from pronounced covalent to ionic bonding and can lead to unexpected structural topologies including interpenetrated frameworks or some degree of porosity. On the other hand, the bimetallic compounds, e.g. containing an alkali metal and an alkaline earth metal or a d- or f-block metals, have a tendency for formation of discrete composite complexes. This structural feature is due to the often-significant difference in Pauling electronegativity of the two metals. The less electronegative alkali metal tends to act as a counter ion in the solid state and the more electronegative metal tend to coordinate with a dominantly covalent interaction to BH_4^- . The alkali metal scandium borohydrides, $\text{MSc}(\text{BH}_4)_4$, $\text{M} = \text{Li}, \text{Na}, \text{K}, \text{Rb}, \text{Cs}$, are an illustrative example all containing distinct $[\text{Sc}(\text{BH}_4)_4]^-$ complexes [127–129]. It is worth noting that scandium borohydride, $\text{Sc}(\text{BH}_4)_3$, has not been isolated in a pure form. There are also bimetallic borohydrides with polynuclear complexes, such as $\text{LiZn}_2(\text{BH}_4)_5$, containing $[\text{Zn}_2(\text{BH}_4)_5]^-$ as an interpenetrated framework, or $\text{LiCe}(\text{BH}_4)_3\text{Cl}$, containing

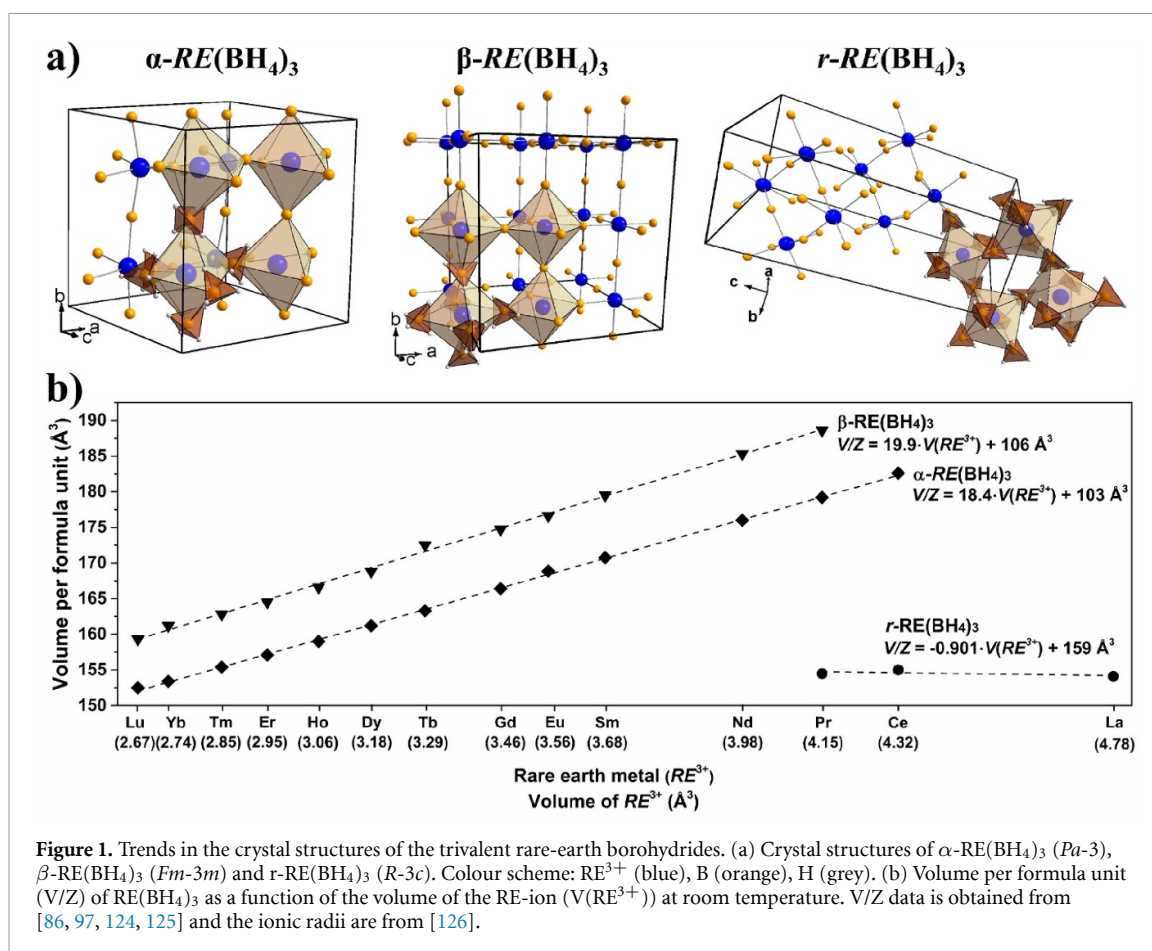
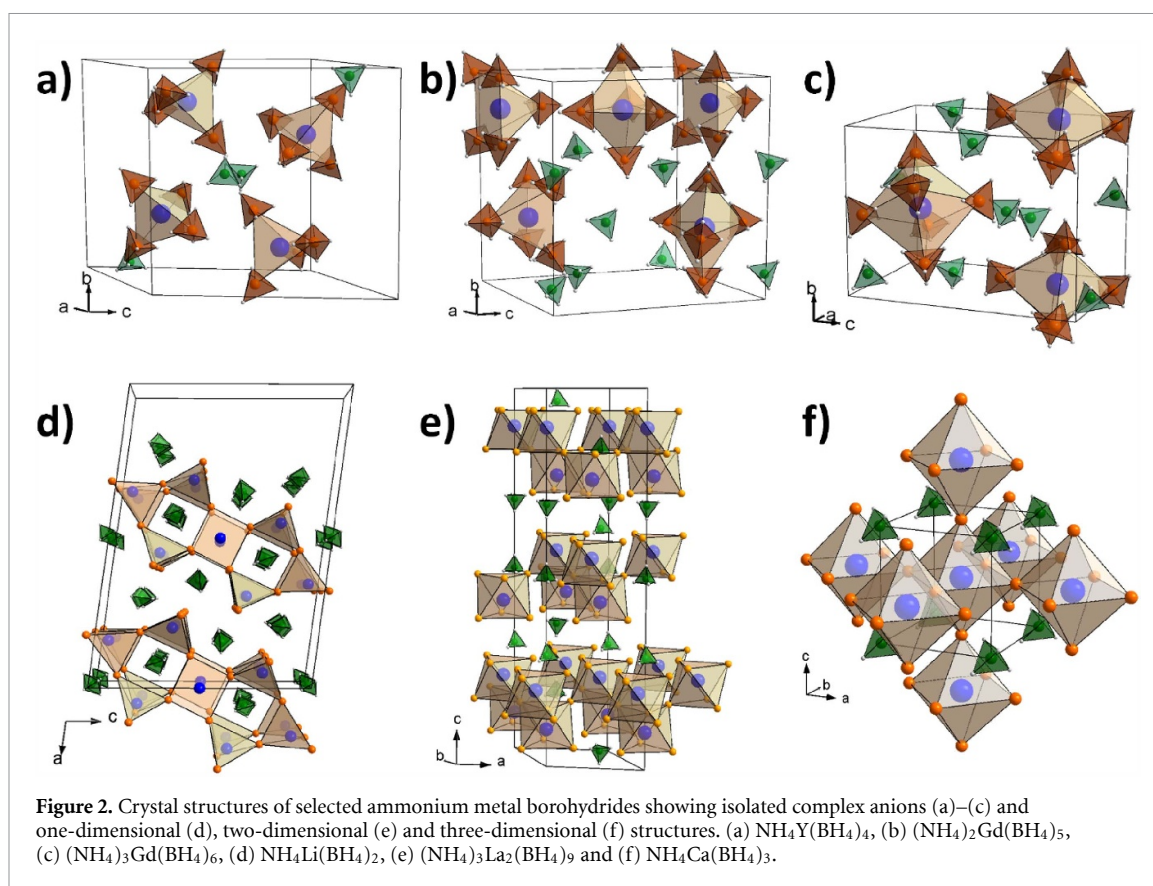


Figure 1. Trends in the crystal structures of the trivalent rare-earth borohydrides. (a) Crystal structures of α -RE(BH₄)₃ (*Pa*-3), β -RE(BH₄)₃ (*Fm*-3*m*) and *r*-RE(BH₄)₃ (*R*-3*c*). Colour scheme: RE³⁺ (blue), B (orange), H (grey). (b) Volume per formula unit (V/Z) of RE(BH₄)₃ as a function of the volume of the RE-ion (V(RE³⁺)) at room temperature. V/Z data is obtained from [86, 97, 124, 125] and the ionic radii are from [126].

tetranuclear anionic clusters [Ce₄Cl₄(BH₄)₁₂]⁴⁻ with a distorted cubane Ce₄Cl₄ core which are charge-balanced by Li⁺ cations [130].

Ammonium borohydride, NH₄BH₄, is interesting from a dynamical and hydrogen storage perspective, due to the extreme hydrogen densities of $\rho_m = 24.5 \text{ wt\% H}_2$ and $\rho_v = 157 \text{ g H}_2 \text{ l}^{-1}$, and to the significant amount of dihydrogen interactions arising in the compound between NH₄⁺ and BH₄⁻. NH₄BH₄ is unstable at ambient conditions with a ‘half-life’ of *ca.* 6 h [131, 132]. However, by reacting this material with Ca(BH₄)₂, a composite with intermediate stability was formed, with $T_{\text{dec}} \sim 100 \text{ }^\circ\text{C}$ [106, 133]. This inspired the design and synthesis of a large variety of ammonium-metal borohydrides, (NH₄)_xM(BH₄)_y, with M = Li, Mg, Al, Sc, Sr, Y, Mn, La, Gd, all with high ρ_m of 9.2–24.5 wt% H₂ [108, 134–136]. No reaction was observed with NaBH₄, while a solid-solution was formed with KBH₄ [108]. This exposed an intriguing structural variety, ranging from structures built from isolated tetrahedral, five-fold or octahedral anionic [M(BH₄)_n] complexes, to structures built from one-dimensional chain-like frameworks, two-dimensional layers to three-dimensional framework structures, which are summarized in figure 2. In all cases, the NH₄⁺ was considered as a counter ion, similar to the alkali metals in bimetallic borohydrides. Dihydrogen interactions between complex NH₄⁺ and BH₄⁻ ions contribute to the structural diversity and flexibility, but due to the similar size of $r(\text{NH}_4^+) = 1.48 \text{ \AA}$, $r(\text{K}^+) = 1.38 \text{ \AA}$, and $r(\text{Rb}^+) = 1.52 \text{ \AA}$, several of the NH₄⁺ compounds show resemblance to the K- and Rb-analogues [108]. However, a new composition and structure type was reported for (NH₄)₃La₂(BH₄)₉, which forms a new two-dimensional layered structure. Interestingly, it was found that structures with three-dimensional framework display significantly longer shortest-dihydrogen bonds (>2.18 Å), while structures with lower dimensionality all displayed shorter bonds with the shortest dihydrogen bonds in the range 1.59–1.82 Å [108].

Quasielastic neutron scattering (QENS) can be used to determine the dynamic processes, such as jump rotation or diffusion. Borohydrides are a near ideal probe, when the boron-11 isotope is used, as hydrogen motions can be probed due to its strong incoherent cross section. All motions are noted as a visible broadening next to the elastic line. QENS has been employed in many different borohydrides over the years and a sensible overview has been published in [137]. QENS has been employed on the γ - and amorphous phase of Mg(BH₄)₂, and on Pr(BH₄)₃ [115, 124]. Mg(BH₄)₂ shows a definite broadening of the elastic line



after the sample has turned amorphous, implying that this broadening is a result of the high rotational mobility of the BH_4^- group [115]. $\text{Pr}(\text{BH}_4)_3$ was also investigated, due to its unusual structural variety, with a stepwise negative thermal expansion [123]. QENS data displayed a definite thermal response during the heating procedure and the mean square displacement value also showed a dependency on the cooling rate, meaning that the high temperature structure was well preserved during cooling [124]. The structural and vibrational properties of NH_4BH_4 have recently been investigated with inelastic and QENS, which revealed the onset of fast NH_4^+ dynamics at $\sim -223^\circ\text{C}$ ($\sim 50\text{ K}$), while the dynamics are almost frozen below this temperature [138, 139]. Upon further heating, the BH_4^- dynamics has an onset at $\sim -148^\circ\text{C}$ ($\sim 125\text{ K}$). The reorientational motions were investigated with QENS, revealing a fast and complex reorientation of NH_4^+ , while BH_4^- can be described as a cubic arrangement with 50% occupancy on the H positions [138], the latter in agreement with the proposed crystal structure determined by x-ray diffraction [132]. Density functional theory (DFT) calculations revealed a non-directional nature of the dihydrogen bonds, and only a weak tendency for long-range ordering [139].

2.2.3. Derivatives of metal borohydrides with neutral molecules

Introduction of neutral molecules into metal borohydrides is a valuable approach to further increase their compositional and structural diversity and to tailor their chemical and physical properties. The selected molecules in most cases contain an electron pair donating atom, such as N, O, or S, which tends to coordinate to the metal in the structure via a covalent bond. Thus, a range of solvated metal borohydrides have been observed through the preparation of metal borohydrides or during subsequent reaction with a solvent [95]. The complete series of rare-earth metal borohydrides (REBs) with dimethyl sulphide ($\text{S}(\text{CH}_3)_2$) has been investigated, where $\text{RE}^{3+} = \text{La}$ form multiple different solvates, $\text{La}(\text{BH}_4)_3 \cdot x\text{S}(\text{CH}_3)_2$, but none of the structures have yet been solved [97, 122]. For the heavier $\text{RE}^{3+} = \text{Ce}$, Pr, two polymorphs have been reported, α - and β - $\text{RE}(\text{BH}_4)_3 \cdot \text{S}(\text{CH}_3)_2$, where α - $\text{RE}(\text{BH}_4)_3 \cdot \text{S}(\text{CH}_3)_2$ is isostructural with the majority of the rare-earths $\text{RE}^{3+} = \text{Y}$, Ce, Pr, Nd, Gd, Tb, Dy, Ho, Er, Tm and Lu [87, 95, 97, 140]. Interestingly, the rare-earths that are sensitive to reduction, $\text{RE}^{3+} = \text{Sm}$, Yb, form different solvates, $\text{RE}(\text{BH}_4)_3 \cdot x\text{S}(\text{CH}_3)_2$, and appear to be a complex mixture of different compounds, where during thermolysis, the solvent is released together with the reduction from RE^{3+} to RE^{2+} [95, 97].

These neutral molecules often contain hydrogen atoms bonded to a more electronegative atoms, which can form dihydrogen bonds with the hydrogen in the borohydride group, e.g. $\text{B}-\text{H}^{\delta-} \cdots ^{\delta+}\text{H}-\text{N}$, in the solid

state. This is illustrated by complexes with ammonia borane, e.g. $\text{Mg}(\text{BH}_4)_2 \cdot 2\text{NH}_3\text{BH}_3$, which possess strong dihydrogen bonds (length $< 2.0 \text{ \AA}$) and the layered structure of $\alpha\text{-Sr}(\text{BH}_4)_2 \cdot \text{NH}_3\text{BH}_3$ consisting of alternating layers of $\text{Sr}(\text{BH}_4)_2$ and NH_3BH_3 , partly stabilised by dihydrogen bonds [141, 142]. Finally, the $\text{Al}(\text{BH}_4)_3 \cdot \text{NH}_3\text{BH}_3$ consists of heteroleptic complexes ($\text{Al}(\text{BH}_4)_3 \cdot \text{NH}_3\text{BH}_3$), where the aluminium cation coordinates to three BH_4^- groups and one NH_3BH_3 molecule [143]. The complexes are ordered in a three-dimensional crystal structure due to weak dihydrogen bonds between the BH_4^- and the $-\text{NH}_3$, which are often bifurcated on the latter side and thus reaching $\text{H} \cdots \text{H}$ distances of more than 2.6 \AA [143].

2.2.4. Anion substitutions

Different types of anion substitution in metal borohydrides have been described, which can be well illustrated by the behaviour of the halides [3]. The small fluoride ion, F^- (1.33 \AA), resembles the hydride ion, H^- (1.40 \AA), and fluorides and hydrides containing the same metal cation are often found to be isostructural. Therefore, fluoride substitution can occur in the borohydride anion forming $\text{B}(\text{H}, \text{F})_4^-$ complexes [144, 145]. This was obtained for various $\text{MBH}_4\text{-MBF}_4$ systems, $\text{M} = \text{Na}$ or K , e.g. by formation of $\text{NaBH}_{2.1}\text{F}_{1.9}$, observed from $200 \text{ }^\circ\text{C}$ to $215 \text{ }^\circ\text{C}$ by synchrotron radiation x-ray powder diffraction (SR-PXD) [145, 146]. Theoretical calculations of thermodynamic properties of orthorhombic $\text{o-LiB}(\text{H}, \text{F})_4$ reveal a tendency of fluorine to prefer boron atoms which already is bonded to F, rather than being statistically distributed over all the available BH_4^- complexes [144, 147]. This is in agreement with the experimentally determined low thermal stability and release of boron trifluoride and diborane gases and the formation of significant amounts of $\text{M}_2\text{B}_{12}\text{H}_{12}$ [145, 146, 148]. Thus, fluorine appears to have too strong of a destabilising effect.

In contrast, the heavier halides, i.e. Cl^- , Br^- , or I^- , chemically resemble the borohydride complex, BH_4^- , and they may substitute this anion in the solid state. An easy anion substitution occurs if the metal borohydride and the metal halide are isostructural. This effect can be observed by moderate heat treatment of mechano-chemically mixed samples and it has been observed for $\text{LiBH}_4\text{-LiBr}$, $\text{LiBH}_4\text{-LiI}$ systems, because $\beta\text{-LiBr}$, $\beta\text{-LiI}$, and h-LiBH_4 are isostructural, as well as in $\text{NaBH}_4\text{-NaCl}$ mixtures, given that NaBH_4 and NaCl are also isostructural [149–152]. These phenomena occur because volume contraction is facilitated by mechano-chemical treatment, i.e. dissolution of the compound with the smaller volume per formula unit (V/Z) into the compound with the larger one. On the other hand, moderate heat treatment lead to thermal expansion, which may facilitate formation of the solid solution with the larger V/Z . Though, upon prolonged heating, solid solutions tend to merge into just one. On the contrary, if the metal borohydride and the metal halide are not isostructural, anion substitution can occur in both compounds, and it may lead to two terminal solid solutions.

In the past few years, interest in intrinsic entropy effects in the solid state has been raised, illustrated by the fact that some polymorphs, e.g. h-LiBH_4 , $\beta\text{-Mg}(\text{BH}_4)_2$, and $\beta\text{-Ca}(\text{BH}_4)_2$ readily dissolve metal halides in the solid state [130, 153]. This effect was assigned to dynamics and an orientational disorder, which often occur in high temperature polymorphs. Therefore, anion substitution often stabilises this structure to lower temperatures.

Since 2009, halide substitution has been adopted to enhance Li^+ conductivity in LiBH_4 [154], stabilizing the high temperature polymorph at room temperature. In the last years, even though the $\text{Li}(\text{BH}_4)_{1-\alpha}(\text{Br})_\alpha$ hexagonal solid solution has been well studied as a solid-state-electrolyte [155], few experimental data exist for hydrogen storage in the $\text{LiBH}_4\text{-LiBr}$ system [150, 156], and only recently a thermodynamic assessment has been reported [157]. The $\text{LiBH}_4\text{-LiBr}$ phase diagram was recently explored experimentally, by means of *in-situ* and *ex-situ* powder x-ray diffraction (PXD), differential scanning calorimetry (DSC), and thermodynamically assessed using the CALPHAD method, coupled with *ab-initio* calculations. The melting behaviour has been determined and a peritectic reaction at $380 \text{ }^\circ\text{C}$ and 0.60 LiBr molar fraction have been reported [157]. By combining DSC and PXD analyses, an enthalpy of mixing ($\Delta H_{\text{Mix}} = -1.0 \pm 0.2 \text{ kJ mol}^{-1}$) for the formation of the $\text{h-Li}(\text{BH}_4)_{0.6}(\text{Br})_{0.4}$ solid solution has been obtained, which was used for the CALPHAD assessment. The resulting phase diagram is reported in figure 3 [157], where it can be observed that the stability of the hexagonal $\text{Li}(\text{BH}_4)_{1-\alpha}(\text{Br})_\alpha$ solid solution at room temperature is in the $0.30 \leq \alpha \leq 0.55$ range. LiBr can stabilize the hexagonal structure of LiBH_4 at room temperature, whereas LiCl is soluble in LiBH_4 only at high temperatures in the hexagonal phase, whereas nearly no solubility has been observed in the orthorhombic phase, as shown in figure 3 [158]. Being isostructural, LiBr and LiCl show a full solubility in the cubic phase [159].

A ternary hexagonal solid solution, $\text{h-Li}(\text{BH}_4)_{1-\alpha-\beta}(\text{Br})_\alpha(\text{Cl})_\beta$, containing both chloride and bromide can be stabilized at room temperature (figure 3) [155]. The $\text{h-Li}(\text{BH}_4)_{1-\alpha-\beta}(\text{Br})_\alpha(\text{Cl})_\beta$ lattice parameters has been defined by PXD analysis and Rietveld refinement. It has been reported that both the a and the c lattice parameters, as well as the volume, of the $\text{h-Li}(\text{BH}_4)_{1-\alpha-\beta}(\text{Br})_\alpha(\text{Cl})_\beta$ phase, decrease with the increase of halides content. The contraction of lattice parameters is almost linear with increasing Cl^- concentration. When Br^- replaces the borohydride anions, the decrease of lattice parameters and volume is less pronounced

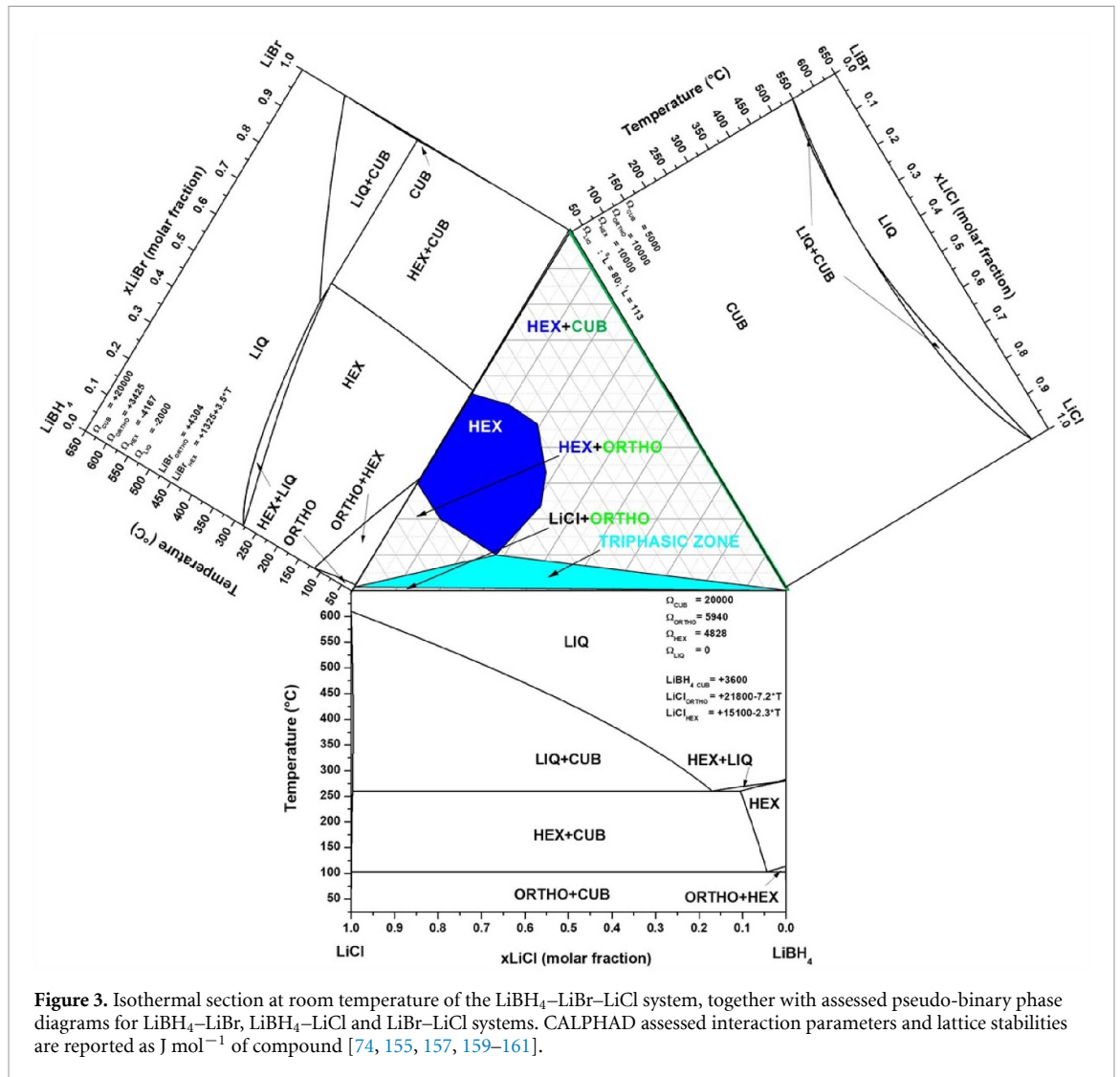


Figure 3. Isothermal section at room temperature of the $\text{LiBH}_4\text{-LiBr-LiCl}$ system, together with assessed pseudo-binary phase diagrams for $\text{LiBH}_4\text{-LiBr}$, $\text{LiBH}_4\text{-LiCl}$ and LiBr-LiCl systems. CALPHAD assessed interaction parameters and lattice stabilities are reported as J mol^{-1} of compound [74, 155, 157, 159–161].

with respect to Cl^- . This behaviour is expected after halogenation, due to the smaller ionic radii of Cl^- ($r(\text{Cl}^-) = 1.81 \text{ \AA}$) and Br^- ($r(\text{Br}^-) = 1.96 \text{ \AA}$) [126] compared to that of BH_4^- ($r(\text{BH}_4^-) = 2.03 \text{ \AA}$) [68]. Finally, the effect of the composition and the structure dimensions of the $\text{h-Li}(\text{BH}_4)_{1-\alpha-\beta}(\text{Br})_\alpha(\text{Cl})_\beta$ solid solution on the Li-ion conductivity has been investigated, showing that the highest value of room temperature Li-ion conductivity in the ternary solid solution is reached for the $\text{h-Li}(\text{BH}_4)_{0.7}(\text{Br})_{0.2}(\text{Cl})_{0.1}$ sample ($1.3 \times 10^{-5} \text{ S cm}^{-1}$ at $30 \text{ }^\circ\text{C}$) [155]. It is worth noting that the incorporation of chlorine in the hexagonal phase leads to a lower weight of the solid solution, i.e. increasing the energy density in terms of electrolyte materials [155].

In contrast to metal borohydride-halide solid solutions with fully anion disordered structures, a few compounds have fully ordered structures, such as $\text{KZn}(\text{BH}_4)\text{Cl}_2$ [162] and lithium REB halides, $\text{LiRE}(\text{BH}_4)_3\text{X}$, ($\text{RE} = \text{La, Ce, Pr, Gd, Sm}$; $\text{X} = \text{Cl, Br, I}$) [86, 89, 90, 92, 121, 163].

Fluoride substitutions have been obtained in RHCs, such as $(\text{CaH}_2/\text{CaF}_2)\text{-MgB}_2$, $\text{Mg-LiBH}_4\text{-FeF}_3$, LiH-LiF-MgB_2 , and $\text{Ca}(\text{BH}_4)_2\text{-MgF}_2$ system, which often have been cycled a few times with hydrogen release and uptake, but they suffer from decreasing capacity due to the high stability of metal fluorides, MF_x , and loss of boron due to formation of gaseous boron trifluoride, BF_3 [164–171].

2.2.5. Cation substitutions

Tailoring approaches to improve thermodynamics and kinetics of hydrogen release and uptake in borohydrides have been evidenced when mixed cations solid solutions or eutectic mixtures have been investigated [112, 172, 173]. Available phase diagrams in cation mixed pseudo binary systems are presented in figure 4, together with information on solid and liquid phases. As a matter of fact, after literature and experimental analysis on $\text{LiBH}_4\text{-NaBH}_4$ [160], $\text{LiBH}_4\text{-KBH}_4$ [174], and $\text{NaBH}_4\text{-KBH}_4$ [175], pseudo-binary systems were fully assessed, describing solid and liquid phases involved in each phase diagram [2, 161].

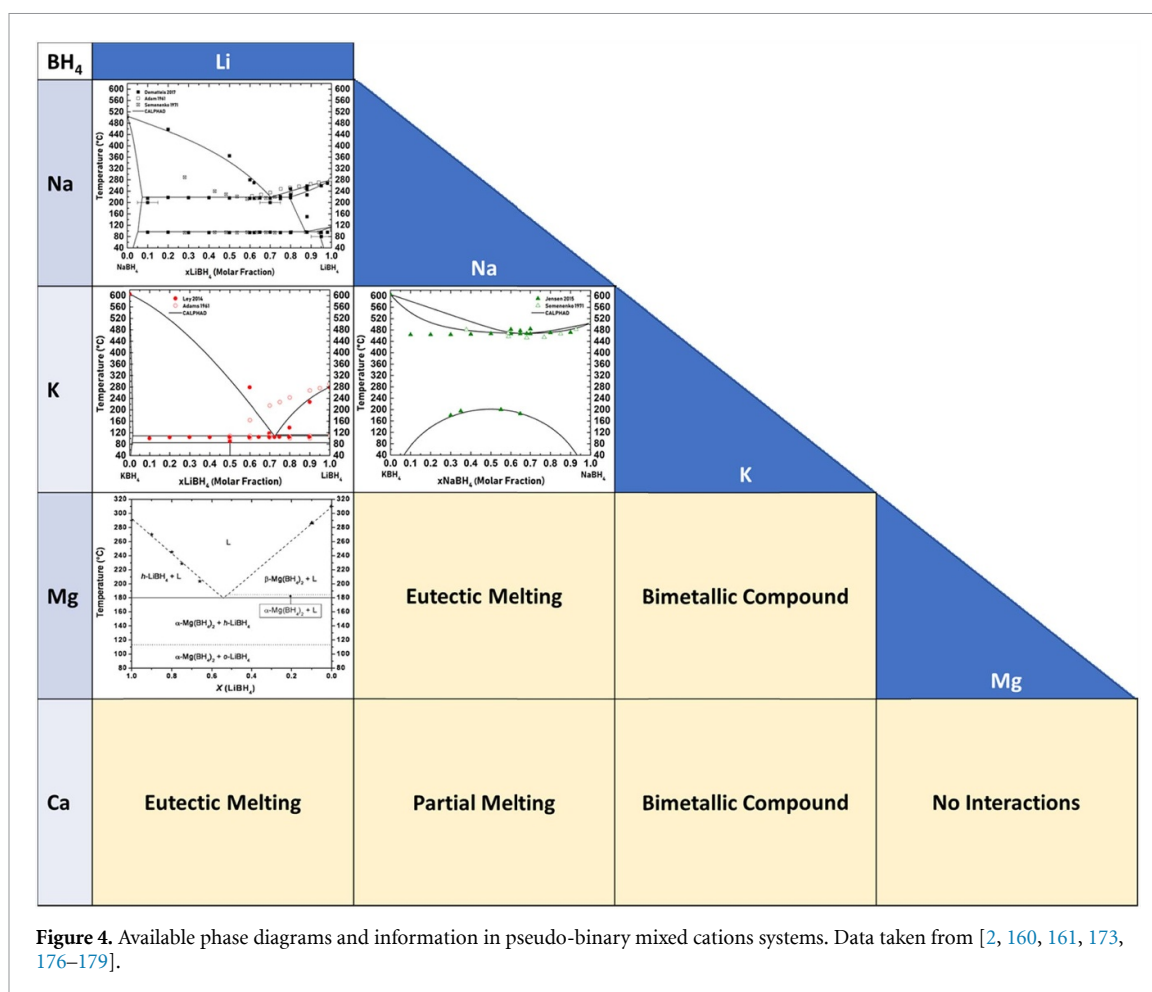


Figure 4. Available phase diagrams and information in pseudo-binary mixed cations systems. Data taken from [2, 160, 161, 173, 176–179].

Eutectic melting is clearly observed in the lithium borohydride-potassium borohydride ($\text{LiBH}_4\text{--KBH}_4$) phase diagram, by a rather deep melting point at $T_{\text{mp}} = 105^\circ\text{C}$ [174]. This feature was utilised to nanoconfine the $\text{LiBH}_4\text{--KBH}_4$ system via melt infiltration into a CMK-3 type carbon, which successfully absorbed 2.5–3 wt% H_2 in five consecutive absorption-desorption cycles at $T = 400^\circ\text{C}\text{--}500^\circ\text{C}$ [180]. A stoichiometric bimetallic compound, $\text{LiK}(\text{BH}_4)_2$ can be prepared mechanochemically from the pure borohydrides, because the volume per formula unit (V/Z) of this compound is smaller than that of the reactants [174]. Interestingly, the binary compound does not form upon cooling.

In contrast, the sodium borohydride-potassium borohydride ($\text{NaBH}_4\text{--KBH}_4$) system forms a solid solution upon thermal treatment at $200 < T < 450^\circ\text{C}$, apparently with solubility in the full range of compositions. Upon cooling, a solid solution, $\text{Na}_x\text{K}_{1-x}(\text{BH}_4)$ easily crystallises. The difference in melting properties is due to the fact that the volume of the solid solution is larger than that of the reactants and its formation is facilitated by thermal expansion [174, 175].

When multiple cations are involved in mixtures of borohydrides, the liquid phase is usually stabilized at lower temperature with respect to pure components, either because of the formation of eutectics or thermal minima. Due to this liquid stabilisation, hydrogen evolution is obtained from the liquid at lower temperature. The formation of a stable liquid at low temperature is also beneficial for nanoconfinement approaches to form nanosized materials, with enhanced hydrogen kinetics and cyclability properties [181–184]. The favourable effect of nanosizing has recently been confirmed and evidenced in theoretical studies and calculations for the decomposition of pure $\text{Ca}(\text{BH}_4)_2$ [185].

Furthermore, when complex mixed cations in ternary, quaternary, or even quinary equimolar mixtures are investigated, the formation of low-melting borohydrides is confirmed, with a limited formation of solid solutions and stoichiometric compounds [186, 187]. Mixed cation borohydrides interact more in the liquid phase than in the solid. On the other hand, the study of double charged cations mixture, as in the case of the $\text{Mg}(\text{BH}_4)_2$ and $\text{Ca}(\text{BH}_4)_2$ system, evidences a very limited interaction in the solid state, while a low temperature liquid was not observed, but a decreased decomposition temperature through complex reaction steps has been reported [179].

2.2.6. Thermal properties and reactivity

Hydrogen release and uptake from metal borohydrides remains not fully understood and the reactions are often relatively slow and require high temperatures and pressures to bypass the high kinetic barriers. This is illustrated by general difficulties in measuring reliable thermodynamic data for metal borohydrides by the Sievert's method [188]. In some cases, more than one decomposition reaction appears to be involved, which may depend on physical conditions, such as partial pressures, temperature and/or composition of the samples. Melting reactions, formation of viscous liquids with associated bubbling, and frothing during thermolysis of metal borohydrides is also a challenge for physical measurements, such as thermogravimetric analysis or manometric gas release analysis.

An illustrative example is the decomposition of lithium borohydride, LiBH_4 . The effect of pressure and temperature on equilibrium phases for LiBH_4 decomposition processes has been assessed by the CALPHAD method [74]. It mainly decomposes to $\text{Li}_2\text{B}_{12}\text{H}_{12}$ at elevated hydrogen partial pressures, $p(\text{H}_2) = 50$ bar during heating to 600°C for 5 h [189]. At lower hydrogen pressures, an increasing amount of amorphous boron is observed, and $\text{Li}_2\text{B}_{12}\text{H}_{12}$ may decompose to hydrogen-poor $\text{Li}_2\text{B}_{12}\text{H}_{12-x}$ [190]. Thus, $\text{Li}_2\text{B}_{12}\text{H}_{12}$ may be avoided depending on the decomposition conditions, to facilitate a successive hydrogen uptake, since $\text{Li}_2\text{B}_{12}\text{H}_{12}$ is not able to be hydrogenated back into LiBH_4 , even under extreme conditions (e.g. $T = 400^\circ\text{C}$ and $p(\text{H}_2) \leq 970$ bar) [191].

Divalent metals appear to have a higher tendency to form metal borides as compared to alkali metals. Under hydrogen atmosphere, magnesium borohydride decomposition is somewhat suppressed and melting is observed at 270°C , followed by a first crystallisation of MgH_2 , then Mg, and finally MgB_2 at 510°C [192]. However, non-crystalline *closo*-boranes may also act as intermediate products during decomposition of $\text{Mg}(\text{BH}_4)_2$ in vacuum [189]. It should be recognized that the decomposition of $\text{Mg}(\text{BH}_4)_2$ is complex [193] and sensitive to the nature of the starting materials and reaction conditions; reviews by Saldan [194] and Zavorotynska *et al* [15] have tabulated many of the reported pathways. The formation of metal borides, MB_x , during decomposition has been considered key to enable rehydrogenation into the respective metal borohydride, e.g. studies on $\text{MgB}_2\text{-MH}_x$ ($M = \text{Li, Na, Mg, Ca}$) systems, revealing the formation of $\text{M}(\text{BH}_4)_n$ ($M = \text{Li, Na, Ca}$) either by direct hydrogenation or by ball-milling under elevated hydrogen pressures [195–197]. Similarly, 75% and 60% of $\text{Mg}(\text{BH}_4)_2$ and $\text{Ca}(\text{BH}_4)_2$ was formed by direct hydrogenation at high hydrogen pressure (>700 bar) and elevated temperature of MgB_2 and CaB_6 , respectively [198, 199]. The high-pressure hydrogenation of MgB_2 also results in the macroscopic fusing of particles, which is thought to prevent further hydrogenation [200]. Lastly, AlB_2 as an additive to MH_x ($M = \text{Li, Na, Ca}$) also proved to enable the formation of the respective metal hydride and up to 83 mol% of NaBH_4 was formed [201].

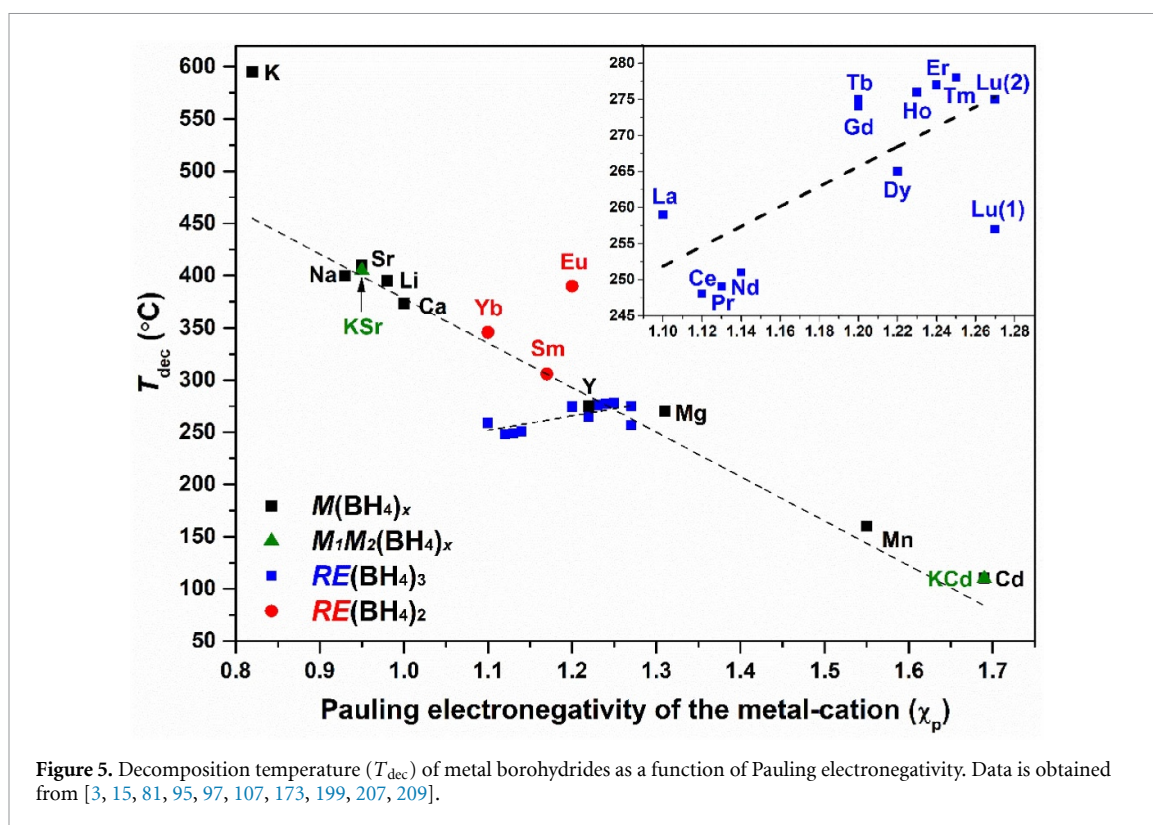
The decomposition pathway of $\text{Mg}(\text{BH}_4)_2$ is different in dynamic vacuum and lower temperatures where $\text{Mg}(\text{B}_3\text{H}_8)_2$ was observed as the major decomposition product at 265°C and $\text{MgB}_4\text{H}_{10}$ was also proposed as an intermediate product [202, 203]. Lower dehydrogenation temperatures over longer time tend to increase the amount of larger borates and a greater quantity of $\text{Mg}(\text{B}_3\text{H}_8)_2$ was obtained after five weeks at 200°C in vacuum [204]. Interestingly, $\text{Mg}(\text{B}_3\text{H}_8)_2$ takes up hydrogen at 250°C and $p(\text{H}_2) = 120$ bar, to transform into $\text{Mg}(\text{BH}_4)_2$ after 48 h [204]. Composites of $\text{Mg}(\text{B}_3\text{H}_8)_2\cdot 2\text{THF-MgH}_2$ (1:2) are even more prone to absorb hydrogen, e.g. at $p(\text{H}_2) = 50$ bar and $T = 200^\circ\text{C}$ after only 2 h [205].

$\text{Al}(\text{BH}_4)_3\cdot\text{NH}_3\text{BH}_3$ showed particular promise as a hydrogen storage material as the hydrogen release temperature was observed at 70°C in an endothermic event ($\Delta H \sim 39$ kJ mol⁻¹), although rehydrogenation attempts at moderate conditions, i.e. 70°C – 100°C and $p(\text{H}_2) = 150$ bar, were unsuccessful [143]. Further derivatives of the compound were investigated, e.g. $\text{Al}(\text{BH}_4)_3\cdot\text{CH}_3\text{NH}_2\text{BH}_3$, but the slight modification of the ligand accompanies large differences in the hydrogen storage properties and a preferential release of B_2H_6 instead of H_2 was observed [206].

Bi- and trimetallic borohydrides tend to dissociate to the monometallic borohydrides upon heating to the temperature of the least stable component, and then the metal borohydrides decompose individually. In some cases, they may also form eutectic melting composites, as described above. In case the bi- and trimetallic borohydrides are created from less stable metal borohydrides, i.e. they contain the metals Al, Sc, Mn, Zn, or Cd, then the corresponding metal borohydride compositions will decompose upon dissociation, often involving release of diborane [130, 207, 208].

The stability of metal borohydrides is to some extent influenced by the Pauling electronegativity of the metal, i.e. the higher χ_p , the lower the decomposition temperature, T_{dec} [119]. However, the opposite tendency was recently observed for the series of rare earth metal borohydrides, as shown in figure 5 [97]. It was also found that the $\text{RE}(\text{BH}_4)_2$ is more stable than the $\text{RE}(\text{BH}_4)_3$, which is ascribed to the lower charge density on the RE-ion.

Additives have been much debated in the scientific literature regarding the identification of a catalyst for the formation/breaking of the B–H bond. To date, no clear evidence of the existence of such a catalyst exists, but some additives appear to have a positive effect on the reaction kinetics, as grain refiners or enhancing the



nucleation sites formation for reaction products. In most cases, the high reactivity of metal borohydrides leads to chemical reactions also with typically inert additives, such as gold and quartz [210].

Nanoconfinement has been explored as an effective strategy to alter the thermodynamic and kinetic properties of borohydrides for hydrogen storage. In addition to affecting reaction enthalpy, changing sizes or morphology can also alter reaction pathways, by shifting the thermodynamic equilibrium for forming different compounds or phases. Other advantages include the promotion of reversible hydrogen desorption/adsorption through accelerated kinetics. In combination with synthesis and characterization, advanced simulation techniques have been used to provide mechanistic understanding of how the thermodynamic and kinetic properties are tuned by nanoconfinement. One target material for these studies has been the Mg–B–H system, which has one of the highest theoretical capacities among the borohydride systems. The effect of pressure and temperature on equilibrium phases for $\text{Mg}(\text{BH}_4)_2$ has been assessed by the CALPHAD method [16]. Jeong *et al* [211] evaluated the free energies and nucleation barriers for phase transformation between the α , β , and γ -phases of $\text{Mg}(\text{BH}_4)_2$ using classical nucleation theory and revealed that there is a subtle balance between the thermodynamic driving force and nucleation kinetics that controls polymorphism in $\text{Mg}(\text{BH}_4)_2$ [211]. These simulations successfully explained the experimental observations of obtaining distinct $\text{Mg}(\text{BH}_4)_2$ phases by following different synthetic routes. In addition, the simulation results provided guidance for future control of borohydride phases through synthesis within well-controlled thermal and chemical environments.

Apart from introducing physical interactions to preserve particle size, a nanoconfining host can also chemically interact with metal hydrides to directly modify dehydrogenation pathways. One example for confined borohydrides can be found in the recent study by Schneemann *et al* [212], in which a metal-organic framework (MOF), $\text{Zr}_6\text{O}_4(\text{OH})_4(\text{bpydc})_6$ ($\text{bpydc}^{2-} = 2,2'$ -bipyridine-5,5'-dicarboxylate) was used to confine $\text{Mg}(\text{BH}_4)_2$ and enhance hydrogen desorption kinetics. First-principles simulations confirmed that observed improvements for hydrogen desorption are attributable to the $\text{Mg}(\text{BH}_4)_2$ interaction with the MOF functional groups (both the ligands and metal centre). It was shown that the activation energies for B–H dissociation are greatly reduced at the Mg sites that are directly coordinated with the N and O atoms in the MOF. The chemical interactions between infiltrated $\text{Mg}(\text{BH}_4)_2$ and the MOF host were probed by comparing simulated and measured x-ray absorption spectra, demonstrating the power of an integrated theory-experiment approach to unravel the reaction mechanisms and identify thermodynamic and kinetic limitations for multistep processes. More generally, the study affirms the merit of tuning complex metal hydride dehydrogenation reaction kinetics by manipulating local chemistry at host-hydride interfaces.

Other recent studies have focused on the Mg–B–H system from the fully dehydrogenated MgB_2 product to identify pathways and limitations. One such fundamental investigation focused on the structure of the

MgB₂ surface, which significantly impacts the nature of initial H₂ interactions during phase decomposition [213]. The authors combined first principles-derived global optimization and free energy sampling methods with experimental synthesis and spectroscopic characterization to investigate the surface atomic structure. They showed that longstanding assumptions in the chemical community regarding the static nature of boron surface structures in MgB₂ and related layered metal diboride compounds may be incorrect; instead, the surfaces are disordered and fluctuate dynamically under conditions relevant to hydrogenation. This dynamic and highly heterogeneous surface environment introduces intrinsic heterogeneity of surface reactivity for H₂ activation and initial H binding, which can translate to uneven hydrogen uptake behaviour as the reaction progresses. Another study by Ray *et al* [214] directly probed the interaction of exposed MgB₂ edges with H₂ using *ab-initio* molecular dynamics accelerated by elevated temperature and pressure conditions. Building on an earlier investigation hypothesizing that such edges can uptake limited quantities of H₂ at far more reasonable conditions than the bulk material [215], the authors generated edge-enriched models to show that these areas are indeed active for hydrogenation. They subsequently mapped out possible chemical reaction pathways in the pre-nucleation regime, illustrating how chemistry might proceed at the buried solid interfaces.

To increase the concentration of reactive edges, Li *et al* [216] synthesized nanoscale Mg–B materials in the absence of a nanoconfining host using a solvent-assisted ball milling approach [216]. Although such morphologies are difficult to maintain upon cycling, they provide insight into the independent size effects that govern nanoscale behaviour. The authors showed that partial hydrogenation could be achieved at 280 °C, which is 100 °C below the threshold for bulk MgB₂ hydrogenation, with a tenfold enhancement in the H–H dissociation rate. DFT calculations were used to reveal the fundamental surface chemistry and interaction with remaining oleate solvent molecules, which were found to further mitigate oxidation.

2.3. Borates

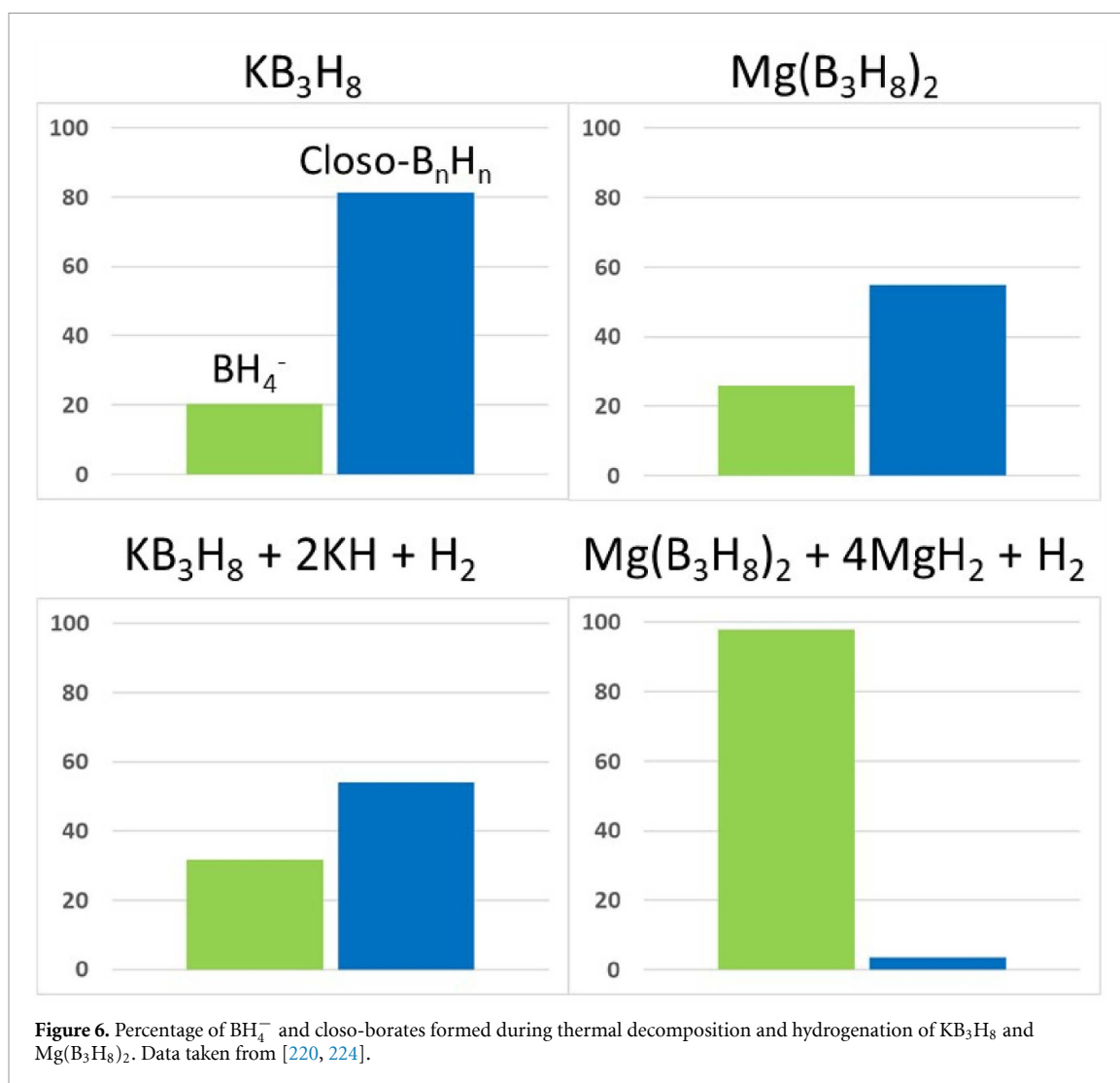
Boranes, B_xH_y, are known to have a very diverse chemistry, with all known neutral compounds being flammable, sometimes even explosive, when coming in contact with air, and they are usually rather toxic. However, anionic complexes also exist, where some are highly stable and relevant for design and development of novel ‘energy materials’, both for solid-state batteries or hydrogen storage. Here, the review focuses on ‘smaller borates’, such as B₃H₈[−], and ‘larger borates’ dominated by the *closo*-borates, such as B₁₀H₁₀^{2−} and B₁₂H₁₂^{2−} [217].

As introduced above, Mg(B₃H₈)₂ is of interest due to its potential to undergo a reversible dehydrogenation-rehydrogenation cycle with Mg(BH₄)₂ at moderate temperatures [204]:



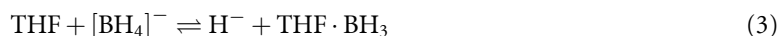
Most syntheses of Mg(B₃H₈)₂ result in compounds containing coordinated solvent molecules, and it is only recently that a solvent-free synthesis has been reported [218], albeit with poor crystallinity and two equivalents of NaBr intermixed within the solid. Monovalent KB₃H₈ is more readily synthesized, solvent-free, and it is interesting to compare this compound with Mg(B₃H₈)₂. KB₃H₈ exhibits a complex structural behaviour, with four polymorphs observed between −3 °C and 57 °C [219, 220]. The structural changes are related to the reorientational dynamics of the B₃H₈[−] anion, in which bridging H atoms are situated outside only 2 of the 3 sides formed by the triangle of B atoms. Similar complex polymorphism has recently also been reported for CsB₃H₈ [221]. The dynamics and lack of three-dimensional crystallinity are likely reasons why B₃H₈[−] forms during dehydrogenation of Mg(BH₄)₂, despite unfavourable thermodynamic predictions [222]. Similarly, another recent DFT study confirmed that the solid-state reactive environment provides a unique energy landscape that can stabilize formation of B₃H₈[−] and other species kinetically [223]. B₃H₈[−] has not been observed during KBH₄ dehydrogenation because the decomposition occurs at temperatures above which KB₃H₈ is stable.

The thermal decomposition of KB₃H₈ and Mg(B₃H₈)₂ shows some similarities, but their reaction with hydrogen and metal hydrides is noticeably different, as shown in figure 6. Mg(B₃H₈)₂ begins to lose H₂ at ≈100 °C [224], while for KB₃H₈ it initiates at ≈150 °C–200 °C [220]. Both disproportionate into the corresponding borohydride and some combination of *closo*-borates B₁₀H₁₀^{2−} and B₁₂H₁₂^{2−}. According to equation (2) above, hydrogenation to the corresponding borohydride will require both H₂ gas and a metal hydride. However, this does not appear to take place for KB₃H₈ + KH. Although a slightly different balance of BH₄[−] and *closo*-borates was observed compared to heating KB₃H₈ alone in an inert atmosphere, this appears to be because less dehydrogenation took place after heating at 200 °C under 460 bar H₂ [220]. PXD suggested that the amount of KH had not changed significantly, but B₉H₉^{2−}, B₁₀H₁₀^{2−}, and B₁₂H₁₂^{2−} were all observed after heating under high H₂ pressure. Only B₁₂H₁₂^{2−} formed when heating under an inert atmosphere. In contrast, Mg(B₃H₈)₂ ball-milled with MgH₂ is readily hydrogenated to borohydride with just 6 bar H₂ pressure (figure 6) [224].



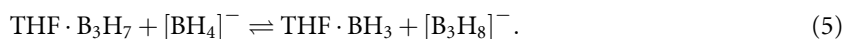
This is surprising given that the reverse reaction, formation of Mg(B₃H₈)₂, is observed during the decomposition of Mg(BH₄)₂. However, the nature of Mg(B₃H₈)₂ is different in the two cases: the material which is hydrogenated starts as a discrete and partially crystalline form, while that made during Mg(BH₄)₂ decomposition is amorphous and intimately mixed with hydride and other borate anions. This substantially changes the formation energy for B₃H₈⁻ [223, 225, 226]. The reason for the stark difference between hydrogenation of KB₃H₈ and Mg(B₃H₈)₂ is not clear and should be investigated in future studies.

Lewis bases, such as ether solvents, also affect the reaction chemistry of hydridoborates. Tetrahydrofuran (THF) and dimethoxyethane (monoglyme) promote dehydrogenation of Mg(BH₄)₂ at lower temperature, and direct the products toward Mg(B₃H₈)₂ and MgB₁₀H₁₀ [227], instead of the irreversible MgB₁₂H₁₂. The chain length of glymes has a strong and surprisingly non-systematic effect on the dehydrogenation products [228]. Stoichiometric additions of monoglyme, triglyme, or tetraglyme all promote dehydrogenation at low temperature (200 °C or less) while the diglyme complex appears to be stable. Increasing the quantity of monoglyme increases the quantity of BH₄⁻ undergoing dehydrogenation, but reduces selectivity toward B₁₀H₁₀²⁻, while increasing the quantity of tetraglyme shuts down dehydrogenation completely [228]. These results suggest that Lewis bases undergo complex interactions, most likely with both the metal ion as well as neutral boranes and potentially anionic hydridoborates. For example, THF may assist the formation of B₂H₇⁻ by ‘shuttling’ BH₃ between borohydrides and leaving a hydride [228]:



Further reaction of B₂H₇⁻ with BH₃ and elimination of H₂ would form the observed product B₃H₈⁻. A similar mechanism involving a complex of THF with a neutral borane has been proposed in the synthesis of

hydridoborates [229]. This work showed how the THF adduct of the neutral triborane B_3H_7 is formed from an acidic solution of KB_3H_8 . Subsequent reaction of $THF \cdot B_3H_7$ with Na or Li borohydride forms the corresponding alkali octahydridoborate:



This synthetic study is consistent with the dehydrogenation studies showing that utilizing Lewis base adducts provides an approach for directing reactions toward favourable, i.e. reversible, borates.

Larger *arachno*-borates, such as $B_{11}H_{14}^-$, also show great promise as energy materials. Their stability is generally in between the smaller borates and the larger *closo*-borates. As such, it has been shown that the $B_{11}H_{14}^-$ anion can degrade to $B_{11}H_{13}OH^-$ upon heating in an acidic environment [230]. The hydrated $LiB_{11}H_{14} \cdot (H_2O)_n$ and $NaB_{11}H_{14} \cdot (H_2O)_n$ salts show exceptional ionic conductivity above $1 \times 10^{-4} \text{ S cm}^{-1}$ and $1 \times 10^{-3} \text{ S cm}^{-1}$ at room temperature, respectively [230].

The *closo*-borates, such as $B_{10}H_{10}^{2-}$ and $B_{12}H_{12}^{2-}$, only have terminal hydrogen atoms, i.e. bonded to boron with a single covalent bond (2c, 2e bond) and are therefore rather stable. Metal *closo*-borates are often synthesised by cation exchange in aqueous solutions, this includes calcium decahydrido-*closo*-decaborate, α - and β - $CaB_{10}H_{10}$, where a variety of hydrates are also described, $CaB_{10}H_{10} \cdot xH_2O$, $x = 1, 4, 5, 6, 7$ [231]. Owing to their high stability, this class of material has been considered a ‘hydrogen sink’ for the release and uptake of hydrogen and it was expected to hamper their reversible hydrogen storage.

Hydrogen release and absorption reactions in boron-based hydrides has been debated in the past and a full description has not yet been obtained due to the complex chemistry of borates. To an extent, this is due to the possibility of several simultaneous reaction mechanisms, which depend on physical conditions, such as hydrogen partial pressures and temperature. Additional computational studies will be of great value to provide further insight into the reversible pathways.

Initially, the composites, $M_2B_{12}H_{12}$ -10MH, $M = Li, Na$ or K were hydrogenated at somewhat harsh conditions, $p(H_2) = 1000 \text{ bar}$ and $500 \text{ }^\circ\text{C}$ for 72 h, where the corresponding metal borohydrides were obtained as the reaction products, MBH_4 , $M = Li, Na$ or K [180, 215]. Later, hydrogenation studies of *closo*-polyborate containing composites, $M_2B_{10}H_{10}$ -8MH and $M_2B_{12}H_{12}$ -10MH, $M = Li$ or Na , using less harsh conditions, were carried out allowing partial hydrogenation and formation of the respective metal borohydride, MBH_4 , at $T = 300 \text{ }^\circ\text{C}$, $p(H_2) = 500 \text{ bar}$ over 24–48 h. It became clear that the $M_2B_{10}H_{10}$ -8MH composites react more readily with hydrogen gas compared to $M_2B_{12}H_{12}$ -10MH and that the sodium-containing composites are more reactive compared to the lithium analogues. Several intermediate compounds were observed, but not fully identified, which may suggest that the two *closo*-borate cages, $B_{10}H_{10}^{2-}$ and $B_{12}H_{12}^{2-}$, are hydrogenated via different mechanisms.

Recently, a wide range of metal *closo*-borates, both mono- and divalent metals, such as $Ag_2B_{10}H_{10}$, $Ag_2B_{12}H_{12}$, $SrB_{10}H_{10}$, and $MnB_{10}H_{10}$, have been prepared, characterized and investigated [232, 233]. Two types of anion substitution have been shown to be possible for these materials, which is best illustrated by iodine substitution in the solid state and formation of $Ag_3B_{10}H_{10}I$ and $Ag_3B_{12}H_{12}I$ [232], while a series of partially iodinated *closo*-decaborates, $M_2[B_{10}H_{10-n}I_n]$ ($M = Li, Na$; $n = 1, 2, 10$), have been observed [234]. *Closo*-borates can also be per-halogenated, illustrated by the series of compounds $Na_2B_{12}X_{12}$, $X = Cl, Br, I$ [235, 236]. Interestingly, a range of other substituents can also be associated to the *closo*-cages with high stability, illustrated by investigation of hydroxylated *closo*-dodecaborates $M_2B_{12}(OH)_{12}$, $M = Li, Na, K$, and Cs . Derivatives with neutral molecules have also been discovered, mainly with protic hydrogens which coordinate via hydrogen bonding, but also others containing donor atoms which can coordinate to a metal in the structure, such as NH_3 , H_2O etc observed for e.g. $CaB_{10}H_{10} \cdot xH_2O$, $x = 1, 4, 5, 6, 7$ [231].

Interestingly, other solvated *closo*-borate derivatives show low temperature melting behaviour with $Li_2B_{12}H_{12}$ solvated with either acetonitrile or THF melting below $150 \text{ }^\circ\text{C}$ [237]. The molten *closo*-borates can then be melt-infiltrated into porous scaffolds and then demonstrate high ionic conductivity in the molten state ($\sim 1 \times 10^{-4} \text{ S cm}^{-1}$) [237]. The high stability also allows substitution directly in to the *closo*-polyborate anions, e.g. with carbon creating a distinct class of *closo*-carborate based materials. Currently, these new materials have high academic interest, but their complicated synthetic route, and therefore high price, hamper their widespread utilisation in all-solid-state batteries.

2.4. Ammines

Ammonia readily reacts with metal borohydrides and ammine derivatives are described for the majority of the known metal borohydrides, with ammonia contents ranging from $x = 0.5$ –8 per metal ion. There are also few reports of ammine metal *closo*-borates, which appear to coordinate a greater amount of NH_3 , possibly stabilized by the larger anion [238–240]. Ammine metal-dodecahydro-*closo*-dodecaborates, $M_xB_{12}H_{12} \cdot nNH_3$ ($M = Li, Na, Ca$, n in the range 2–7), but also $Na_2B_{10}H_{10} \cdot nNH_3$ ($n = 1, 2$) have been described recently

[238, 241]. Table 2 provides an overview of all known ammine metal borohydrides and the corresponding structural dimensionality. The highest amount of ammonia is absorbed in $\text{Zr}(\text{BH}_4)_4 \cdot 8\text{NH}_3$ [111, 242], while low charge-density metal ions such as MBH_4 ($M = \text{Na}, \text{K}, \text{Rb}$ and Cs) do not coordinate ammonia [3]. The largest range of structures are observed for $\text{Y}(\text{BH}_4)_3 \cdot x\text{NH}_3$, with $x = 1, \alpha - 2, \beta - 2, \alpha - 3, \beta - 3, 5, 6, 7$, where α and β refer to a low- and high temperature polymorph, respectively [96, 98, 110, 243, 244]. The yttrium compounds are isostructural with several members of the ammine REBs [96].

As described above, the crystal structures of metal borohydrides often consist of three-dimensional frameworks formed by bridging BH_4^- groups, resulting in connected tetrahedral $[\text{M}(\text{BH}_4)_4]$ or octahedral $[\text{M}(\text{BH}_4)_6]$ complexes [68]. Ammonia interrupts these frameworks, and the dimensionality of the structures decreases with increasing ammonia content. In all structures of ammine metal borohydrides, NH_3 coordinates to the metal-ion via its lone pair, while the coordination of BH_4^- is more flexible and it may act as a bridging and terminal ligand and as a counter ion, accommodating the desired coordination of the metal ion. This is well illustrated by the series of $\text{Y}(\text{BH}_4)_3 \cdot x\text{NH}_3$ [96, 98, 110]. $\text{Y}(\text{BH}_4)_3 \cdot \text{NH}_3$ forms two-dimensional layers through bridging BH_4^- groups, connecting the $\text{Y}(\text{NH}_3)(\text{BH}_4)_5$ octahedra. The layers are held together by dihydrogen interactions between NH_3 and BH_4^- . $\text{Y}(\text{BH}_4)_3 \cdot 2\text{NH}_3$ forms one-dimensional zig-zag (α) or straight (β) chains via bridging BH_4^- groups connecting the $\text{Y}(\text{NH}_3)_2(\text{BH}_4)_4$ octahedra. Both α - and β - $\text{Y}(\text{BH}_4)_3 \cdot 3\text{NH}_3$ are built from neutral $\text{Y}(\text{NH}_3)_3(\text{BH}_4)_3$ octahedral complexes, while $\text{Y}(\text{BH}_4)_3 \cdot 5\text{NH}_3$ is built from $[(\text{NH}_3)_5(\text{BH}_4)_2]^+$ complex ions, and it is a rare example of borohydride groups acting as both a coordinating ligand and counter ion in the same compound. $\text{Y}(\text{BH}_4)_3 \cdot x\text{NH}_3$ ($x = 6$ and 7) are both built from cationic $\text{Y}(\text{NH}_3)_x^{3+}$ complexes, where all BH_4^- act as counter ions. Note that the structure of $\text{Y}(\text{BH}_4)_3 \cdot 5\text{NH}_3$ and both the structure and composition of $\text{Y}(\text{BH}_4)_3 \cdot 3\text{NH}_3$ were recently revised, where the latter was previously suggested to have the composition $\text{Y}(\text{BH}_4)_3 \cdot 4\text{NH}_3$ [96, 110, 243, 244].

In an ‘open’ system, the thermal stability of ammine metal borohydrides and the composition of the released gas, i.e. H_2 vs NH_3 , can be correlated to the M–N bond strength and to the thermal stability of the metal borohydrides, as shown in figure 7 [3, 96, 109]. Other factors have also been suggested to affect the thermal stability and gas-composition, e.g. strong dihydrogen bonds and the relative amount of NH_3 to BH_4^- , but these hypotheses have been disproved by the ammine metal borohydrides with a Pauling electronegativity (χ_P) less than 1.05.

As shown before, the thermal stability of metal borohydrides are approximately inversely proportional to the χ_P of the metal, illustrated by the black dotted line in figure 7 [119, 265]. Thus, the composition of the released gas during thermolysis of ammine metal borohydrides in an open system can roughly be divided into the red, blue and green regions in figure 7 as regarding the Pauling electronegativity:

- Red region ($\chi_P < 1.05$): these compounds have a low charge-density cation (weak M–N bond) and a high thermal stability of the metal borohydride, resulting in the release of NH_3 .
- Blue region ($\chi_P \sim 1.05\text{--}1.58$): these compounds often release NH_3 when the NH_3/BH_4 ratio is higher than 1. When the ratio is ≤ 1 , the thermal stability of the ammine metal borohydride and the metal borohydride is often similar, i.e. the BH_4^- groups are sufficiently destabilized to react with NH_3 , resulting in the release of H_2 . However, lowering the NH_3 release temperature by vacuum may favor the release of NH_3 over H_2 [3].
- Green region ($\chi_P > 1.58$): these compounds have a higher thermal stability than the corresponding metal borohydrides. Theoretical calculations indicate that metal borohydrides are thermodynamically destabilized by ammonia, but NH_3 may provide a kinetic stabilization due to a shielding effect, which obstructs the usual decomposition mechanism [259, 266]. Consequently, these compounds mainly release H_2 .

The divalent $\text{RE}(\text{BH}_4)_2 \cdot x\text{NH}_3$ ($\text{RE} = \text{Sm}, \text{Eu}, \text{Yb}$) are exceptions to this simple relation with χ_P , as they only release NH_3 during thermolysis, despite having a $\chi_P \sim 1.1\text{--}1.2$. This is related to the higher thermal stability of the metal borohydride [3, 97]. Calculations of the ionic potentials of the cations may provide a more accurate correlation, as demonstrated for the metal borohydrides [136, 267, 268].

The partial pressure of ammonia during decomposition strongly affects the decomposition temperature and the composition of the released gas. The ammonia release temperatures are significantly lowered by vacuum compared to a closed capillary, as observed for $\text{RE}(\text{BH}_4)_3 \cdot x\text{NH}_3$ ($\text{RE} = \text{La}, \text{Ce}$) [98]. A high partial pressure of NH_3 can facilitate the release of H_2 , as observed for thermolysis of $\text{LiBH}_4 \cdot \text{NH}_3$ and $\text{Ca}(\text{BH}_4)_2 \cdot x\text{NH}_3$ ($x = 1, 2$) in a closed vessel [252, 269]. Alternative strategies that can promote hydrogen evolution include fluorine-substitution [270], catalysis using metal nanoparticles or metal halides [271–273], or by nano-confinement [274, 275].

Table 2. Ammine metal borohydrides with known composition and the dimensionality of the structures. 3D: three-dimensional frameworks; 2D: two-dimensional layers; 1D: one-dimensional chains; 0D: neutral molecular complexes; Cl: complex cations and anions; L: liquid at ambient conditions; U: unknown crystal structure.

Compounds	Ammonia content, x in $M(\text{BH}_4)_n \cdot x\text{NH}_3$								References	
	1/2	1	2	3	4	5	6	7		8
Mono-metallic										
$\text{LiBH}_4 \cdot x\text{NH}_3$	2D	1D	L ^a	U ^a	—	—	—	—	—	[245–247]
$\text{Be}(\text{BH}_4)_2 \cdot x\text{NH}_3$	—	—	—	—	Cl	—	—	—	—	[248]
$\text{Mg}(\text{BH}_4)_2 \cdot x\text{NH}_3$	—	1D	0D	0D	—	—	Cl	—	—	[249–251]
$\text{Ca}(\text{BH}_4)_2 \cdot x\text{NH}_3$	—	3D	2D	—	0D	—	Cl ^a	—	—	[109, 252, 253]
$\text{Sr}(\text{BH}_4)_2 \cdot x\text{NH}_3$	—	2D	2D	—	0D ^a	—	—	—	—	[109, 253, 254]
$\text{Ba}(\text{BH}_4)_2 \cdot x\text{NH}_3$	—	3D	2D ^a	—	—	—	—	—	—	[255]
$\text{Al}(\text{BH}_4)_3 \cdot x\text{NH}_3$	—	0D	—	—	—	—	Cl	—	—	[256, 257]
$\text{Ti}(\text{BH}_4)_3 \cdot x\text{NH}_3$	—	—	—	U	—	U	—	—	—	[258]
$\text{V}(\text{BH}_4)_3 \cdot x\text{NH}_3$	—	—	—	0D	—	—	—	—	—	[259]
$\text{Mn}(\text{BH}_4)_2 \cdot x\text{NH}_3$	—	U	0D	0D	—	—	Cl	—	—	[251]
$\text{Fe}(\text{BH}_4)_2 \cdot x\text{NH}_3$	—	—	—	—	—	—	Cl ^a	—	—	[113]
$\text{Co}(\text{BH}_4)_2 \cdot x\text{NH}_3$	—	—	—	—	—	—	Cl ^a	—	—	[113]
$\text{Zn}(\text{BH}_4)_2 \cdot x\text{NH}_3$	—	—	0D	—	U	—	—	—	—	[260]
$\text{Zr}(\text{BH}_4)_4 \cdot x\text{NH}_3$	—	—	—	—	—	—	—	—	Cl	[242]
$\text{Y}(\text{BH}_4)_3 \cdot x\text{NH}_3$	—	2D	1D (α, β)	0D (α, β)	—	Cl	Cl	Cl	—	[96, 98, 110, 243, 244]
$\text{La}(\text{BH}_4)_3 \cdot x\text{NH}_3$	—	—	—	0D	0D	—	Cl	—	—	[96, 98, 110]
$\text{Ce}(\text{BH}_4)_3 \cdot x\text{NH}_3$	—	—	—	0D	0D	Cl	Cl	—	—	[96, 98, 110]
$\text{Pr}(\text{BH}_4)_3 \cdot x\text{NH}_3$	—	—	—	0D	0D	Cl	Cl	Cl	—	[96]
$\text{Nd}(\text{BH}_4)_3 \cdot x\text{NH}_3$	—	—	—	0D	0D	Cl	Cl	Cl	—	[96]
$\text{Sm}(\text{BH}_4)_2 \cdot x\text{NH}_3$	—	2D	2D	—	—	—	—	—	—	[96]
$\text{Eu}(\text{BH}_4)_2 \cdot x\text{NH}_3$	—	2D	2D	—	—	—	—	—	—	[96]
$\text{Gd}(\text{BH}_4)_3 \cdot x\text{NH}_3$	—	—	—	0D	—	Cl	Cl	Cl	—	[96, 110]
$\text{Tb}(\text{BH}_4)_3 \cdot x\text{NH}_3$	—	—	—	0D	Cl	Cl	—	Cl	—	[96]
$\text{Dy}(\text{BH}_4)_3 \cdot x\text{NH}_3$	—	—	—	0D	Cl	Cl	Cl	Cl	—	[96, 110]
$\text{Ho}(\text{BH}_4)_3 \cdot x\text{NH}_3$	—	—	—	0D	—	Cl	—	Cl	—	[96]
$\text{Er}(\text{BH}_4)_3 \cdot x\text{NH}_3$	—	—	—	0D	—	Cl	—	Cl	—	[96]
$\text{Tm}(\text{BH}_4)_3 \cdot x\text{NH}_3$	—	—	—	0D	—	Cl	—	Cl	—	[96]
$\text{Yb}(\text{BH}_4)_3 \cdot x\text{NH}_3$	—	—	—	—	—	Cl	—	Cl	—	[96]
$\text{Yb}(\text{BH}_4)_2 \cdot x\text{NH}_3$	—	3D	2D	—	0D	—	—	—	—	[96]
$\text{Lu}(\text{BH}_4)_3 \cdot x\text{NH}_3$	—	—	—	—	—	—	—	Cl	—	[96]

(Continued.)

Table 2. (Continued.)

Compounds	Ammonia content, x in $M(\text{BH}_4)_n \cdot x\text{NH}_3$								References	
	1/2	1	2	3	4	5	6	7		8
Bi-cationic										
$\text{LiMg}(\text{BH}_4)_3 \cdot x\text{NH}_3$	—	—	3D	—	—	—	—	—	—	[261]
$\text{Li}_2\text{Mg}(\text{BH}_4)_4 \cdot x\text{NH}_3$	—	—	—	—	—	—	Cl	—	—	[110, 262]
$\text{NH}_4\text{Mg}(\text{BH}_4)_3 \cdot x\text{NH}_3$	—	—	3D	—	—	—	—	—	—	[108]
$\text{Li}_2\text{Al}(\text{BH}_4)_5 \cdot x\text{NH}_3$	—	—	—	—	—	—	Cl	—	—	[263]
$\text{LiSc}(\text{BH}_4)_4 \cdot x\text{NH}_3$	—	—	—	—	1D	—	—	—	—	[259]
$\text{Li}_2\text{Ti}(\text{BH}_4)_5 \cdot x\text{NH}_3$	—	—	—	—	—	U	—	—	—	[258]
$\text{LiMn}(\text{BH}_4)_3 \cdot x\text{NH}_3$	—	—	3D	—	—	—	—	—	—	[108]
$\text{Li}_2\text{Mn}(\text{BH}_4)_4 \cdot x\text{NH}_3$	—	—	—	—	—	—	Cl	—	—	[251]
$\text{NH}_4\text{Mn}(\text{BH}_4)_3 \cdot x\text{NH}_3$	—	—	3D	—	—	—	—	—	—	[108]
$\text{Li}_2\text{Fe}(\text{BH}_4)_4 \cdot x\text{NH}_3$	—	—	—	—	—	—	Cl	—	—	[113]
$\text{NaZn}(\text{BH}_4)_3 \cdot x\text{NH}_3$	—	—	Cl	—	—	—	—	—	—	[264]
$\text{NH}_4\text{Y}(\text{BH}_4)_4 \cdot x\text{NH}_3$	—	Cl	—	—	—	—	—	—	—	[108]
$(\text{NH}_4)_2\text{Y}(\text{BH}_4)_5 \cdot x\text{NH}_3$	—	Cl	—	—	—	—	—	—	—	[108]
$\text{NH}_4\text{La}(\text{BH}_4)_4 \cdot x\text{NH}_3$	—	1D	—	—	—	—	—	—	—	[108]
$\text{NH}_4\text{Gd}(\text{BH}_4)_4 \cdot x\text{NH}_3$	—	1D	—	—	—	—	—	—	—	[108]
Solid solutions										
$\text{Mg}_{1-y}\text{Mn}_y(\text{BH}_4)_2 \cdot x\text{NH}_3$	—	—	—	—	—	—	Cl	—	—	[251]
$\text{Co}(\text{BH}_4)_{2-y}\text{Cl}_y \cdot x\text{NH}_3$	—	—	—	—	—	—	Cl ^a	—	—	[113]

^a Unstable at room temperature.

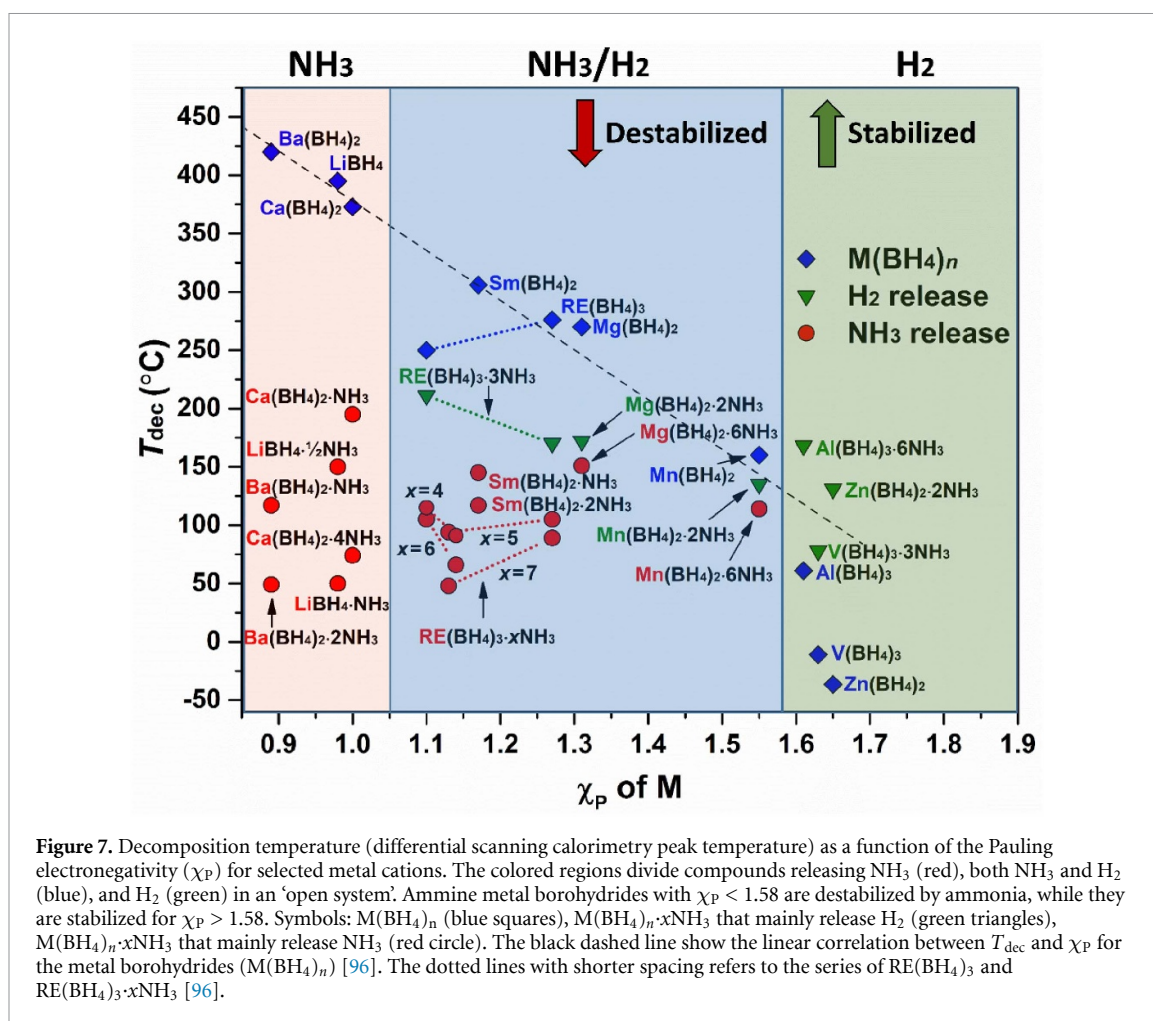


Figure 7. Decomposition temperature (differential scanning calorimetry peak temperature) as a function of the Pauling electronegativity (χ_P) for selected metal cations. The colored regions divide compounds releasing NH_3 (red), both NH_3 and H_2 (blue), and H_2 (green) in an ‘open system’. Ammine metal borohydrides with $\chi_P < 1.58$ are destabilized by ammonia, while they are stabilized for $\chi_P > 1.58$. Symbols: $\text{M}(\text{BH}_4)_n$ (blue squares), $\text{M}(\text{BH}_4)_n \cdot x\text{NH}_3$ that mainly release H_2 (green triangles), $\text{M}(\text{BH}_4)_n \cdot x\text{NH}_3$ that mainly release NH_3 (red circle). The black dashed line shows the linear correlation between T_{dec} and χ_P for the metal borohydrides ($\text{M}(\text{BH}_4)_n$) [96]. The dotted lines with shorter spacing refer to the series of $\text{RE}(\text{BH}_4)_3$ and $\text{RE}(\text{BH}_4)_3 \cdot x\text{NH}_3$ [96].

2.5. Amides and imides

The reaction of ammonia with alkali and alkaline earth metals or metal hydrides leads to the formation of amides such as LiNH_2 , NaNH_2 , KNH_2 , $\text{Mg}(\text{NH}_2)_2$, $\text{Ca}(\text{NH}_2)_2$ and $\text{Ba}(\text{NH}_2)_2$. The partial decomposition of the amides often leads to the formation of imides, for instance Li_2NH , Na_2NH , MgNH , CaNH and BaNH . The amides first came to the limelight in the early 2000’s, when it was reported that the combination of LiNH_2 and LiH releases reversibly about 6.5 wt% hydrogen at around 250 °C [276]. This is unlike the pure LiNH_2 and LiH that release hydrogen at temperature above 300 °C and 550 °C, respectively. In fact, the enthalpy and entropy associated with the decomposition of $\text{LiNH}_2 + \text{LiH}$ to hydrogen is $\Delta H = 38.9 \text{ kJ mol}^{-1} \text{ H}_2$ and $\Delta S = 111.98 \text{ J K}^{-1} \text{ mol}^{-1} \text{ H}_2$, respectively, implying that an equilibrium pressure of $p(\text{H}_2) = 1 \text{ bar}$ at 74 °C is expected [277]. Hence, the use of different catalysts was explored to reduce the decomposition temperature of the mixture. This also led to several efforts to explore other metal amides and their combinations with metal hydrides for hydrogen storage applications [278–282].

Although research on applications of amides/imides for hydrogen storage materials is still progressing [283–293], most recent efforts have been focused on their application as catalysts or co-catalysts in ammonia synthesis and decomposition, as solid-state electrolytes for batteries, and novel amide/imides with multifunctional energy applications [285, 294–302]. For instance, by ball milling mixtures of lithium amide, lithium imide and lithium nitride–hydride, Makepeace *et al* [296] recently reported an amide-imide solid solution with wide-ranging anion compositions. Samples from majority of the lithium amide through to pure lithium imide and majority lithium nitride–hydride show a highly disordered anti-fluorite structure, with evidence for greater nitride–hydride incorporation at high temperatures. In contrast, the tetragonal lithium amide and nitride–hydride structures show very limited compositional variation.

Raman spectroscopy of lithium amide–lithium imide samples show that the amide and imide groups in stoichiometric and nonstoichiometric environments can be differentiated by the different frequency of the N–H stretch, as they show distinct bands in both environments. Thus, continuous variation in the local NH_x environment (evidenced by N–H stretch) is observed as a function of the composition [303]. This rich library of stoichiometric compounds and solid solutions is a basis for expanded investigations into composition

control and tailored hydrogen storage properties in M–N–H materials or mixtures. Additionally, they have been proposed for variety of applications such as ion conduction, ammonia storage, catalysts/co-catalysts for ammonia synthesis and catalytic decomposition [296]. Furthermore, it has been recently reported that novel compounds are formed in the $\text{LiBH}_4\text{--LiNH}_2$ system, and nanocomposites of them with mesoporous silica have been explored [301]. After heating or ball milling mixtures of LiBH_4 and LiNH_2 , the presence of multiple $\text{Li}(\text{BH}_4)_{1-x}(\text{NH}_2)_x$ phases is clearly observed by PXD and further corroborated with DSC and diffuse reflectance infrared Fourier transform spectroscopy (DRIFTS) analysis. By DSC, different $\text{LiBH}_4\text{--LiNH}_2$ phases can be distinguished by their specific melting temperature, revealing up to three different phases; such as $\text{Li}_2(\text{BH}_4)(\text{NH}_2)$, $\text{Li}_3(\text{BH}_4)(\text{NH}_2)_2$ and $\text{Li}_4(\text{BH}_4)(\text{NH}_2)_3$ in the prepared $\text{LiBH}_4\text{--LiNH}_2$ mixtures, depending on the composition of the starting materials and the synthesis temperature [304]. The different phases show different properties both for reversible hydrogen release and Li ion conduction. For instance, lower hydrogen release temperature is favoured for the phases with low LiNH_2 content, while the Li-ion conductivity increases with increasing LiNH_2 (up to 50 mol% LiNH_2) content and then decreases above 50% LiNH_2 in the mixture [301].

In terms of hydrogen storage properties of amide-imides, Gizer *et al* [284] recently investigated the influence of a $\text{K}_2\text{Mn}(\text{NH}_2)_4$ additive on the hydrogen sorption properties of the $\text{Mg}(\text{NH}_2)_2 + 2\text{LiH}$ (i.e. Li–Mg–N–H) system. It was demonstrated that the addition of $\text{K}_2\text{Mn}(\text{NH}_2)_4$ (5 mol%) leads to a decrease of the peak dehydrogenation temperature from 200 to 172 °C, with a hydrogen storage capacity of 4.2 wt% maintained over 25 hydrogen sorption cycles. *In-situ* synchrotron radiation-PXD analysis revealed that $\text{K}_2\text{Mn}(\text{NH}_2)_4$ decomposes into Mn_4N and a potassium compound, most likely amorphous or nanocrystalline KH. Therefore, the increased hydrogen sorption kinetics was ascribed to the presence of KH and Mn_4N , which alter the hydrogen sorption properties of the system [284]. In a related study, the hydrogen sorption properties of the ternary amide-hydride $\text{LiAl}(\text{NH}_2)_4\text{--LiAlH}_4$ system was investigated by means of mechanical milling and thermal methods. It was shown that the mixture decomposes spontaneously at ambient conditions during mechanical milling, releasing 70% of the H_2 (six equiv. of H_2 or 5.7 wt% H_2) within 2 h of mechanical milling. The hydrogen release rate increases with increasing amount of LiAlH_4 , suggesting an ion migration mediated dehydrogenation. The hydrogen release reaction occurs via the formation of Li_3AlH_6 as an intermediate, and LiH and AlN as the final products, with a total of eight equiv. of H_2 (7.5 wt%). For the physically mixed $\text{LiAl}(\text{NH}_2)_4\text{--LiAlH}_4$ (1:3) which are not in intimate contact, NH_3 mediated dehydrogenation is prone to occur. However, the decomposed residue, $\text{LiAl}(\text{NH}_2)_2$ reacted with LiAlH_4 , leading to rapid hydrogen release. The basicity of the hydrides was found to be an important point in triggering amide-hydride interactions, which leads to low hydrogen release temperatures [286]. In another recent study, Zhang *et al* [291] examined the effects of Na addition on the reversible hydrogen uptake of $\text{Mg}(\text{NH}_2)_2\text{--MgH}_2$ system. The addition of the Na leads to the formation of NaMgH_3 . They demonstrated that the replacement of NaMgH_3 for MgH_2 suppresses ammonia release and improves the hydrogen desorption property of the $\text{Mg}(\text{NH}_2)_2\text{--NaMgH}_3$ system. At high temperature (190 °C), the formation of $\text{NaMg}(\text{NH}_2)(\text{NH})$ was detected, suggesting that the addition of Na alters the reaction pathway. The authors demonstrated that the formation $\text{NaMg}(\text{NH}_2)(\text{NH})$ is responsible for the partial reversibility (1.8 wt% of hydrogen at 10 bar and 190 °C) observed in the $\text{Mg}(\text{NH}_2)_2\text{--NaMgH}_3$ system [291].

The system Li_2NH and LiBH_4 was recently studied. The $\text{Li}_2\text{NH--LiBH}_4$ sample (in a molar ratio of 1:1) shows very good hydrogenation kinetics, with hydrogen absorption starting at 37 °C at 50 bar, which is more than 100 °C lower than that of pristine Li_2NH , and amongst the mildest reported for amide systems [285]. The $\text{Li}_5(\text{BH}_4)_3\text{NH}$ complex hydride, obtained by ball milling LiBH_4 and Li_2NH in various molar ratios, has been identified. The crystal structure has been solved in space group *Pnma*, and refined coupling DFT and synchrotron radiation x-ray powder diffraction data [305].

Finally, lithium amide/lithium nitride system has a high gravimetric capacity (10.3 wt%), making it an attractive material for hydrogen storage applications. However, in the bulk, the H_2 release temperature exceeds 400 °C, and the compounds exhibits slow hydrogen release kinetics and poor reversibility, hindering their applications for reversible hydrogen storage. It has been shown recently that nanoconfinement using porous carbon can lower the dehydrogenation temperature of the material, which was attributed to the thermodynamically penalizing role of internal ‘nanointerfaces’ [306]. More recent work is tackling this mechanism in greater detail, focusing on the additional role of hydride-host interactions to understand changes in reactivity. Through a combination of *ab-initio* molecular dynamics and electronic structure calculations alongside experimental nanoconfinement studies in N-doped carbons, the effect of nanoporous carbon host on Li–N–H thermodynamics has been explicitly probed [307]. Authors have found that charge transfer and confinement effects exerted by carbon hosts can significantly stabilize the dehydrogenated Li_3N phase over the hydrogenated phases. This points to the strong interfacial interaction between a nanoporous carbon host and Li_3N as an additional tunable factor for achieving lower dehydrogenation energy in Li–N–H system.

2.6. Transition metals complex hydrides

The first known transition metal complex hydride, K_2ReH_9 , was fully described in 1964 [308]. Despite the fact that there are now more than a hundred known types of hydrides divided in almost 50 structure types discovered over past decade [8, 9] not many of them bring too much of the attention as potential materials for hydrogen and heat storage, mainly due to the high cost of materials, high thermal stability, not straightforward reversibility, etc.

Mainly due to the relatively low cost, complex hydrides based on iron (Mg_2FeH_6), nickel (Mg_2NiH_4) and cobalt (Mg_2CoH_5) are being intensively studied till now, since they display attractive properties, which can be relevant for hydrogen storage applications. For instance, although its gravimetric hydrogen density, $\rho_m = 5.5$ wt% H_2 is lower than that of MgH_2 , Mg_2FeH_6 exhibits the highest volumetric hydrogen density, $\rho_v = 150$ g H_2 l^{-1} , among the known metal hydrides and it has excellent hydrogen sorption cycling properties. For instance, no irreversible capacity losses were observed over 600 cycles carried out between 450 °C and 550 °C and at pressures between 65 and 75 bar [27]. These properties make Mg_2FeH_6 a promising hydrogen storage material for stationary applications at high temperatures (near 450 °C) [309].

Ball milling is the most commonly used method for mixing Mg and Fe powders and subsequent hydrogenation at high temperature under hydrogen pressure produces Mg_2FeH_6 . Recently, cold roll milling (CRM) has also been adopted to produce Mg/Fe nanocomposite powder with a layered structure [310]. In the CRM process, Mg and Fe powders are premixed with a small amount of oleylamine as a process control agent. The pre-mixed powders were milled using an in-house-made vertical roll milling machine at 50 rpm in air. The milling machine has two vertical rolls of 100 mm in diameter, a vibrational powder feeder capable of regulating the amount and speed of the powder feeding, and an inlet chute for stable spill-free powder entry between the rolls. The fine layered structure improves the hydrogenation reaction kinetics by reducing the diffusion distance of Mg and/or MgH_2 through the refinement of Fe particles, which is particularly critical when the hydrogenation temperature is lower than 400 °C [311, 312]. The layer thickness of Fe particles can be controlled by varying the number of CRM passes. The Mg and Fe layers become thinner with increasing number of rolling passes, namely down to 10 nm in the case of Fe, which is enough to support the fast formation of Mg_2FeH_6 . If CRM process is done in air, the preferential oxidation of Mg is unavoidable and the higher the number of CRM passes, the higher the MgO content in the Mg/Fe composite powder. Repeated CRM effectively decreased the Fe layer thickness up to a sufficient value for the fast formation of Mg_2FeH_6 , but too much CRM passes decreased the hydrogen storage capacity due to inevitable oxidation of Mg in air. The thickness of the Fe layer plays an important role in the initial stage, whereas the degree of oxidation and the distribution of oxides have more influence on the formation of Mg_2FeH_6 in the long term by consuming Mg. Both microstructure refinement and minimal oxidation are the prerequisites for efficient Mg_2FeH_6 synthesis, with the former condition being achievable by optimizing the number of millings, and the latter by performing CRM under an inert atmosphere.

Recently the synthesis of Mg_2FeH_6 by ball milling and subsequent sintering was conducted with the use of both plain and highly alloyed austenitic stainless steel (AISI 316L) instead of pure iron [313, 314]. The idea was to see if the alloying elements interfere and influence the synthesis process, as well as if they change the thermodynamic properties of the obtained compound. Using steel (or even steel scrap or scrap in general [315, 316]) might be a way of reducing the price of the material when it is supposed to be used in high quantities as a heat or hydrogen storage medium. It was found that, in the case of plain steel, the properties of the obtained material do not change and the carbon present in the steel does not interact with the hydride nor form solid solutions. It was confirmed, however, that the mechanical properties of the steel (high hardness) may influence the milling process itself, thus contributing to the lowering of the reaction yield. In case of manufacturing from AISI 316L steel, the main finding was that the single phase, austenitic structure of the steel during ball milling undergoes the mechanically induced martensitic transformation and the martensite readily reacts with the magnesium hydride. The final product is likely composed of quaternary Mg–Fe–Cr hydride, possessing different equilibrium pressure as compared to pure Mg_2FeH_6 and Mg_2NiH_4 .

The synthesis of Mg-based transition-metal complex hydrides containing Fe, Co, or Ni can also be achieved in one processing step by ball milling elemental powder mixtures in a reactive hydrogen atmosphere [102, 317]. The reactive mechanochemical synthesis has the advantage of enhancing hydrogen sorption kinetics, due to the formation of fresh surfaces and reduced particle sizes, allowing hydride formation after only a few hours of milling. It should be noted that, while fresh surfaces are consumed with hydrogen cycling and are critical during the milling process, reduced particle sizes are retained upon cycling [318], playing a beneficial role in maintaining good hydrogen cycling kinetics. Reactive milling has been also successfully used for the synthesis of Mg-based complex hydrides with more than one TM, resulting in the formation of quaternary hydrides such as $Mg_2(FeH_6)_{0.5}(CoH_5)_{0.5}$ [319, 320].

Recently, the properties of $Mg_2Fe_xCo_{(1-x)}D_y$ complex deuterides with different Fe–Co and D contents ($0 \leq x \leq 1$ and $5 \leq y \leq 6$) were reported and the results were compared with ternary Mg_2CoD_5 and

Mg₂FeD₆ compounds [34]. Deuterium was used to allow the structural study with powder neutron diffraction. The crystal structure characterization of the milling products shows that, depending on the relative content of Fe and Co (Fe_xCo_{1-x}), the following hydrides are formed: Mg₂(FeD₆)_{0.09}(CoD₅)_{0.91}, Mg₂(FeD₆)_{0.3}(CoD₅)_{0.7}, Mg₂(FeD₆)_{0.4}(CoD₅)_{0.6}, Mg₂(FeD₆)_{0.5}(CoD₅)_{0.5}, Mg₂(FeD₆)_{0.7}(CoD₅)_{0.3} and Mg₂(FeD₆)_{0.9}(CoD₅)_{0.1}. In all cases, Fe and Co randomly occupy the same crystallographic site, creating solid solutions containing both FeD₆⁴⁻ and CoD₅⁴⁻ complex anions. For $x = 1$, Mg₂(FeD₆)_{0.09}(CoD₅)_{0.91} was found to be isostructural either with Mg₂CoD₅ (tetragonal *P4/nmm*), whereas for $x \geq 5$, the quaternary hydrides have the same cubic *Fm $\bar{3}m$* structure as Mg₂FeD₆ and Mg₂CoD₅ at high temperatures. For $x = 0.3$, the presence of a two-phase region, where the tetragonal and cubic phases coexist, was found and supported by the assessment of the stability of the hydrides from experimental and literature data.

All Mg₂Fe_xCo_(1-x)D_y quaternary complex hydrides were shown to have a similar hydrogen desorption process and to be relatively stable, but their desorption temperature (maximum desorption temperature $T_{\text{dec}} \cong 277$ °C) was below that of MgH₂. The activation energy Ea_{des} (87–89 kJ mol⁻¹) and enthalpy ΔH_{des} (about 70 kJ mol⁻¹ H₂) of desorption were reported to be independent from the relative amount of complex anions. Desorption of hydrogen results in the formation of Mg and (FeCo) solid solutions, which are found unevenly distributed. Nonetheless, the reversible hydrogenation to form the quaternary hydrides is observed at 30 bar of H₂ and 400 °C for Mg₂(FeH₆)_{0.5}(CoH₅)_{0.5}.

Complex transition-metal hydrides containing hydride complexes with hydrogen coordination number exceeding six are quite rare, due to the presence of high energy barriers for their formation process [321]. In addition, if the temperature is raised to promote the formation reaction, the target hydrides will decompose, and, conversely, the reaction will have difficulty in proceeding below the decomposition temperature. One way of overcoming this situation is to apply high hydrogen pressures, of the order of several GPa. As a result, the target hydrides are thermodynamically stabilized, and the temperature can be raised without decomposition to a region where the decomposition reaction would proceed under ambient pressure. Several new hydrides, including Li₅MoH₁₁ with the nine-fold H coordination hydride complexes MoH₉³⁻ have been synthesized recently [322–329] using a high-temperature and high-pressure technique, as developed by Fukai *et al* [330].

2.7. RHCs

Many borohydrides possess very high gravimetric energy densities (i.e. LiBH₄-18.5 wt%, MgBH₄-14.8 wt%), which makes them interesting for hydrogen storage applications. However, their use in practical applications is hindered while they are thermodynamically stable and poorly reversible. Combining borohydrides, with other hydrides, the reaction enthalpy of the system is decreased, compared to the decomposition enthalpy of the single components. These systems are called ‘RHCs’, referring to mixtures of different metal hydrides reacting with each other during dehydrogenation, rather than decomposing individually. Similar approach was already shown by Reilly and Wiswall in 1967, where MgH₂ and MgCu₂ reacts with each other to form Mg₂Cu upon hydrogen release [331]. Major disadvantage of this system is the significant capacity reduction due to addition of MgCu₂, which does not contribute to the total hydrogen capacity. First example of RHCs were reported by Chen *et al* in 2002 (LiNH₂ + LiH system). Following this work, Bark [196, 332] and Vajo [333] reported destabilization of LiBH₄ by combining it with MgH₂. Desorption of this system is a two step reaction process. When the backpressure of 5 bar of H₂ is supplied (above the equilibrium pressure of LiBH₄ alone), firstly MgH₂ decomposes and later on, magnesium reacts with LiBH₄ to form MgB₂. Absorption reaction can be carried out in single step for the MgB₂-LiH composite at moderate pressure-temperature conditions (250 °C, 50 bar) [334]. So far, extensive research is conducted on the RHCs to understand the reaction mechanisms, cycling properties and suitable additives which may help to lower the operation temperatures further [335–342]. In a recent study, Zhao *et al* developed a novel process, where MgH₂ is ball milled in conjunction with aerosol spraying of LiBH₄ dissolved in THF [343]. Hydrogen release could be carried out in three steps: (a) H₂ release from the decomposition of nano-LiBH₄ and then decomposition product Li₂B₁₂H₁₂ reacts with nano-MgH₂ to release H₂, (b) H₂ release from the decomposition of nano-Mg(BH₄)₂, and (c) H₂ release from the decomposition of nano-MgH₂. These desorption reactions lead to 4.1 wt% H₂ release below 265 °C, which is one of the highest quantities for this system up to date. However, H₂ capacity of the composite degrades gradually over hydrogenation and dehydrogenation cycles at 265 °C, mainly due to gradual increases in crystallite and particle sizes. From one side, designing the systems at nano-scale gives the opportunity to establish RHCs in solid state with improved kinetics and lower operating temperatures. From the other side, stability of these nano-composites at the operating temperatures of RHCs is of great importance, since it is known that two main reactants, LiH and MgB₂ segregate continuously upon cycling [344]. Therefore, the use of a scaffolding material is an option which may help to improve the cycling stability while keeping the reactants confined. Le *et al* introduced an inert polymer, poly(4-methyl-1-pentene) or shortly TPXTM, in order to improve the cycling stability of

titanium(III) chloride-aluminum chloride added $2\text{LiH} + \text{MgB}_2$. The presence of TPXTM does not affect the reaction pathway of the RHC, which is also supported with determined rate-limiting reactions, and it improves the cycling stability. Decrement in the capacity after ten hydrogenation/dehydrogenation cycles is only 0.05 wt%, while it is 0.32 wt% for the system without TPXTM. Prevention of the phase segregation between the two main phases, due to the presence of scaffolding polymer surrounding the particles, is thought to be the reason for this improvement. One of the main challenges in the design of RHC based hydrogen storage systems is to develop reliable kinetic models to describe sorption reactions. These models are beneficial to save time and evaluate the feasibility of the system. To ensure the potential of RHCs for the real applications, thermodynamic and kinetic investigations are carried out by Neves *et al* [345]. In this study, TiCl_3 added $\text{LiBH}_4/\text{MgH}_2$ is examined under absorption conditions. Enthalpy and entropy are found to be $34 \text{ kJ mol}^{-1} \text{ H}_2$ and $70 \text{ J K}^{-1} \text{ mol}^{-1} \text{ H}_2$. Separable variable method is applied to investigate absorption conditions of the developed Li-RHC. Applying this model, the effects of temperature, pressure and transformation of the hydride forming material are considered in the rate expression. According to the results, transformation of the forming hydride is limited by the movement of the not-hydrogenated/hydrogenated material interface, described by the one-dimensional interface-controlled model with a fixed number of nuclei and constant interface velocity, also known as Johnson–Mehl–Avrami–Erofev–Kolmogorov (JMAEK) with $n = 1$ model. After taking the driving force component into account, the apparent activation energy E_a and pre-exponential factor A are, respectively, $1.8 \times 10^8 \text{ s}^{-1}$ and $146 \text{ kJ mol}^{-1} \text{ H}_2$. Developed models could be applied to model the hydrogen storage tanks with RHC materials through FEM simulations, or combined with novel computational approaches as machine learning, in order to better understand and optimize their designs. Modification of the RHCs with an appropriate additive is also an important step towards designing materials with fast reaction kinetics. In a recent study, catalytic role of NbF_5 and ScCl_3 during the hydrogenation and dehydrogenation reactions were investigated [340, 346]. Addition of NbF_5 reduces the dehydrogenation time required for the $\text{LiBH}_4/\text{MgH}_2$ composite from 45 h to 1.5 h. During ball milling, NbF_5 transforms to NbB_2 , which remains stable in the subsequent cycles. In details, Nb reacts with LiBH_4 generating NbB_2 , while F is partially substituting hydrogen in LiH and LiBH_4 . While in larger amounts the latter leads to a favourable thermodynamic change in the reaction enthalpy, in smaller amounts this effect is negligible [3, 167, 168]. Nano-sized NbB_2 particles in the grain boundaries act as nucleation seeds for the nucleation and growth of MgB_2 . Presence of NbB_2 nanoparticles considerably lowers the interfacial tension between the matrix and MgB_2 nuclei, which can lead to a smaller energy barrier for the nucleation and growth process for MgB_2 phase in the doped $\text{LiBH}_4/\text{MgH}_2$ system. Similar to NbF_5 , ScCl_3 transforms to ScB_2 nanoparticles during the ball milling. Formation of ScB_2 nanoparticles with a stable nanostructure serving as grain refiner and acting as nucleation agent, providing nucleation sites and reducing the energy barrier for nucleation and growth of the MgB_2 phase. The resulting smaller nanostructures result in a larger surface area and shorter diffusion path ways, leading to improved reaction kinetics. In order to investigate the affect of additives on RHCs in detail, advance characterization techniques; such as small angle x-ray scattering/ultra small angle x-ray scattering, anomalous x-ray scattering, small angle neutron scattering, *in-situ* SR-PXD, high resolution transmission electron microscopy, can provide the key informations related to the role of additive in the matrix. With the outcome from these advance characterization techniques with experimental results and computer simulations, current research is still ongoing to further reduce the operating temperatures and improve the reaction kinetics of the RHCs.

3. New trends and properties

As illustrated in the present review, complex hydride-based materials and systems have been extensively investigated in academia to define the best synthesis and processing methods, structural and physical properties, thermodynamics, and kinetics of involved reactions, and developing combined experimental, theoretical, modelling, and calculation methods to further understand and tailor these materials towards possible applications.

Research was first boosted by a great interest in hydrogen storage applications in the solid state, owing to their elevated gravimetric and volumetric content of hydrogen, mainly bonded in the complex anion. High hydrogen density can guarantee low weight and modest volume of storage, as in the case of borohydrides and alanates, advantageous for mobile applications. On the other hand, modest hydrogen density, typical of transition metal complex hydrides, can also be considered for stationary hydrogen storage in compact volumes. Extreme hydrogen densities have been reached in e.g. $\text{M}(\text{BH}_4)_n \cdot x\text{NH}_3$, NH_4BH_4 and $\text{NH}_4\text{-M-BH}_4$ systems [98, 129, 238, 329].

However, the drawback evidenced by basic research on these systems was their limited reversibility and cycling properties, related to harsh conditions of pressure and temperature for hydrogen release and uptake,

in addition with a material sensitivity to moisture and water, which make them relatively unusable in integrated systems that include hydrogen production from water by electrolysis and its final use in a fuel cell in mild conditions [79]. For this reason, advanced feasibility analysis of integrated systems or life cycle assessment studies based on complex hydrides are limited [78] and they are instead usually focused on metal hydrides [347–349]. In the case of real applications for hydrogen storage, magnesium based materials [67, 350, 351] or metal hydrides have been explored [352–356], considering complex hydrides only when included in the formulation of RHCs mixtures [77, 182, 334, 357, 358].

The wide possibility of applications for which complex hydrides have been explored underline how chemical and structural diversity is key for developing new multifunctional materials. Basic research evidenced new trends as it will be described hereafter, however, further applicative studies involving complex hydrides should be considered to further prove their properties on a large scale.

Recent reviews extensively present the advances of complex hydride based research [2, 72, 359–361], evidencing how the focus is shifting towards alternative applications beside hydrogen storage [43–45].

Applications in the field of solar thermal or heat storage require cycling properties and adequate thermodynamics, which once again are more advantageous in the case of metal hydrides or limited to few examples in transition metal complex hydrides [49, 362–372].

A renaissance of elemental properties studies on complex hydrides has started together with the exploration of their ionic conductivity to be used as solid state electrolytes in batteries or as electrodes [71, 285, 295, 301, 360, 373–380].

Due to the high number of Li-ion conducting borohydrides reported in literature, a statistical analysis has been performed for the most conductive and studied ones, e.g. LiBH_4 , $\text{Li}_2\text{BH}_4\text{NH}_2$, $\text{Li}_4\text{BH}_4(\text{NH}_2)_3$, and $\text{Li}_5(\text{BH}_4)_3\text{NH}$, to obtain the average values [375]. In addition, the energy limits of a certain migration map periodicities have been obtained with DFT calculations. A clear correlation between the experimental and calculated values for Li-ion mobility was obtained, suggesting that DFT and topological analysis can adequately explain ion conductivity in complex hydrides.

The effect of the composition and the structure dimensions of the $\text{h-Li}(\text{BH}_4)_{1-\alpha-\beta}(\text{Br})_\alpha(\text{Cl})_\beta$ solid solution on the Li-ion conductivity has been investigated, showing that the highest value of RT Li-ion conductivity in the ternary solid solution is reached for $\text{h-Li}(\text{BH}_4)_{0.7}(\text{Br})_{0.2}(\text{Cl})_{0.1}$ sample ($1.3 \times 10^{-5} \text{ S cm}^{-1}$ at 30°C) [155].

Recently, a total of 11 polymorphs of the compositions $\text{M}(\text{HCB}_{11}\text{H}_5\text{X}_6)$, $\text{M} = \text{Li, Na, X} = \text{Cl, Br}$ were reported representing a new series of halogenated *closo*-carborates. These exhibit order-disorder polymorphic transitions in the temperature range 203°C and 305°C . The high temperature polymorphs of these materials have superionic Li^+ or Na^+ conductivity, which is associated with the disordered structures [381]. Theoretical investigations reveal that the cation mobility in these systems is associated with the strength of the interaction with the anionic network and the dynamics of the anions, which open new routes for design of functional materials. A possible new type of proton conductor was also recently reported among the *closo*-borates, with a potential as solid-state ionic H^+ conductors. The structures containing the complex ammonium-ammonia cation N_2H_7^+ , with synthesis, crystal structures, and properties of $(\text{NH}_4)_2\text{B}_{10}\text{H}_{10} \cdot x\text{NH}_3$, $x = 1/2, 1$ (α and β) and $(\text{NH}_4)_2\text{B}_{12}\text{H}_{12} \cdot x\text{NH}_3$ ($x = 1$ and 2) are reported in ref [240]. The significant recent interest in this class of materials is mainly due to the possible design of fast ion conductors for solid state batteries. In particular, entropy effects, i.e. anion dynamics, have proven a powerful phenomenon for tuning ion conductivity. There are several studies of metal borates using static solid-state NMR or neutron spectroscopy that show a correlation between cation translational diffusion and dynamics of the anion lattice [219, 382–386].

It has been theoretically demonstrated that $\text{Li}_5\text{MoH}_{11}$ containing MoH_9^{3-} exhibits an unprecedentedly high lithium-ion conductivity at room temperature [387]. The key to the high ionic conductivity lies in the peculiar dynamics of MoH_9^{3-} , called ‘pseudorotation’ [388]. In fact, unlike rigid-body rotation, pseudorotation only requires small displacements of highly mobile hydrogen atoms, and thus is easily activated, leading to an order-disorder phase transition with significant cation diffusion at low temperature. The pseudorotation occurs due to the presence of energetically competing metastable coordination geometries that can easily be interconverted, especially for hydride complexes with high hydrogen coordination number exceeding six. This mechanism is quite general and may be applicable to a wide range of complex transition metal hydrides containing hydride complexes with high hydrogen coordination.

The use of complex hydrides as catalyst or electrocatalyst in reactions mainly involved studies on ammonia synthesis and decomposition [294, 299, 389], or CO_2 storage and conversion [390, 391]. In particular, the use of metal amides/imides as catalyst or co-catalyst with transition metals is one of the latest developments in the low temperature/pressure ammonia synthesis [297–300] and several new catalysts based on amide/imide materials has been recently reported [294].

Recently, new types of physical properties have been explored in lanthanide-bearing borohydrides related to solid state phosphors and magnetic refrigeration. Furthermore optical and magnetic properties have been reported, but they should be further explored [123, 124, 392].

REBs have received much attention over the years [2, 121] with respect to hydrogen storage materials [393, 394] or as solid state ion conductors for battery applications [92, 163, 395]. However, investigation of $\text{RE}(\text{BH}_4)_2(\text{THF})_2$ ($\text{RE} = \text{Eu}, \text{Yb}$) revealed the interesting property of bright blue luminescence from $\text{Eu}(\text{BH}_4)_2(\text{THF})_2$ with a quantum yield of 75% [396]. A few perovskite-type metal borohydrides were investigated with respect to luminescent properties too, and it was found that $\text{CsEu}(\text{BH}_4)_3$ exhibits a 20 nm red shift compared to pristine $\text{Eu}(\text{BH}_4)_2$ [106]. Interestingly, *closo*-borates were also investigated regarding their photoluminescence, where ultraviolet emission was observable from Sc, Y, and La as well as Li, Na, and Eu-based $\text{B}_{10}\text{H}_{10}^{2-}$ and $\text{B}_{12}\text{H}_{12}^{2-}$ compounds, while visible light emission was postulated from *arachno*-borates [397].

Finally, magnetic properties have been investigated for most of the REBs with $\text{K}_2\text{Gd}(\text{BH}_4)_5$ standing out as the most promising with a magnetic entropy change of $54.6 \text{ J kg}^{-1} \text{ K}^{-1}$ at 7 T, which is among the highest reported for inorganic materials [97, 398, 399]. The entropy change may be advantageous in application such as magnetic refrigerants.

The presence of unpaired f-electrons in $\text{Tb}(\text{BH}_4)_3$ and $\text{Tb}(\text{BH}_4)_3 \cdot \text{S}(\text{CH}_3)_2$ allowed for an investigation of the local structure of the Tb^{3+} ion using luminescence spectroscopy, where the latter resulted in an increased splitting of the f-f transitions [140]. Obtained data were compared to Density Functional Density calculations coupled with the Hubbard correction (DFT + U), which revealed that the calculations overestimate both the free ion electron-electron repulsion, the spin-orbit parameters as well as the crystal field parameters.

The rare earth metal borohydrides $\alpha\text{-Pr}(\text{BH}_4)_3$ and $\text{LiCe}(\text{BH}_4)_3\text{Cl}$ are both paramagnetic compounds as Pr^{3+} and Ce^{3+} have two and one unpaired electrons respectively. This gives rise to paramagnetic electron spin-nuclear spin interactions, which significantly affect the ^{11}B MAS NMR spectra of these compounds [400]. Even at a spinning frequency of 12.0 kHz the observed manifolds of spinning sidebands (ssb) in the ^{11}B MAS NMR spectra are highly asymmetric and resemble the ssb patterns for the chemical shift anisotropy interaction for spin- $1/2$ nuclei. The observed isotropic chemical shifts, δ_{obs} , are dominated by the contribution from the isotropic hyperfine shift, $\delta_{\text{iso}}^{\text{hf}}$, representing the contribution from the unpaired electrons. $\delta_{\text{iso}}^{\text{hf}}$ and the paramagnetic shift anisotropy, estimated by comparison with the isostructural and diamagnetic compounds $\alpha\text{-Y}(\text{BH}_4)_3$ and $\text{LiLa}(\text{BH}_4)_3\text{Cl}$, are approximately 5 and 4 times larger, respectively, for the ^{11}B site in $\alpha\text{-Pr}(\text{BH}_4)_3$ as compared to $\text{LiCe}(\text{BH}_4)_3\text{Cl}$ [400]. The great difference in both hyperfine shift and paramagnetic shift anisotropy are ascribed to the metal-borohydride contacts, i.e. two Pr^{3+} ions are in the vicinity of BH_4^- in $\alpha\text{-Pr}(\text{BH}_4)_3$, whereas only one Ce^{3+} is in the vicinity of BH_4^- in $\text{LiCe}(\text{BH}_4)_3\text{Cl}$, but it is also ascribed to the electronic spin state of the metal ions as the coupling parameters scale with $S(S + 1)$, where S is the electronic spin state. Finally, the anisotropic dipolar interactions show a $1 r^{-3}$ dependency, where r is the ^{11}B nuclear spin-paramagnetic electron spin distance. It may be possible to utilize this dependency for the determination of internuclear distances in similar systems [400].

Finally, a niche application that has been evidenced recently is the use of hydrides for radiation shielding in space [401, 402], which should be considered and investigated for complex hydrides too.

4. Outlooks and conclusions

The proficient synthesis of new compounds, chemical availability and flexibility of complex hydrides has been evidenced by the prolific literature publications and the detailed study of their crystal structure [3, 97, 112, 217, 403, 404].

Synthesis routes include wet chemistry [95, 405] and especially mechano-chemistry [101, 102, 207, 406], that can be easily scaled up, while structural investigations include the use of either x-ray or neutron diffraction and spectroscopies (e.g. Raman, NMR, FT-IR (Fourier transform infrared) etc) [158, 228, 388–398].

The interest has moved to a deeper analysis and understanding of the local structure of complex hydrides to understand the role of amorphous phase or defects on hydrogen storage and especially on ion migration path to enhance ion conductivity [115]. The study of local structure by PDF should be further expanded in the future, focusing on both solid and liquid phases, as in the case of borohydrides, borates and eutectic mixtures.

As previously introduced, the research on complex hydrides has spotlighted some general trends based on chemical bonds between different elements and hydrogen in these complex anions, which evidenced dihydrogen bonds as the interaction of the future. Before, it was suggested that this bond strength can determine the hydrogen release, however it has been shown that there is no relation between the bond

strength and the decomposition temperature, nevertheless dihydrogen bonds strongly contribute to structural flexibility in the solid state and cation mobility and possibly also other interesting properties.

The direct correlation of decomposition temperature with Pauling electronegativity was reported but in the case of $\text{RE}(\text{BH}_4)_n$, the opposite trend has been observed. These correlations and trends have been widely exploited to tailor hydrogenation properties of complex hydrides, especially by cation or anion substitutions. Furthermore, nanoscaling and nanoconfinement have emerged as a particularly promising strategy for improving kinetics of complex hydrides, as illustrated in several of the aforementioned examples [52–55, 57, 58, 60, 64, 211, 212, 216, 306, 407]. Strategies can leverage ‘non-innocent’ chemical interactions with the confining medium, reduced diffusion lengths, confinement stress effects, lowered nucleation barriers, and surface/interface energy penalties to speed reaction rates or alter reaction pathways [52, 54, 60, 64, 212, 306]. Many of these strategies were recently reviewed in a comprehensive article on nanostructured metal hydrides for hydrogen storage [407]. Further research along these lines, including improved fundamental mechanistic understanding of nanoconfinement, may aid in the selection of ideal complex hydride formulations and host matrices for practical low-pressure, high-capacity storage solutions.

The future opportunities in tailoring these systems must involve a massive exploitation of thermodynamics evaluation and modelling efforts. Challenges and opportunities in modelling and simulations are based on a proficient determination of thermo-chemical properties of newly discovered materials, which requires huge calculations and theoretical thermodynamic modelling to build up a comprehensive database, coupled with a massive experimental effort. It has been demonstrated that the CALPHAD approach is beneficial to create and expand thermodynamic calculations on complex hydrides systems, but it needs to be updated and integrated while new materials are discovered and investigated [16, 75, 161, 408]. A continuous flow of thermodynamic data will also allow the development of machine learning techniques to be applied to complex hydrides, as it has been demonstrated on metal hydrides [409–412]. This approach will combine an ocean of data on these systems and reveal new trends and correlations to further develop a rational design of target-based materials and new promising compositions or mixtures.

It is worth noting that high throughput *ab-initio* calculations can be a huge support to thermodynamic assessments, and they can be integrated and compared with available experimental data owing to the CALPHAD approach, which leads to a comprehensive modelling of investigated system. To our knowledge no other possible approaches have been proposed for modelling thermodynamics of hydrides systems.

Recent advances in modelling and simulation have provided additional insight into complex hydride reactions [60, 64, 211–213, 215, 225, 306, 407, 413–415]. These solid-state reactions are notoriously complex, thus simulations must consider non-idealities that alter thermodynamics, as well as impacting reaction and diffusion kinetics [415]. Recent computational activities have incorporated interfaces and interfacial energy penalties more directly in thermodynamic and kinetic investigations of reaction pathways in complex hydrides, with a focus on nanoscale materials [60, 64, 211, 306, 415]. It is also increasingly being realized that diffusion in complex hydrides is likely dominated by interfacial, surface, and grain boundary pathways, rather than bulk defect dynamics. Investigations are underway to quantify the contributions of these diffusion pathways more directly.

The role of phase nucleation is also being considered more prominently. Nucleation is a multi-step process for complex hydrides, which involves transformations of chemical species in addition to phase-level reorganizations. Recently, a model was developed to account for this multi-step reactions within a classical nucleation theory context [413]. A separate study was also published detailing how local morphology and dimensionality of complex hydride clusters, surfaces, and bulk crystals play a role in determining reaction pathways and nucleation barriers in the solid state [225]. These calculations can be the basis for a more quantitative approach to nucleation prediction.

For nanoconfined complex hydrides, an emerging area of interest for computation is the development of approaches for predicting interaction effects with the confining host for different particle sizes. Recent investigations have addressed this challenge by combining advanced free-energy sampling methods with direct computation of hydride-host interactions [60, 64]. This methodology provides an avenue for predicting both size-dependent and host-dependent reaction enthalpies, while simultaneously providing insights into kinetic effects in confined systems. The approach has been successfully deployed to study carbon-confined nanoscale Li–Al–H [60] and Al–H [64] systems and it is currently being applied to the Li–N–H system. An additional investigation pathway has focused on the integration of spectroscopic techniques and *ab-initio* modelling to investigate the chemical interaction with the confining medium and the impact on phase behaviour [60, 64, 212, 215, 414]. Examples include recent work on borohydrides, which invoked computational models and direct spectroscopic calculations to interpret experiments and elucidate the interfacial chemistry [212, 213, 215]. An analogous approach combining spectroscopy and simulations was also recently raised to investigate the effects of native surface oxidation on NaAlH_4 dehydrogenation kinetics [66].

A recent paper by Wood *et al* [415] highlighted four areas where advances beyond idealized models have helped to elucidate key phenomena in metal hydrides, with an emphasis on nanoscale and nanoconfined systems. These included the role of surfaces and interfaces in determining enthalpy and reaction pathways; the role of anharmonicity at surfaces and interfaces in determining entropy-enthalpy compensation effects; the role of solid mechanics in altering properties of confined systems in stiff matrices; and the role of surface contamination in altering chemical pathways and barriers for dissociation and diffusion. Although not exhaustive, these examples nicely illustrate the types of advances that are required to achieve parity between theoretical predictions and experimental realities, and they can be also applied in the future on complex hydride systems.

Data availability statement

No new data were created or analysed in this study.

Acknowledgments

This paper was realised within the framework of the Hydrogen Technology Collaboration Programme (TCP) of the International Energy Agency (IEA) in Task 40 ‘Energy storage and conversion based on hydrogen’. Work at Pacific Northwest National Laboratory (PNNL) and Lawrence Livermore National Laboratory (LLNL) was supported by the Hydrogen Materials Advanced Research Consortium (HyMARC), established as part of the Energy Materials Network under the U.S. Department of Energy, Office of Energy Efficiency and Renewable Energy, Fuel Cell Technologies Office. PNNL is a multiprogram national laboratory operated by Battelle for the U.S. Department of Energy (DOE). Work at LLNL was performed under the auspices of the DOE under Contract DE-AC52-07NA27344. Kasper T Møller would like to acknowledge the Carlsberg Foundation for a Reintegration Fellowship (CF19-0465). Funding from the Danish Ministry of Higher Education and Science through the SMART Lighthouse, the independent research fund Denmark for technology and production (Grants 9041-00226B and 0217-00327B) and the Carlsberg Foundation are gratefully acknowledged. C E Buckley (CEB), Mark Paskevicius (MP) and T D Humphries (TDH) acknowledge financial support from the Australian Research Council for Grants LP120101848, LP150100730 (CEB, TDH), DP150101708 (CEB), FT160100303 (MP), LE140100075 (CEB, MP), LE0989180 (CEB) and LE0775551 (CEB). Shin-ichi Orimo acknowledges funding from JSPS KAKENHI (Hydrogenomics, JP18H05513). Shigeyuki Takagi acknowledges funding from JSPS KAKENHI (19H05514, 20K20438). P Ngene and P E de Jongh acknowledge funding from NWO (Dutch Research Council) Materials for sustainability (739.017.009) and NWO ECHO (712.015.005) grants. Y W Cho and Y-S Lee acknowledge funding from National Research Foundation of Korea (NRF-2020M1A2A2080881).

ORCID iDs

Erika Michela Dematteis  <https://orcid.org/0000-0002-3680-4196>

Mads B Amdisen  <https://orcid.org/0000-0003-2663-8988>

Tom Autrey  <https://orcid.org/0000-0002-7983-3667>

Jussara Barale  <https://orcid.org/0000-0002-6014-0465>

Mark E Bowden  <https://orcid.org/0000-0003-3812-3340>

Craig E Buckley  <https://orcid.org/0000-0002-3075-1863>

Young Whan Cho  <https://orcid.org/0000-0001-9909-0082>

Martin Dornheim  <https://orcid.org/0000-0001-8491-435X>

Petra de Jongh  <https://orcid.org/0000-0002-2216-2620>

Jakob B Grinderslev  <https://orcid.org/0000-0001-7645-1383>

Gökhan Gizer  <https://orcid.org/0000-0002-1268-8610>

Valerio Gulino  <https://orcid.org/0000-0002-5808-7802>

Bjørn C Hauback  <https://orcid.org/0000-0002-2717-6941>

Michael Heere  <https://orcid.org/0000-0002-7826-1425>

Tae Wook Heo  <https://orcid.org/0000-0002-0765-3480>



Terry D Humphries  <https://orcid.org/0000-0003-1015-4495>

Torben R Jensen  <https://orcid.org/0000-0002-4278-3221>

Shin Young Kang  <https://orcid.org/0000-0001-9035-8169>

Young-Su Lee  <https://orcid.org/0000-0002-3160-6633>

Hai-Wen Li  <https://orcid.org/0000-0001-7223-1754>

Sichi Li  <https://orcid.org/0000-0002-2565-5906>
Kasper T Møller  <https://orcid.org/0000-0002-1970-6703>
Peter Ngene  <https://orcid.org/0000-0003-3691-0623>
Shin-ichi Orimo  <https://orcid.org/0000-0002-4216-0446>
Mark Paskevicius  <https://orcid.org/0000-0003-2677-3434>
Marek Polanski  <https://orcid.org/0000-0003-0163-514X>
Shigeyuki Takagi  <https://orcid.org/0000-0002-8434-7946>
Liwen Wan  <https://orcid.org/0000-0002-5391-0804>
Brandon C Wood  <https://orcid.org/0000-0002-1450-9719>
Michael Hirscher  <https://orcid.org/0000-0002-3143-2119>
Marcello Baricco  <https://orcid.org/0000-0002-2856-9894>

References

- [1] Holleman A F and Wiberg E 1995 *Inorganic Chemistry* (Berlin: Walter de Gruyter)
- [2] Hadjixenophontos E *et al* 2020 A review of the MSCA ITN ECOSTORE—novel complex metal hydrides for efficient and compact storage of renewable energy as hydrogen and electricity *Inorganics* **8** 17
- [3] Paskevicius M, Jepsen L H, Schouwink P, Černý R, Ravnsbæk D B, Filinchuk Y, Dornheim M, Besenbacher F and Jensen T R 2017 Metal borohydrides and derivatives—synthesis, structure and properties *Chem. Soc. Rev.* **46** 1565–634
- [4] Polanski M, Nielsen T K, Cerenius Y, Bystrzycki J and Jensen T R 2010 Synthesis and decomposition mechanisms of Mg_2FeH_6 studied by *in-situ* synchrotron x-ray diffraction and high-pressure DSC *Int. J. Hydrog. Energy* **35** 3578–82
- [5] Polanski M, Płociński T, Kuncie I and Bystrzycki J 2010 Dynamic synthesis of ternary Mg_2FeH_6 *Int. J. Hydrog. Energy* **35** 1257–66
- [6] Norek M, Nielsen T K, Polanski M, Kuncie I, Płociński T, Jaroszewicz L R, Cerenius Y, Jensen T R and Bystrzycki J 2011 Synthesis and decomposition mechanisms of ternary Mg_2CoH_5 studied using *in situ* synchrotron x-ray diffraction *Int. J. Hydrog. Energy* **36** 10760–70
- [7] Polanski M, Nielsen T K, Kuncie I, Norek M, Płociński T, Jaroszewicz L R, Gundlach C, Jensen T R and Bystrzycki J 2013 Mg_2NiH_4 synthesis and decomposition reactions *Int. J. Hydrog. Energy* **38** 4003–10
- [8] Yvon K and Renaudin G 2011 Hydrides: solid state transition metal complexes *Encyclopedia of Inorganic and Bioinorganic Chemistry* (Chichester: Wiley)
- [9] Humphries T D, Sheppard D A and Buckley C E 2017 Recent advances in the 18-electron complex transition metal hydrides of Ni, Fe, Co and Ru *Coord. Chem. Rev.* **342** 19–33
- [10] Sai Raman S S, Davidson D J, Bobet J-L and Srivastava O N 2002 Investigations on the synthesis, structural and microstructural characterizations of Mg-based K_2PtCl_6 type (Mg_2FeH_6) hydrogen storage material prepared by mechanical alloying *J. Alloys Compd.* **333** 282–90
- [11] Zolliker P, Yvon K, Jorgensen J D and Rotella F J 1986 Structural studies of the hydrogen storage material magnesium nickel hydride (Mg_2NiH_4). 2. Monoclinic low-temperature structure *Inorg. Chem.* **25** 3590–3
- [12] Yvon K, Schefer J and Stucki F 1981 Structural studies of the hydrogen storage material Mg_2NiH_4 . 1. Cubic high-temperature structure *Inorg. Chem.* **20** 2776–8
- [13] Smith M B and Bass G E 1963 Heats and free energies of formation of the alkali aluminum hydrides and of cesium hydride *J. Chem. Eng. Data* **8** 342–6
- [14] Martelli P, Caputo R, Remhof A, Mauron P, Borgschulte A and Züttel A 2010 Stability and decomposition of $NaBH_4$ *J. Phys. Chem. C* **114** 7173–7
- [15] Zavorotynska O, El-Kharbachi A, Deledda S and Hauback B C 2016 Recent progress in magnesium borohydride $Mg(BH_4)_2$: fundamentals and applications for energy storage *Int. J. Hydrog. Energy* **41** 14387–403
- [16] Pinat E R, Albanese E, Civalleri B and Baricco M 2015 Thermodynamic modelling of $Mg(BH_4)_2$ *J. Alloys Compd.* **645** S64–S68
- [17] Block J and Gray A P 1965 The thermal decomposition of lithium aluminum hydride *Inorg. Chem.* **4** 304–5
- [18] Chen J, Kuriyama N, Xu Q, Takeshita H T and Sakai T 2001 Reversible hydrogen storage via titanium-catalyzed $LiAlH_4$ and Li_3AlH_6 *J. Phys. Chem. B* **105** 11214–20
- [19] Brinks H W and Hauback B C 2003 The structure of Li_3AlD_6 *J. Alloys Compd.* **354** 143–7
- [20] Blanchard D, Brinks H, Hauback B and Norby P 2004 Desorption of $LiAlH_4$ with Ti- and V-based additives *Mater. Sci. Eng. B* **108** 54–59
- [21] Chung S-C and Morioka H 2004 Thermochemistry and crystal structures of lithium, sodium and potassium alanates as determined by *ab initio* simulations *J. Alloys Compd.* **372** 92–96
- [22] Na Ranong C, Höhne M, Franzen J, Hapke J, Fieg G, Dornheim M, Eigen N, Bellosta von Colbe J M and Metz O 2009 Concept, design and manufacture of a prototype hydrogen storage tank based on sodium alanate *Chem. Eng. Technol.* **32** 1154–63
- [23] Canton P, Fichtner M, Frommen C and Léon A 2006 Synchrotron x-ray studies of Ti-doped $NaAlH_4$ *J. Phys. Chem. B* **110** 3051–4
- [24] Rönnebro E, Noréus D, Kadir K, Reiser A and Bogdanovic B 2000 Investigation of the perovskite related structures of $NaMgH_3$, $NaMgF_3$ and Na_3AlH_6 *J. Alloys Compd.* **299** 101–6
- [25] Jacobs H and Juza R 1972 Neubestimmung der Kristallstruktur des Lithiumamids *Z. Anorg. Allg. Chem.* **391** 271–9
- [26] Chen P, Xiong Z, Luo J, Lin J and Tan K L 2002 Interaction of hydrogen with metal nitrides and imides *Nature* **420** 302–4
- [27] Bogdanović B, Reiser A, Schlichte K, Spliethoff B and Tesche B 2002 Thermodynamics and dynamics of the Mg–Fe–H system and its potential for thermochemical thermal energy storage *J. Alloys Compd.* **345** 77–89
- [28] Puszkiel J A, Larochette P A and Gennari F C 2008 Thermodynamic and kinetic studies of Mg–Fe–H after mechanical milling followed by sintering *J. Alloys Compd.* **463** 134–42
- [29] Puszkiel J *et al* 2013 Sorption behavior of the MgH_2 – Mg_2FeH_6 hydride storage system synthesized by mechanical milling followed by sintering *Int. J. Hydrog. Energy* **38** 14618–30
- [30] Puszkiel J A, Arneodo Larochette P and Gennari F C 2009 Hydrogen storage properties of Mg_xFe (x: 2, 3 and 15) compounds produced by reactive ball milling *J. Power Sources* **186** 185–93

- [31] Zolliker P, Yvon K, Fischer P and Schefer J 1985 Dimagnesium cobalt(I) pentahydride, Mg_2CoH_5 , containing square-pyramidal pentahydrocobaltate(4-) (CoH_5^{4-}) anions *Inorg. Chem.* **24** 4177–80
- [32] Anon 2020 Materials data on Mg_2CoH_5 by materials project *Materials Project United States* (<https://doi.org/10.17188/1280145>)
- [33] Verón M G and Gennari F C 2014 Thermodynamic behavior of the Mg–Co–H system: the effect of hydrogen cycling *J. Alloys Compd.* **614** 317–22
- [34] Barale J, Deledda S, Dematteis E M, Sørby M H, Baricco M and Hauback B C 2020 Synthesis and characterization of magnesium-iron-cobalt complex hydrides *Sci. Rep.* **10** 9000
- [35] Fernández I G, Meyer G O and Gennari F C 2008 Hydriding/dehydriding behavior of Mg_2CoH_5 produced by reactive mechanical milling *J. Alloys Compd.* **464** 111–7
- [36] Zlotea C, Oumellal Y, Berrú J J S and Aguey-Zinsou K-F 2018 On the feasibility of the bottom-up synthesis of Mg_2CoH_5 nanoparticles supported on a porous carbon and their hydrogen desorption behaviour *Nano-Struct. Nano-Objects* **16** 144–50
- [37] Martínez-Coronado R, Retuerto M, Torres B, Martínez-Lope M J, Fernández-Díaz M T and Alonso J A 2013 High-pressure synthesis, crystal structure and cyclability of the Mg_2NiH_4 hydride *Int. J. Hydrog. Energy* **38** 5738–45
- [38] Reilly J J and Wiswall R H 1968 Reaction of hydrogen with alloys of magnesium and nickel and the formation of Mg_2NiH_4 *Inorg. Chem.* **7** 2254–6
- [39] Muthukumar P, Maiya M P, Srinivasa Murthy S, Vijay R and Sundaresan R 2008 Tests on mechanically alloyed Mg_2Ni for hydrogen storage *J. Alloys Compd.* **452** 456–61
- [40] Liu X, Zhu Y and Li L 2007 Hydriding characteristics of Mg_2NiMg_2Ni prepared by mechanical milling of the product of hydriding combustion synthesis *Int. J. Hydrog. Energy* **32** 2450–4
- [41] David W I F, Jones M O, Gregory D H, Jewell C M, Johnson S R, Walton A and Edwards P P 2007 A mechanism for non-stoichiometry in the lithium amide/lithium imide hydrogen storage reaction *J. Am. Chem. Soc.* **129** 1594–601
- [42] Lohstroh W, Roth A, Hahn H and Fichtner M 2010 Thermodynamic effects in nanoscale $NaAlH_4$ *ChemPhysChem* **11** 789–92
- [43] Milanese C et al 2019 Complex hydrides for energy storage *Int. J. Hydrog. Energy* **44** 7860–74
- [44] El Kharbachi A et al 2020 Metal hydrides and related materials. Energy carriers for novel hydrogen and electrochemical storage *J. Phys. Chem. C* **124** 7599–607
- [45] Bannenberg L J et al 2020 Metal (boro-) hydrides for high energy density storage and relevant emerging technologies *Int. J. Hydrog. Energy* **45** 33687–730
- [46] Bogdanović B and Schwickardi M 2001 Ti-doped $NaAlH_4$ as a hydrogen-storage material—preparation by Ti-catalyzed hydrogenation of aluminum powder in conjunction with sodium hydride *Appl. Phys. A* **72** 221–3
- [47] Hauback B C 2008 Structures of aluminium-based light weight hydrides *Z. Kristallogr.* **223** 636–48
- [48] Graetz J 2009 New approaches to hydrogen storage *Chem. Soc. Rev.* **38** 73–82
- [49] Møller K, Sheppard D, Ravnsbæk D, Buckley C, Akiba E, Li H-W and Jensen T 2017 Complex metal hydrides for hydrogen, thermal and electrochemical energy storage *Energies* **10** 1645
- [50] Sheppard D A, Jepsen L H, Rowles M R, Paskevicius M, Jensen T R and Buckley C E 2019 Decomposition pathway of $KAlH_4$ altered by the addition of Al_2S_3 *Dalt. Trans.* **48** 5048–57
- [51] Sheppard D A, Jepsen L H, Jensen T R, Paskevicius M and Buckley C E 2013 New directions for hydrogen storage: sulphur destabilised sodium aluminium hydride *J. Mater. Chem. A* **1** 12775
- [52] Nielsen T K, Javadian P, Polanski M, Besenbacher F, Bystrzycki J and Jensen T R 2012 Nanoconfined $NaAlH_4$: determination of distinct prolific effects from pore size, crystallite size, and surface interactions *J. Phys. Chem. C* **116** 21046–51
- [53] Nielsen T K, Javadian P, Polanski M, Besenbacher F, Bystrzycki J, Skibsted J and Jensen T R 2014 Nanoconfined $NaAlH_4$: prolific effects from increased surface area and pore volume *Nanoscale* **6** 599–607
- [54] Nielsen T K, Polanski M, Zasada D, Javadian P, Besenbacher F, Bystrzycki J, Skibsted J and Jensen T R 2011 Improved hydrogen storage kinetics of nanoconfined $NaAlH_4$ catalyzed with $TiCl_3$ nanoparticles *ACS Nano* **5** 4056–64
- [55] Paskevicius M et al 2016 Cyclic stability and structure of nanoconfined Ti-doped $NaAlH_4$ *Int. J. Hydrog. Energy* **41** 4159–67
- [56] Huen P, Peru F, Charalambopoulou G, Steriotis T A, Jensen T R and Ravnsbæk D B 2017 Nanoconfined $NaAlH_4$ conversion electrodes for Li batteries *ACS Omega* **2** 1956–67
- [57] Ianni E, Sofianos M V, Sheppard D A, Rowles M R, Humphries T D, Liu S and Buckley C E 2018 Synthesis and characterisation of a porous Al scaffold sintered from $NaAlH_4$ *J. Mater. Sci.* **53** 1076–87
- [58] Sofianos M V, Chaudhary A-L, Paskevicius M, Sheppard D A, Humphries T D, Dornheim M and Buckley C E 2019 Hydrogen storage properties of eutectic metal borohydrides melt-infiltrated into porous Al scaffolds *J. Alloys Compd.* **775** 474–80
- [59] Ianni E, Sofianos M V, Rowles M R, Sheppard D A, Humphries T D and Buckley C E 2018 Synthesis of $NaAlH_4/Al$ composites and their applications in hydrogen storage *Int. J. Hydrog. Energy* **43** 17309–17
- [60] Cho Y et al 2021 Reversing the irreversible: thermodynamic stabilization of $LiAlH_4$ nanoconfined within a nitrogen-doped carbon host *ACS Nano* **15** 10163–74
- [61] Humphries T D, Birkmire D, McGrady G S, Hauback B C and Jensen C M 2017 Regeneration of $LiAlH_4$ at sub-ambient temperatures studied by multinuclear NMR spectroscopy *J. Alloys Compd.* **723** 1150–4
- [62] Humphries T D, Birkmire D, Hauback B C, McGrady G S and Jensen C M 2013 *In situ* high pressure NMR study of the direct synthesis of $LiAlH_4$ *J. Mater. Chem. A* **1** 2974
- [63] Lacina D, Yang L, Chopra I, Muckerman J, Chabal Y and Graetz J 2012 Investigation of $LiAlH_4$ –THF formation by direct hydrogenation of catalyzed Al and LiH *Phys. Chem. Chem. Phys.* **14** 6569
- [64] Stavila V et al 2021 Defying thermodynamics: stabilization of alane within covalent triazine frameworks for reversible hydrogen storage *Angew. Chem.* **133** 26019–28
- [65] Konovalov S K and Bulychev B M 1995 The P,T-state diagram and solid phase synthesis of aluminum hydride *Inorg. Chem.* **34** 172–5
- [66] White J L et al 2019 Identifying the role of dynamic surface hydroxides in the dehydrogenation of Ti-doped $NaAlH_4$ *ACS Appl. Mater. Interfaces* **11** 4930–41
- [67] Hirscher M et al 2020 Materials for hydrogen-based energy storage—past, recent progress and future outlook *J. Alloys Compd.* **827** 153548
- [68] Černý R and Schouwink P 2015 The crystal chemistry of inorganic metal borohydrides and their relation to metal oxides *Acta Crystallogr. B* **71** 619–40
- [69] Møller K T, Jensen T R, Akiba E and Li H-W 2017 Hydrogen—a sustainable energy carrier *Prog. Nat. Sci. Mater. Int.* **27** 34–40
- [70] Suárez-Alcántara K and Tena García J R 2021 Metal borohydrides beyond groups I and II: a review *Materials* **14** 2561
- [71] Hagemann H 2019 Boron hydrogen compounds for hydrogen storage and as solid ionic conductors *Chim. Int. J. Chem.* **73** 868–73

- [72] Callini E *et al* 2016 Complex and liquid hydrides for energy storage *Appl. Phys. A* **122** 353
- [73] Dematteis E M, Jensen S R, Jensen T R and Baricco M 2020 Heat capacity and thermodynamic properties of alkali and alkali-earth borohydrides *J. Chem. Thermodyn.* **143** 106055
- [74] El Kharbachi A, Pinatel E, Nuta I and Baricco M 2012 A thermodynamic assessment of LiBH_4 *Calphad* **39** 80–90
- [75] Baricco M, Palumbo M, Pinatel E, Corno M and Ugliengo P 2010 Thermodynamic database for hydrogen storage materials *Adv. Sci. Technol.* **72** 213–8
- [76] Jepsen L H, Ley M B, Lee Y-S, Cho Y W, Dornheim M, Jensen J O, Filinchuk Y, Jørgensen J E, Besenbacher F and Jensen T R 2014 Boron–nitrogen based hydrides and reactive composites for hydrogen storage *Mater. Today* **17** 129–35
- [77] Dematteis E M, Vaunois S, Pistidda C, Dornheim M and Baricco M 2018 Reactive hydride composite of Mg_2NiH_4 with borohydrides eutectic mixtures *Crystals* **8** 90
- [78] Baricco M, Bang M, Fichtner M, Hauback B, Linder M, Luetto C, Moretto P and Sgroi M 2017 SSH_2S : hydrogen storage in complex hydrides for an auxiliary power unit based on high temperature proton exchange membrane fuel cells *J. Power Sources* **342** 853–60
- [79] Dematteis E M, Barale J, Corno M, Sciuolo A, Baricco M and Rizzi P 2021 Solid-state hydrogen storage systems and the relevance of a gender perspective *Energies* **14** 6158
- [80] Schlesinger H I, Brown H C and Finholt A E 1953 The preparation of sodium borohydride by the high temperature reaction of sodium hydride with borate esters *J. Am. Chem. Soc.* **75** 205–9
- [81] Richter B, Ravnsbæk D B, Tumanov N, Filinchuk Y and Jensen T R 2015 Manganese borohydride; synthesis and characterization *Dalt. Trans.* **44** 3988–96
- [82] Ravnsbæk D B, Nickels E A, Černý R, Olesen C H, David W I F, Edwards P P, Filinchuk Y and Jensen T R 2013 Novel alkali earth borohydride $\text{Sr}(\text{BH}_4)_2$ and borohydride-chloride $\text{Sr}(\text{BH}_4)\text{Cl}$ *Inorg. Chem.* **52** 10877–85
- [83] Schlesinger H I, Brown H C and Hyde E K 1953 The preparation of other borohydrides by metathetical reactions utilizing the alkali metal borohydrides *J. Am. Chem. Soc.* **75** 209–13
- [84] Yan Y, Li H-W, Sato T, Umeda N, Miwa K, Towata S and Orimo S 2009 Dehydrogenating and rehydrogenating properties of yttrium borohydride $\text{Y}(\text{BH}_4)_3$ prepared by liquid-phase synthesis *Int. J. Hydrog. Energy* **34** 5732–6
- [85] Li H-W, Kikuchi K, Nakamori Y, Miwa K, Towata S and Orimo S 2007 Effects of ball milling and additives on dehydrogenating behaviors of well-crystallized $\text{Mg}(\text{BH}_4)_2$ *Scr. Mater.* **57** 679–82
- [86] Olsen J E, Frommen C, Jensen T R, Riktor M D, Sørby M H and Hauback B C 2014 Structure and thermal properties of composites with RE-borohydrides (RE = La, Ce, Pr, Nd, Sm, Eu, Gd, Tb, Er, Yb or Lu) and LiBH_4 *RSC Adv.* **4** 1570–82
- [87] Ley M B, Paskevicius M, Schouwink P, Richter B, Sheppard D A, Buckley C E and Jensen T R 2014 Novel solvates $\text{M}(\text{BH}_4)_3\text{S}(\text{CH}_3)_2$ and properties of halide-free $\text{M}(\text{BH}_4)_3$ (M = Y or Gd) *Dalt. Trans.* **43** 13333–42
- [88] Humphries T D, Ley M B, Frommen C, Munroe K T, Jensen T R and Hauback B C 2015 Crystal structure and *in situ* decomposition of $\text{Eu}(\text{BH}_4)_2$ and $\text{Sm}(\text{BH}_4)_2$ *J. Mater. Chem. A* **3** 691–8
- [89] Ley M B, Ravnsbæk D B, Filinchuk Y, Lee Y-S, Janot R, Cho Y W, Skibsted J and Jensen T R 2012 $\text{LiCe}(\text{BH}_4)_3\text{Cl}$, a new lithium-ion conductor and hydrogen storage material with isolated tetranuclear anionic clusters *Chem. Mater.* **24** 1654–63
- [90] Frommen C, Sørby M H, Ravindran P, Vajeeston P, Fjellvåg H and Hauback B C 2011 Synthesis, crystal structure, and thermal properties of the first mixed-metal and anion-substituted rare earth borohydride $\text{LiCe}(\text{BH}_4)_3\text{Cl}$ *J. Phys. Chem. C* **115** 23591–602
- [91] Olsen J E, Frommen C, Sørby M H and Hauback B C 2013 Crystal structures and properties of solvent-free $\text{LiYb}(\text{BH}_4)_{4-x}\text{Cl}_x$, $\text{Yb}(\text{BH}_4)_3$ and $\text{Yb}(\text{BH}_4)_{2-x}\text{Cl}_x$ *RSC Adv.* **3** 10764
- [92] Ley M B, Boulineau S, Janot R, Filinchuk Y and Jensen T R 2012 New Li ion conductors and solid state hydrogen storage materials: $\text{LiM}(\text{BH}_4)_3\text{Cl}$, M = La, Gd *J. Phys. Chem. C* **116** 21267–76
- [93] Grube E, Olesen C H, Ravnsbæk D B and Jensen T R 2016 Barium borohydride chlorides: synthesis, crystal structures and thermal properties *Dalt. Trans.* **45** 8291–9
- [94] Anon (available at: www.katchem.cz)
- [95] Richter B, Grinderslev J B, Møller K T, Paskevicius M and Jensen T R 2018 From metal hydrides to metal borohydrides *Inorg. Chem.* **57** 10768–80
- [96] Grinderslev J B and Jensen T R 2021 Trends in the series of ammine rare-earth-metal borohydrides: relating structural and thermal properties *Inorg. Chem.* **60** 2573–89
- [97] Grinderslev J B, Møller K T, Bremholm M and Jensen T R 2019 Trends in synthesis, crystal structure, and thermal and magnetic properties of rare-earth metal borohydrides *Inorg. Chem.* **58** 5503–17
- [98] Grinderslev J B, Ley M B, Lee Y-S, Jepsen L H, Jørgensen M, Cho Y W, Skibsted J and Jensen T R 2020 Ammine lanthanum and cerium borohydrides, $\text{M}(\text{BH}_4)_3 \cdot n\text{NH}_3$; trends in synthesis, structures, and thermal properties *Inorg. Chem.* **59** 7768–78
- [99] Yang Y, Liu Y, Li Y, Gao M and Pan H 2013 Synthesis and thermal decomposition behaviors of magnesium borohydride ammoniates with controllable composition as hydrogen storage materials *Chem. Asian J.* **8** 476–81
- [100] Yan Y, Grinderslev J B, Jørgensen M, Skov L N, Skibsted J and Jensen T R 2020 Ammine magnesium borohydride nanocomposites for all-solid-state magnesium batteries *ACS Appl. Energy Mater.* **3** 9264–70
- [101] Huot J *et al* 2019 Mechanochemistry of metal hydrides: recent advances *Materials* **12** 2778
- [102] Huot J, Ravnsbæk D B, Zhang J, Cuevas F, Latroche M and Jensen T R 2013 Mechanochemical synthesis of hydrogen storage materials *Prog. Mater. Sci.* **58** 30–75
- [103] Černý R, Chul Kim K, Penin N, D'Anna V, Hagemann H and Sholl D S 2010 $\text{AZn}_2(\text{BH}_4)_5$ (A = Li, Na) and $\text{NaZn}(\text{BH}_4)_3$: structural studies *J. Phys. Chem. C* **114** 19127–33
- [104] Møller K T, Jørgensen M, Fogh A S and Jensen T R 2017 Perovskite alkali metal samarium borohydrides: crystal structures and thermal decomposition *Dalt. Trans.* **46** 11905–12
- [105] Nickels E A, Jones M O, David W I F, Johnson S R, Lowton R L, Sommariva M and Edwards P P 2008 Tuning the decomposition temperature in complex hydrides: synthesis of a mixed alkali metal borohydride *Angew. Chem., Int. Ed.* **47** 2817–9
- [106] Schouwink P, Ley M B, Tissot A, Hagemann H, Jensen T R, Smrčok Ľ and Černý R 2014 Structure and properties of complex hydride perovskite materials *Nat. Commun.* **5** 5706
- [107] Møller K T, Ley M B, Schouwink P, Černý R and Jensen T R 2016 Synthesis and thermal stability of perovskite alkali metal strontium borohydrides *Dalt. Trans.* **45** 831–40
- [108] Grinderslev J B, Jepsen L H, Lee Y-S, Møller K T, Cho Y W, Černý R and Jensen T R 2020 Structural diversity and trends in properties of an array of hydrogen-rich ammonium metal borohydrides *Inorg. Chem.* **59** 12733–47

- [109] Jepsen L H, Lee Y-S, Černý R, Sarusie R S, Cho Y W, Besenbacher F and Jensen T R 2015 Ammine calcium and strontium borohydrides: syntheses, structures, and properties *ChemSusChem* **8** 3472–82
- [110] Jepsen L H, Ley M B, Černý R, Lee Y-S, Cho Y W, Ravnsbæk D, Besenbacher F, Skibsted J and Jensen T R 2015 Trends in syntheses, structures, and properties for three series of ammine rare-earth metal borohydrides, $M(\text{BH}_4)_3 \cdot n\text{NH}_3$ ($M = \text{Y, Gd, and Dy}$) *Inorg. Chem.* **54** 7402–14
- [111] Rude L H, Corno M, Ugliengo P, Baricco M, Lee Y-S, Cho Y W, Besenbacher F, Overgaard J and Jensen T R 2012 Synthesis and structural investigation of $\text{Zr}(\text{BH}_4)_4$ *J. Phys. Chem. C* **116** 20239–45
- [112] Rude L H et al 2011 Tailoring properties of borohydrides for hydrogen storage: a review *Phys. Status Solidi* **208** 1754–73
- [113] Roedern E and Jensen T R 2015 Ammine-stabilized transition-metal borohydrides of iron, cobalt, and chromium: synthesis and characterization *Inorg. Chem.* **54** 10477–82
- [114] Heere M, Zavorotynska O, Deledda S, Sørby M H, Book D, Steriotis T and Hauback B C 2018 Effect of additives, ball milling and isotopic exchange in porous magnesium borohydride *RSC Adv.* **8** 27645–53
- [115] Heere M, Hansen A-L, Payandeh S, Aslan N, Gizer G, Sørby M H, Hauback B C, Pistidda C, Dornheim M and Lohstroh W 2020 Dynamics of porous and amorphous magnesium borohydride to understand solid state Mg-ion-conductors *Sci. Rep.* **10** 9080
- [116] Pistidda C et al 2010 Synthesis of amorphous $\text{Mg}(\text{BH}_4)_2$ from MgB_2 and H_2 at room temperature *J. Alloys Compd.* **508** 212–5
- [117] Filinchuk Y, Richter B, Jensen T R, Dmitriev V, Chernyshov D and Hagemann H 2011 Porous and dense magnesium borohydride frameworks: synthesis, stability, and reversible absorption of guest species *Angew. Chem., Int. Ed.* **50** 11162–6
- [118] Ban V, Soloninin A V, Skripov A V, Hadermann J, Abakumov A and Filinchuk Y 2014 Pressure-collapsed amorphous $\text{Mg}(\text{BH}_4)_2$: an ultradense complex hydride showing a reversible transition to the porous framework *J. Phys. Chem. C* **118** 23402–8
- [119] Nakamori Y, Miwa K, Ninomiya A, Li H, Ohba N, Towata S, Züttel A and Orimo S 2006 Correlation between thermodynamical stabilities of metal borohydrides and cation electronegativities: first-principles calculations and experiments *Phys. Rev. B* **74** 045126
- [120] Flacau R, Ratcliffe C I, Desgreniers S, Yao Y, Klug D D, Pallister P, Moudrakovski I L and Ripmeester J A 2010 Structure and dynamics of ammonium borohydride *Chem. Commun.* **46** 9164
- [121] Frommen C, Sørby M, Heere M, Humphries T, Olsen J and Hauback B 2017 Rare earth borohydrides—crystal structures and thermal properties *Energies* **10** 2115
- [122] Ley M B, Jørgensen M, Černý R, Filinchuk Y and Jensen T R 2016 From $\text{M}(\text{BH}_4)_3$ ($M = \text{La, Ce}$) borohydride frameworks to controllable synthesis of porous hydrides and ion conductors *Inorg. Chem.* **55** 9748–56
- [123] Payandeh Gharibdoust S, Heere M, Nervi C, Sørby M H, Hauback B C and Jensen T R 2018 Synthesis, structure, and polymorphic transitions of praseodymium(iii) and neodymium(iii) borohydride, $\text{Pr}(\text{BH}_4)_3$ and $\text{Nd}(\text{BH}_4)_3$ *Dalt. Trans.* **47** 8307–19
- [124] Gigante A, Payandeh S, Grinderslev J B, Heere M, Embs J P, Jensen T R, Burankova T, Remhof A and Hagemann H 2021 Structural and dynamic studies of $\text{Pr}(\text{11BH}_4)_3$ *Int. J. Hydrog. Energy* **46** 32126–34
- [125] Wegner W, Jaroń T and Grochala W 2018 Preparation of a series of lanthanide borohydrides and their thermal decomposition to refractory lanthanide borides *J. Alloys Compd.* **744** 57–63
- [126] Shannon R D 1976 Revised effective ionic radii and systematic studies of interatomic distances in halides and chalcogenides *Acta Crystallogr. A* **32** 751–67
- [127] Černý R, Severa G, Ravnsbæk D B, Filinchuk Y, D'Anna V, Hagemann H, Haase D, Jensen C M and Jensen T R 2010 $\text{NaSc}(\text{BH}_4)_4$: a novel scandium-based borohydride *J. Phys. Chem. C* **114** 1357–64
- [128] Hagemann H, Longhini M, Kaminski J W, Wesolowski T A, Černý R, Penin N, Sørby M H, Hauback B C, Severa G and Jensen C M 2008 $\text{LiSc}(\text{BH}_4)_4$: a novel salt of Li^+ and discrete $\text{Sc}(\text{BH}_4)_4^-$ complex anions *J. Phys. Chem. A* **112** 7551–5
- [129] Černý R, Ravnsbæk D B, Severa G, Filinchuk Y, D'Anna V, Hagemann H, Haase D, Skibsted J, Jensen C M and Jensen T R 2010 Structure and characterization of $\text{KSc}(\text{BH}_4)_4$ *J. Phys. Chem. C* **114** 19540–9
- [130] Ravnsbæk D, Filinchuk Y, Cerenius Y, Jakobsen H J, Besenbacher F, Skibsted J and Jensen T R 2009 A series of mixed-metal borohydrides *Angew. Chem., Int. Ed.* **48** 6659–63
- [131] Nielsen T K, Karkamkar A, Bowden M, Besenbacher F, Jensen T R and Autrey T 2013 Methods to stabilize and destabilize ammonium borohydride *Dalt. Trans.* **42** 680–7
- [132] Karkamkar A, Kathmann S M, Schenter G K, Heldebrant D J, Hess N, Gutowski M and Autrey T 2009 Thermodynamic and structural investigations of ammonium borohydride, a solid with a highest content of thermodynamically and kinetically accessible hydrogen *Chem. Mater.* **21** 4356–8
- [133] Schouwink P, Morelle F, Sadikin Y, Filinchuk Y and Černý R 2015 Increasing hydrogen density with the cation-anion pair $\text{BH}_4^- - \text{NH}_4^+$ in perovskite-type $\text{NH}_4\text{Ca}(\text{BH}_4)_3$ *Energies* **8** 8286–99
- [134] Wegner W, Fijalkowski K J and Grochala W 2020 A low temperature pyrolytic route to amorphous quasi-hexagonal boron nitride from hydrogen rich $(\text{NH}_4)_3\text{Mg}(\text{BH}_4)_5$ *Dalt. Trans.* **49** 336–42
- [135] Starobrat A, Jaroń T and Grochala W 2018 New hydrogen-rich ammonium metal borohydrides, $\text{NH}_4[\text{M}(\text{BH}_4)_4]$, $M = \text{Y, Sc, Al}$, as potential H_2 sources *Dalt. Trans.* **47** 4442–8
- [136] Dovgaliuk I, Safin D A, Tumanov N A, Morelle F, Moulai A, Černý R, Łodziana Z, Devillers M and Filinchuk Y 2017 Solid aluminum borohydrides for prospective hydrogen storage *ChemSusChem* **10** 4725–34
- [137] Lohstroh W and Heere M 2020 Structure and dynamics of borohydrides studied by neutron scattering techniques: a review *J. Phys. Soc. Japan* **89** 051011
- [138] Andersson M S, Grinderslev J B, Jensen T R, García Sakai V, Häussermann U, Udovic T J and Karlsson M 2020 Interplay of NH_4^+ and BH_4^- reorientational dynamics in NH_4BH_4 *Phys. Rev. Mater.* **4** 085002
- [139] Filippov S, Grinderslev J B, Andersson M S, Armstrong J, Karlsson M, Jensen T R, Klarbring J, Simak S I and Häussermann U 2019 Analysis of dihydrogen bonding in ammonium borohydride *J. Phys. Chem. C* **123** 28631–9
- [140] Christmann J, Mansouri A, Grinderslev J B, Jensen T R and Hagemann H 2020 Probing the local symmetry of Tb^{3+} in borohydrides using luminescence spectroscopy *J. Lumin.* **221** 117065
- [141] Jørgensen M, Lee Y-S, Bjerring M, Jepsen L H, Akbey Ü, Cho Y W and Jensen T R 2018 Disorder induced polymorphic transitions in the high hydrogen density compound $\text{Sr}(\text{BH}_4)_2(\text{NH}_3\text{BH}_3)_2$ *Dalt. Trans.* **47** 16737–46
- [142] Jepsen L H, Ban V, Møller K T, Lee Y-S, Cho Y W, Besenbacher F, Filinchuk Y, Skibsted J and Jensen T R 2014 Synthesis, crystal structure, thermal decomposition, and ^{11}B MAS NMR characterization of $\text{Mg}(\text{BH}_4)_2(\text{NH}_3\text{BH}_3)_2$ *J. Phys. Chem. C* **118** 12141–53
- [143] Dovgaliuk I, Le Duff C S, Robeyns K, Devillers M and Filinchuk Y 2015 Mild dehydrogenation of ammonia borane complexed with aluminum borohydride *Chem. Mater.* **27** 768–77

- [144] Corno M, Pinatel E, Ugliengo P and Baricco M 2011 A computational study on the effect of fluorine substitution in LiBH_4 *J. Alloys Compd.* **509** S679–83
- [145] Rude L H et al 2013 Hydrogen–fluorine exchange in NaBH_4 – NaBF_4 *Phys. Chem. Chem. Phys.* **15** 18185
- [146] Heyn R H, Saldan I, Sørby M H, Frommen C, Arstad B, Bougza A M, Fjellvåg H and Hauback B C 2013 Structural and spectroscopic characterization of potassium fluoroborohydrides *Phys. Chem. Chem. Phys.* **15** 11226
- [147] Pinatel E R, Corno M, Ugliengo P and Baricco M 2014 Effects of metastability on hydrogen sorption in fluorine substituted hydrides *J. Alloys Compd.* **615** S706–10
- [148] Richter B, Ravnsbæk D B, Sharma M, Spyratou A, Hagemann H and Jensen T R 2017 Fluoride substitution in LiBH_4 ; destabilization and decomposition *Phys. Chem. Chem. Phys.* **19** 30157–65
- [149] Olsen J E, Sørby M H and Hauback B C 2011 Chloride-substitution in sodium borohydride *J. Alloys Compd.* **509** L228–31
- [150] Rude L H et al 2011 Bromide substitution in lithium borohydride, LiBH_4 – LiBr *Int. J. Hydrog. Energy* **36** 15664–72
- [151] Rude L H, Groppo E, Arnbjerg L M, Ravnsbæk D B, Malmkjær R A, Filinchuk Y, Baricco M, Besenbacher F and Jensen T R 2011 Iodide substitution in lithium borohydride, LiBH_4 – LiI *J. Alloys Compd.* **509** 8299–305
- [152] Ravnsbæk D B, Rude L H and Jensen T R 2011 Chloride substitution in sodium borohydride *J. Solid State Chem.* **184** 1858–66
- [153] Blanchard D et al 2012 Hindered rotational energy barriers of BH_4 –tetrahedra in β - $\text{Mg}(\text{BH}_4)_2$ from quasielastic neutron scattering and DFT calculations *J. Phys. Chem. C* **116** 2013–23
- [154] Maekawa H, Matsuo M, Takamura H, Ando M, Noda Y, Karahashi T and Orimo S 2009 Halide-stabilized LiBH_4 , a room-temperature lithium fast-ion conductor *J. Am. Chem. Soc.* **131** 894–5
- [155] Gulino V, Brighi M, Dematteis E M, Murgia F, Nervi C, Černý R and Baricco M 2019 Phase stability and fast ion conductivity in the hexagonal LiBH_4 – LiBr – LiCl solid solution *Chem. Mater.* **31** 5133–44
- [156] Cascallana-Matias I, Keen D A, Cussen E J and Gregory D H 2015 Phase behavior in the LiBH_4 – LiBr system and structure of the anion-stabilized fast ionic, high temperature Phase *Chem. Mater.* **27** 7780–7
- [157] Gulino V, Dematteis E M, Corno M, Palumbo M and Baricco M 2021 Theoretical and experimental studies of LiBH_4 – LiBr phase diagram *ACS Appl. Energy Mater.* **4** 7327–37
- [158] Zavorotynska O, Corno M, Pinatel E, Rude L H, Ugliengo P, Jensen T R and Baricco M 2012 Theoretical and experimental study of LiBH_4 – LiCl solid solution *Crystals* **2** 144–58
- [159] Sangster J and Pelton A D 1987 Phase diagrams and thermodynamic properties of the 70 binary alkali halide systems having common ions *J. Phys. Chem. Ref. Data* **16** 509–61
- [160] Dematteis E M, Roedern E, Pinatel E R, Corno M, Jensen T R and Baricco M 2016 A thermodynamic investigation of the LiBH_4 – NaBH_4 system *RSC Adv.* **6** 60101–8
- [161] Dematteis E M, Pinatel E R, Corno M, Jensen T R and Baricco M 2017 Phase diagrams of the LiBH_4 – NaBH_4 – KBH_4 system *Phys. Chem. Chem. Phys.* **19** 25071–9
- [162] Ravnsbæk D B, Sørensen L H, Filinchuk Y, Reed D, Book D, Jakobsen H J, Besenbacher F, Skibsted J and Jensen T R 2010 Mixed-anion and mixed-cation borohydride $\text{KZn}(\text{BH}_4)\text{Cl}_2$: synthesis, structure and thermal decomposition *Eur. J. Inorg. Chem.* **2010** 1608–12
- [163] Payandeh Gharibdoust S, Brighi M, Sadikin Y, Ravnsbæk D B, Černý R, Skibsted J and Jensen T R 2017 Synthesis, structure, and Li-Ion conductivity of $\text{LiLa}(\text{BH}_4)_3$, X, X = Cl, Br, I *J. Phys. Chem. C* **121** 19010–21
- [164] Pistidda C et al 2014 Effect of the partial replacement of CaH_2 with CaF_2 in the mixed system CaH_2 + MgB_2 *J. Phys. Chem. C* **118** 28409–17
- [165] Alcantara K S et al 2012 3CaH_2 + 4MgB_2 + CaF_2 reactive hydride composite as a potential hydrogen storage material: hydrogenation and dehydrogenation pathway *J. Phys. Chem. C* **116** 7207–12
- [166] Puzkiel J et al 2014 Hydrogen storage in Mg – LiBH_4 composites catalyzed by FeF_3 *J. Power Sources* **267** 799–811
- [167] Saldan I et al 2013 Hydrogen sorption in the LiH – LiF – MgB_2 system *J. Phys. Chem. C* **117** 17360–6
- [168] Saldan I, Gosalawit-Utke R, Pistidda C, Bösenberg U, Schulze M, Jensen T R, Taube K, Dornheim M and Klassen T 2012 Influence of stoichiometry on the hydrogen sorption behavior in the LiF – MgB_2 system *J. Phys. Chem. C* **116** 7010–5
- [169] Gosalawit-Utke R et al 2011 $\text{Ca}(\text{BH}_4)_2$ – MgF_2 reversible hydrogen storage: reaction mechanisms and kinetic properties *J. Phys. Chem. C* **115** 3762–8
- [170] Suarez-Alcantara K, Sørby M H, Pistidda C, Karimi F, Saldan I, Hauback B C, Klassen T and Dornheim M 2015 Synchrotron diffraction studies of hydrogen absorption/desorption on CaH_2 + MgB_2 reactive hydride composite mixed with fluorinated compounds *J. Phys. Chem. C* **119** 11430–7
- [171] Bonatto Minella C et al 2011 Effect of transition metal fluorides on the sorption properties and reversible formation of $\text{Ca}(\text{BH}_4)_2$ *J. Phys. Chem. C* **115** 2497–504
- [172] Albanese E, Kalantzopoulos G N, Vitillo J G, Pinatel E, Civalieri B, Deledda S, Bordiga S, Hauback B C and Baricco M 2013 Theoretical and experimental study on $\text{Mg}(\text{BH}_4)_2$ – $\text{Zn}(\text{BH}_4)_2$ mixed borohydrides *J. Alloys Compd.* **580** S282–6
- [173] Paskevicius M, Ley M B, Sheppard D A, Jensen T R and Buckley C E 2013 Eutectic melting in metal borohydrides *Phys. Chem. Chem. Phys.* **15** 19774
- [174] Ley M B, Roedern E and Jensen T R 2014 Eutectic melting of LiBH_4 – KBH_4 *Phys. Chem. Chem. Phys.* **16** 24194–9
- [175] Jensen S R H, Jepsen L H, Skibsted J and Jensen T R 2015 Phase diagram for the NaBH_4 – KBH_4 system and the stability of a $\text{Na}_{(1-x)}\text{K}_x\text{BH}_4$ solid solution *J. Phys. Chem. C* **119** 27919–29
- [176] Bardaji E G, Zhao-Karger Z, Boucharat N, Nale A, van Setten M J, Lohstroh W, Röhm E, Catti M and Fichtner M 2011 LiBH_4 – $\text{Mg}(\text{BH}_4)_2$: a physical mixture of metal borohydrides as hydrogen storage material *J. Phys. Chem. C* **115** 6095–101
- [177] Ley M, Roedern E, Thygesen P and Jensen T 2015 Melting behavior and thermolysis of NaBH_4 – $\text{Mg}(\text{BH}_4)_2$ and NaBH_4 – $\text{Ca}(\text{BH}_4)_2$ composites *Energies* **8** 2701–13
- [178] Schouwink P, D’Anna V, Ley M B, Lawson Daku L M, Richter B, Jensen T R, Hagemann H and Černý R 2012 Bimetallic borohydrides in the system $\text{M}(\text{BH}_4)_2$ – KBH_4 (M = Mg, Mn): on the structural diversity *J. Phys. Chem. C* **116** 10829–40
- [179] Dematteis E M and Baricco M 2019 Hydrogen desorption in $\text{Mg}(\text{BH}_4)_2$ – $\text{Ca}(\text{BH}_4)_2$ system *Energies* **12** 3230
- [180] Peru F, Payandeh S, Charalambopoulou G, Jensen T R and Steriotis T 2020 Hydrogen sorption and reversibility of the LiBH_4 – KBH_4 eutectic system confined in a CMK-3 type carbon via melt infiltration *J. Carbon Res.* **6** 19
- [181] Fang Z Z, Wang P, Rufford T E, Kang X D, Lu G Q and Cheng H M 2008 Kinetic- and thermodynamic-based improvements of lithium borohydride incorporated into activated carbon *Acta Mater.* **56** 6257–63
- [182] Roedern E, Hansen B R S, Ley M B and Jensen T R 2015 Effect of eutectic melting, reactive hydride composites, and nanoconfinement on decomposition and reversibility of LiBH_4 – KBH_4 *J. Phys. Chem. C* **119** 25818–25

- [183] Ampoumogli A, Charalambopoulou G, Javadian P, Richter B, Jensen T R and Steriotis T 2015 Hydrogen desorption and cycling properties of composites based on mesoporous carbons and a $\text{LiBH}_4\text{-Ca}(\text{BH}_4)_2$ eutectic mixture *J. Alloys Compd.* **645** S480–4
- [184] Callini E *et al* 2016 Nanostructured materials for solid-state hydrogen storage: a review of the achievement of COST action MP1103 *Int. J. Hydrog. Energy* **41** 14404–28
- [185] Albanese E, Corno M, Baricco M and Civalleri B 2021 Simulation of nanosizing effects in the decomposition of $\text{Ca}(\text{BH}_4)_2$ through atomistic thin film models *Res. Chem. Intermed.* **47** 345–56
- [186] Dematteis E M, Pistidda C, Dornheim M and Baricco M 2019 Exploring ternary and quaternary mixtures in the $\text{LiBH}_4\text{-NaBH}_4\text{-KBH}_4\text{-Mg}(\text{BH}_4)_2\text{-Ca}(\text{BH}_4)_2$ system *ChemPhysChem* **20** 1348–59
- [187] Dematteis E M, Santoru A, Poletti M G, Pistidda C, Klassen T, Dornheim M and Baricco M 2018 Phase stability and hydrogen desorption in a quinary equimolar mixture of light-metals borohydrides *Int. J. Hydrog. Energy* **43** 16793–803
- [188] Paskevicius M, Sheppard D A and Buckley C E 2010 Thermodynamic changes in mechanochemically synthesized magnesium hydride nanoparticles *J. Am. Chem. Soc.* **132** 5077–83
- [189] Yan Y, Remhof A, Hwang S-J, Li H-W, Mauron P, Orimo S and Züttel A 2012 Pressure and temperature dependence of the decomposition pathway of LiBH_4 *Phys. Chem. Chem. Phys.* **14** 6514
- [190] Pitt M P, Paskevicius M, Brown D H, Sheppard D A and Buckley C E 2013 Thermal Stability of $\text{Li}_2\text{B}_{12}\text{H}_{12}$ and its role in the decomposition of LiBH_4 *J. Am. Chem. Soc.* **135** 6930–41
- [191] Jensen S R H, Paskevicius M, Hansen B R S, Jakobsen A S, Møller K T, White J L, Allendorf M D, Stavila V, Skibsted J and Jensen T R 2018 Hydrogenation properties of lithium and sodium hydride—closo -borate, $[\text{B}_{10}\text{H}_{10}]^{2-}$ and $[\text{B}_{12}\text{H}_{12}]^{2-}$, composites *Phys. Chem. Chem. Phys.* **20** 16266–75
- [192] Paskevicius M, Pitt M P, Webb C J, Sheppard D A, Filso U, Gray E M and Buckley C E 2012 *In-situ* x-ray diffraction study of $\gamma\text{-Mg}(\text{BH}_4)_2$ decomposition *J. Phys. Chem. C* **116** 15231–40
- [193] Johnson S, Demaria J, Ginovska B, Edverson G, Hagemann H and Autrey S T 2022 Exploring detailed reaction pathways for hydrogen storage with borohydrides using DFT calculations *Energy Fuels* **36** 5513–27
- [194] Saldan I 2016 Decomposition and formation of magnesium borohydride *Int. J. Hydrog. Energy* **41** 11201–24
- [195] Barkhordarian G, Jensen T R, Doppiu S, Bösenberg U, Borgschulte A, Gremaud R, Cerenius Y, Dornheim M, Klassen T and Bormann R 2008 Formation of $\text{Ca}(\text{BH}_4)_2$ from hydrogenation of $\text{CaH}_2\text{+MgB}_2$ composite *J. Phys. Chem. C* **112** 2743–9
- [196] Barkhordarian G, Klassen T, Dornheim M and Bormann R 2007 Unexpected kinetic effect of MgB_2 in reactive hydride composites containing complex borohydrides *J. Alloys Compd.* **440** L18–L21
- [197] Garroni S *et al* 2013 Mechanochemical synthesis of NaBH_4 starting from NaH-MgB_2 reactive hydride composite system *Int. J. Hydrog. Energy* **38** 2363–9
- [198] Severa G, Rönnebro E and Jensen C M 2010 Direct hydrogenation of magnesium boride to magnesium borohydride: demonstration of >11 weight percent reversible hydrogen storage *Chem. Commun.* **46** 421–3
- [199] Rönnebro E and Majzoub E H 2007 Calcium borohydride for hydrogen storage: catalysis and reversibility *J. Phys. Chem. B* **111** 12045–7
- [200] Pitt M P, Webb C J, Paskevicius M, Sheptyakov D, Buckley C E and Gray E M 2011 *In situ* neutron diffraction study of the deuteration of isotopic Mg_{11}B_2 *J. Phys. Chem. C* **115** 22669–79
- [201] Møller K T, Fogh A S, Paskevicius M, Skibsted J and Jensen T R 2016 Metal borohydride formation from aluminium boride and metal hydrides *Phys. Chem. Chem. Phys.* **18** 27545–53
- [202] Vitillo J G, Bordiga S and Baricco M 2015 Spectroscopic and structural characterization of thermal decomposition of $\gamma\text{-Mg}(\text{BH}_4)_2$: dynamic vacuum versus H_2 atmosphere *J. Phys. Chem. C* **119** 25340–51
- [203] Yan Y, Remhof A, Rentsch D and Züttel A 2015 The role of $\text{MgB}_{12}\text{H}_{12}$ in the hydrogen desorption process of $\text{Mg}(\text{BH}_4)_2$ *Chem. Commun.* **51** 700–2
- [204] Chong M, Karkamkar A, Autrey T, Orimo S, Jalisatgi S and Jensen C M 2011 Reversible dehydrogenation of magnesium borohydride to magnesium triborane in the solid state under moderate conditions *Chem. Commun.* **47** 1330–2
- [205] Chong M, Matsuo M, Orimo S, Autrey T and Jensen C M 2015 Selective reversible hydrogenation of $\text{Mg}(\text{B}_3\text{H}_8)_2/\text{MgH}_2$ to $\text{Mg}(\text{BH}_4)_2$: pathway to reversible borane-based hydrogen storage? *Inorg. Chem.* **54** 4120–5
- [206] Dovgaliuk I, Møller K T, Robeyns K, Louppe V, Jensen T R and Filinchuk Y 2019 Complexation of ammonia boranes with Al^{3+} *Inorg. Chem.* **58** 4753–60
- [207] Ravnsbaek D B, Sørensen L H, Filinchuk Y, Besenbacher F and Jensen T R 2012 Screening of metal borohydrides by mechanochemistry and diffraction *Angew. Chem., Int. Ed.* **51** 3582–6
- [208] Lindemann I, Domènech Ferrer R, Dunsch L, Filinchuk Y, Černý R, Hagemann H, D'Anna V, Lawson Daku L M, Schultz L and Gutfleisch O 2010 $\text{Al}_3\text{Li}_4(\text{BH}_4)_{13}$: a complex double-cation borohydride with a new structure *Chem. Eur. J.* **16** 8707–12
- [209] Sharma M, Didelot E, Spyratou A, Lawson Daku L M, Černý R and Hagemann H 2016 Halide free $\text{M}(\text{BH}_4)_2$ ($\text{M} = \text{Sr, Ba, and Eu}$) synthesis, structure, and decomposition *Inorg. Chem.* **55** 7090–7
- [210] Mosegaard L, Møller B, Jørgensen J-E, Filinchuk Y, Cerenius Y, Hanson J C, Dimasi E, Besenbacher F and Jensen T R 2008 Reactivity of LiBH_4 : *in situ* synchrotron radiation powder x-ray diffraction study *J. Phys. Chem. C* **112** 1299–303
- [211] Jeong S *et al* 2020 A mechanistic analysis of phase evolution and hydrogen storage behavior in nanocrystalline $\text{Mg}(\text{BH}_4)_2$ within reduced graphene oxide *ACS Nano* **14** 1745–56
- [212] Schneemann A *et al* 2020 Nanoconfinement of molecular magnesium borohydride captured in a bipyridine-functionalized metal–organic framework *ACS Nano* **14** 10294–304
- [213] Li S *et al* 2021 Spontaneous dynamical disordering of borophenes in MgB_2 and related metal borides *Nat. Commun.* **12** 6268
- [214] Ray K G, Klebanoff L E, Lee J R I, Stavila V, Heo T W, Shea P, Baker A A, Kang S Y, Wan L F and Wood B C 2022 *Understanding hydrogenation chemistry at MgB_2 reactive edges from Ab Initio molecular dynamics* *ACS Appl. Mater. Interfaces* **14** 20430–42
- [215] Ray K G *et al* 2017 Elucidating the mechanism of MgB_2 initial hydrogenation via a combined experimental–theoretical study *Phys. Chem. Chem. Phys.* **19** 22646–58
- [216] Liu Y-S *et al* 2020 Nanoscale Mg-B via surfactant ball milling of MgB_2 : morphology, composition, and improved hydrogen storage properties *J. Phys. Chem. C* **124** 21761–71
- [217] Hansen B R S, Paskevicius M, Li H-W, Akiba E and Jensen T R 2016 Metal boranes: progress and applications *Coord. Chem. Rev.* **323** 60–70
- [218] Moury R, Gigante A, Remhof A, Roedern E and Hagemann H 2020 Experimental investigation of $\text{Mg}(\text{B}_3\text{H}_8)_2$ dimensionality, materials for energy storage applications *Dalt. Trans.* **49** 12168–73
- [219] Andersson M S, Grinderslev J B, Chen X-M, Chen X, Häussermann U, Zhou W, Jensen T R, Karlsson M and Udovic T J 2021 Interplay between the reorientational dynamics of the B_3H_8^- anion and the structure in KB_3H_8 *J. Phys. Chem. C* **125** 3716–24

- [220] Grinderslev J B, Møller K T, Yan Y, Chen X-M, Li Y, Li H-W, Zhou W, Skibsted J, Chen X and Jensen T R 2019 Potassium octahydridotriborate: diverse polymorphism in a potential hydrogen storage material and potassium ion conductor *Dalt. Trans.* **48** 8872–81
- [221] Zavorotynska O, Sørby M H, Vitillo J G, Deledda S, Frommen C and Hauback B C 2021 Experimental and computational characterization of phase transitions in CsB₃H₈ *Phys. Chem. Chem. Phys.* **23** 17836–47
- [222] Nayyar I H, Ginovska B, Bowden M, Edverson G and Autrey T 2022 Analysis of intermediates and products from the dehydrogenation of Mg(BH₄)₂ *J. Phys. Chem.* **126** 444–52
- [223] Wan L F, Autrey T and Wood B C 2022 First-principles elucidation of initial dehydrogenation pathways in Mg(BH₄)₂ *J. Phys. Chem. Lett.* **13** 1908–13
- [224] Gigante A et al 2021 Thermal conversion of unsolvated Mg(B₃H₈)₂ to BH₄—in the presence of MgH₂ *ACS Appl. Energy Mater.* **4** 3737–47
- [225] Kang S, Heo T W, Allendorf M D and Wood B C 2019 Morphology-dependent stability of complex metal hydrides and their intermediates using first-principles calculations *ChemPhysChem* **20** 1340–7
- [226] Nayyar I H, Ginovska B, Bowden M, Edverson G, Tran B and Autrey T 2022 Analysis of intermediates and products from the dehydrogenation of Mg(BH₄)₂ *J. Phys. Chem. A* **126** 444–52
- [227] Chong M, Autrey T and Jensen C 2017 Lewis base complexes of magnesium borohydride: enhanced kinetics and product selectivity upon hydrogen release *Inorganics* **5** 89
- [228] Tran B L, Allen T N, Bowden M E, Autrey T and Jensen C M 2021 Effects of glymes on the distribution of Mg(B₁₀H₁₀) and Mg(B₁₂H₁₂) from the thermolysis of Mg(BH₄)₂ *Inorganics* **9** 41
- [229] Liu X-R, Chen X-M, Zhang J, Jensen T R and Chen X 2019 The interconversion between THF·B₃H₇ and B₃H₈[−]: an efficient synthetic method for MB₃H₈ (M = Li and Na) *Dalt. Trans.* **48** 5140–3
- [230] Souza D H P, Møller K T, Moggach S A, Humphries T D, D'Angelo A M, Buckley C E and Paskevicius M 2021 Hydrated alkali-B₁₁H₁₄ salts as potential solid-state electrolytes *J. Mater. Chem. A* **9** 15027–37
- [231] Jørgensen M, Zhou W, Wu H, Udovic T J, Paskevicius M, Černý R and Jensen T R 2021 Polymorphism of calcium decahydrido-closo-decaborate and characterization of its hydrates *Inorg. Chem.* **60** 10943–57
- [232] Paskevicius M, Hansen B R S, Jørgensen M, Richter B and Jensen T R 2017 Multifunctionality of silver closo-boranes *Nat. Commun.* **8** 15136
- [233] Jørgensen M, Lee Y-S, Paskevicius M, Hansen B R S and Jensen T R 2021 Synthesis and crystal structures of decahydro-closo-decaborates of the divalent cations of strontium and manganese *J. Solid State Chem.* **298** 122133
- [234] Li S, Qiu P, Kang J, Ma Y, Zhang Y, Yan Y, Jensen T R, Guo Y, Zhang J and Chen X 2021 Iodine-substituted lithium/sodium closo-decaborates: syntheses, characterization, and solid-state ionic conductivity *ACS Appl. Mater. Interfaces* **13** 17554–64
- [235] Hansen B R S, Paskevicius M, Jørgensen M and Jensen T R 2017 Halogenated sodium-closo-dodecaboranes as solid-state ion conductors *Chem. Mater.* **29** 3423–30
- [236] Bukovsky E V, Peryshkov D V, Wu H, Zhou W, Tang W S, Jones W M, Stavila V, Udovic T J and Strauss S H 2017 Comparison of the coordination of B₁₂F₁₂[−], B₁₂Cl₁₂[−], and B₁₂H₁₂[−] to Na⁺ in the solid state: crystal structures and thermal behavior of Na₂(B₁₂F₁₂), Na₂(H₂O)4(B₁₂F₁₂), Na₂(B₁₂Cl₁₂), and Na₂(H₂O)6(B₁₂C₁₂) *Inorg. Chem.* **56** 4369–79
- [237] Møller K T, Paskevicius M, Andreasen J G, Lee J, Chen-Tan N, Overgaard J, Payandeh S, Silvester D S, Buckley C E and Jensen T R 2019 Molten metal closo-borate solvates *Chem. Commun.* **55** 3410–3
- [238] Jørgensen M, Hansen B R S, Lee Y-S, Cho Y W and Jensen T R 2019 Crystal structures and energy storage properties of ammine sodium decahydro-closo-decaboranes (Na₂B₁₀H₁₀·nNH₃, n = 1, 2) *J. Phys. Chem. C* **123** 20160–6
- [239] Hansen B R S, Tumanov N, Santoru A, Pistidda C, Bednarcik J, Klassen T, Dornheim M, Filinchuk Y and Jensen T R 2017 Synthesis, structures and thermal decomposition of ammine M_xB₁₂H₁₂ complexes (M = Li, Na, Ca) *Dalt. Trans.* **46** 7770–81
- [240] Grinderslev J B, Lee Y-S, Paskevicius M, Møller K T, Yan Y, Cho Y W and Jensen T R 2020 Ammonium–ammonia complexes, N₂H₇⁺, in ammonium closo-borate amines: synthesis, structure, and properties *Inorg. Chem.* **59** 11449–58
- [241] Jørgensen M, Jensen S R H, Humphries T D, Rowles M R, Sofianos M V, Buckley C E, Jensen T R and Paskevicius M 2020 Hydroxylated closo-dodecaborates M₂B₁₂(OH)₁₂ (M = Li, Na, K, and Cs); structural analysis, thermal properties, and solid-state ionic conductivity *J. Phys. Chem. C* **124** 11340–9
- [242] Huang J, Tan Y, Su J, Gu Q, Černý R, Ouyang L, Sun D, Yu X and Zhu M 2015 Synthesis, structure and dehydrogenation of zirconium borohydride octaammoniate *Chem. Commun.* **51** 2794–7
- [243] Yuan F, Gu Q, Guo Y, Sun W, Chen X and Yu X 2012 Structure and hydrogen storage properties of the first rare-earth metal borohydride ammoniate: γ(BH₄)₃·4NH₃ *J. Mater. Chem.* **22** 1061–8
- [244] Grinderslev J B, Andersson M S, Trump B A, Zhou W, Udovic T J, Karlsson M and Jensen T R 2021 Neutron scattering investigations of the global and local structures of ammine yttrium borohydrides *J. Phys. Chem. C* **125** 15415–23
- [245] Yan Y, Grinderslev J B, Lee Y-S, Jørgensen M, Cho Y W, Černý R and Jensen T R 2020 Ammonia-assisted fast Li-ion conductivity in a new hemiammine lithium borohydride, LiBH₄·1/2NH₃ *Chem. Commun.* **56** 3971–4
- [246] Johnson S R, David W I, Royse D M, Sommariva M, Tang C Y, Fabbiani F P, Jones M O and Edwards P P 2009 the monoammoniate of lithium borohydride, Li(NH₃)BH₄: an effective ammonia storage compound *Chem. Asian J.* **4** 849–54
- [247] Sullivan E A and Johnson S 1959 The lithium borohydride–ammonia system P–C–T relationships and densities *J. Phys. Chem.* **63** 233–8
- [248] Semenenko K N, Shilkin S P and Polyakova V B 1975 Synthesis and structure of amines of beryllium and magnesium borohydrides *Bull. Acad. Sci. USSR, Div. Chem. Sci.* **24** 661–3
- [249] Yan Y, Dononelli W, Jørgensen M, Grinderslev J B, Lee Y-S, Cho Y W, Černý R, Hammer B and Jensen T R 2020 The mechanism of Mg₂⁺ conduction in ammine magnesium borohydride promoted by a neutral molecule *Phys. Chem. Chem. Phys.* **22** 9204–9
- [250] Soloveichik G, Her J-H, Stephens P W, Gao Y, Rijssenbeek J, Andrus M and Zhao J-C 2008 Ammine magnesium borohydride complex as a new material for hydrogen storage: structure and properties of Mg(BH₄)₂·2NH₃ *Inorg. Chem.* **47** 4290–8
- [251] Jepsen L H, Ley M B, Filinchuk Y, Besenbacher F and Jensen T R 2015 Tailoring the properties of ammine metal borohydrides for solid-state hydrogen storage *ChemSusChem* **8** 1452–63
- [252] Chu H, Wu G, Xiong Z, Guo J, He T and Chen P 2010 Structure and hydrogen storage properties of calcium borohydride diammoniate *Chem. Mater.* **22** 6021–8
- [253] Tang Z, Tan Y, Gu Q and Yu X 2012 A novel aided-cation strategy to advance the dehydrogenation of calcium borohydride monoammoniate *J. Mater. Chem.* **22** 5312

- [254] Gradišek A, Jepsen L H, Jensen T R and Conradi M S 2016 Nuclear magnetic resonance study of molecular dynamics in ammine metal borohydride $\text{Sr}(\text{BH}_4)_2(\text{NH}_3)_2$ *J. Phys. Chem. C* **120** 24646–54
- [255] Grinderslev J B, Amdisen M B and Jensen T R 2020 Synthesis, crystal structures and thermal properties of ammine barium borohydrides *Inorganics* **8** 57
- [256] Lobkovskij E B, Dorosinskij A L and Semenenko K N 1974 x-ray diffraction of aluminium boron hydride monoammine *Zh. Strukt. Khim.* **15** 70–73
- [257] Semenenko K N, Shilkin S P, Kravchenko O V and Polyakova V B 1974 Structure of hexaammines of aluminum borohydride and chloroborohydrides *Bull. Acad. Sci. USSR, Div. Chem. Sci.* **23** 1379–83
- [258] Yuan F, Gu Q, Chen X, Tan Y, Guo Y and Yu X 2012 Complex ammine titanium(III) borohydrides as advanced solid hydrogen-storage materials with favorable dehydrogenation properties *Chem. Mater.* **24** 3370–9
- [259] Tang Z, Yuan F, Gu Q, Tan Y, Chen X, Jensen C M and Yu X 2013 Scandium and vanadium borohydride ammoniates: enhanced dehydrogenation behavior upon coordinative expansion and establishment of $\text{H}\delta+\cdots-\delta\text{H}$ interactions *Acta Mater.* **61** 3110–9
- [260] Gu Q, Gao L, Guo Y, Tan Y, Tang Z, Wallwork K S, Zhang F and Yu X 2012 Structure and decomposition of zinc borohydride ammonia adduct: towards a pure hydrogen release *Energy Environ. Sci.* **5** 7590
- [261] Sun W, Chen X, Gu Q, Wallwork K S, Tan Y, Tang Z and Yu X 2012 A new ammine dual-cation (Li, Mg) borohydride: synthesis, structure, and dehydrogenation enhancement *Chem. Eur. J.* **18** 6825–34
- [262] Yang Y, Liu Y, Wu H, Zhou W, Gao M and Pan H 2014 An ammonia-stabilized mixed-cation borohydride: synthesis, structure and thermal decomposition behavior *Phys. Chem. Chem. Phys.* **16** 135–43
- [263] Guo Y, Wu H, Zhou W and Yu X 2011 Dehydrogenation tuning of ammine borohydrides using double-metal cations *J. Am. Chem. Soc.* **133** 4690–3
- [264] Xia G, Gu Q, Guo Y and Yu X 2012 Ammine bimetallic (Na, Zn) borohydride for advanced chemical hydrogen storage *J. Mater. Chem.* **22** 7300
- [265] Schrauzer G N 1955 Über ein Periodensystem der Metallboranate *Naturwissenschaften* **42** 438
- [266] Welchman E and Thonhauser T 2017 Decomposition mechanisms in metal borohydrides and their ammoniates *J. Mater. Chem. A* **5** 4084–92
- [267] Błoński P and Łodziana Z 2014 Correlation between the ionic potential and thermal stability of metal borohydrides: first-principles investigations *Phys. Rev. B* **90** 054114
- [268] Dovgaliuk I and Filinchuk Y 2016 Aluminium complexes of B- and N-based hydrides: synthesis, structures and hydrogen storage properties *Int. J. Hydrog. Energy* **41** 15489–504
- [269] Zheng X, Wu G, Li W, Xiong Z, He T, Guo J, Chen H and Chen P 2011 Releasing 17.8 wt% H_2 from lithium borohydride ammoniate *Energy Environ. Sci.* **4** 3593
- [270] Yang Y, Liu Y, Li Y, Gao M and Pan H 2015 Fluorine-substituted $\text{Mg}(\text{BH}_4)_2 \cdot 2\text{NH}_3$ with improved dehydrogenation properties for hydrogen storage *J. Mater. Chem. A* **3** 570–8
- [271] Guo Y, Xia G, Zhu Y, Gao L and Yu X 2010 Hydrogen release from ammine lithium borohydride, $\text{LiBH}_4 \cdot \text{NH}_3$ *Chem. Commun.* **46** 2599
- [272] Mostajeran M, Ye E, Desgreniers S and Baker R T 2017 Base-metal nanoparticle-catalyzed hydrogen release from ammine yttrium and lanthanum borohydrides *Chem. Mater.* **29** 742–51
- [273] Zheng X, Chua Y, Xiong Z, Chen W, Jiang Z, Wu G and Chen P 2015 The effect of NH_3 content on hydrogen release from $\text{LiBH}_4\text{-NH}_3$ system *Int. J. Hydrog. Energy* **40** 4573–8
- [274] Ngene P, Adelhelm P, Beale A M, de Jong K P and de Jongh P E 2010 $\text{LiBH}_4/\text{SBA-15}$ nanocomposites prepared by melt infiltration under hydrogen pressure: synthesis and hydrogen sorption properties *J. Phys. Chem. C* **114** 6163–8
- [275] Yang Y, Liu Y, Li Y, Zhang X, Gao M and Pan H 2015 Towards the endothermic dehydrogenation of nanoconfined magnesium borohydride ammoniate *J. Mater. Chem. A* **3** 11057–65
- [276] Chen P, Xiong Z, Luo J, Lin J and Tan K L 2003 Interaction between lithium amide and lithium hydride *J. Phys. Chem. B* **107** 10967–70
- [277] Xiong Z, Hu J, Wu G, Chen P, Luo W, Gross K and Wang J 2005 Thermodynamic and kinetic investigations of the hydrogen storage in the Li–Mg–N–H system *J. Alloys Compd.* **398** 235–9
- [278] Qiu S, Chu H, Zou Y, Xiang C, Xu F and Sun L 2017 Light metal borohydrides/amides combined hydrogen storage systems: composition, structure and properties *J. Mater. Chem. A* **5** 25112–30
- [279] Garroni S, Santoru A, Cao H, Dornheim M, Klassen T, Milanese C, Gennari F and Pistidda C 2018 recent progress and new perspectives on metal amide and imide systems for solid-state hydrogen storage *Energies* **11** 1027
- [280] Hu J, Liu Y, Wu G, Xiong Z, Chua Y S and Chen P 2008 Improvement of hydrogen storage properties of the Li–Mg–N–H system by addition of LiBH_4 *Chem. Mater.* **20** 4398–402
- [281] Zhang J, Wang Y, Zhang M, Leng Z, Gao M, Hu J, Liu Y and Pan H 2017 Improved overall hydrogen storage properties of a CsH and KH co-doped $\text{Mg}(\text{NH}_2)_2/2\text{LiH}$ system by forming mixed amides of Li–K and Cs–Mg *RSC Adv.* **7** 30357–64
- [282] Sheppard D A, Paskevicius M and Buckley C E 2011 Hydrogen desorption from the $\text{NaNH}_2\text{-MgH}_2$ system *J. Phys. Chem. C* **115** 8407–13
- [283] Liu B, Zhang B, Yuan J, Lv W and Wu Y 2021 Improvement of hydrogen dehydrogenation performance of lithium amide pyrolysis by ball milling with magnesium *Int. J. Hydrog. Energy* **46** 18423–32
- [284] Gizer G, Cao H, Puzskiel J, Pistidda C, Santoru A, Zhang W, He T, Chen P, Klassen T and Dornheim M 2019 Enhancement effect of bimetallic amide $\text{K}_2\text{Mn}(\text{NH}_2)_4$ and *in-situ* formed KH and Mn_3N on the dehydrogenation/hydrogenation properties of Li–Mg–N–H system *Energies* **12** 2779
- [285] Wang H et al 2018 $\text{Li}_2\text{NH-LiBH}_4$: a complex hydride with near ambient hydrogen adsorption and fast lithium ion conduction *Chem. Eur. J.* **24** 1342–7
- [286] Chua Y S, Xiong Z, Wu G and Chen P 2019 Ternary amide-hydride system: a study on $\text{LiAl}(\text{NH}_2)_4\text{-LiAlH}_4$ interaction *J. Alloys Compd.* **790** 597–601
- [287] Goshome K, Jain A, Miyaoka H, Yamamoto H, Kojima Y and Ichikawa T 2019 Eutectic phenomenon of $\text{LiNH}_2\text{-KH}$ composite in MH-NH_3 hydrogen storage system *Molecules* **24** 1348
- [288] Schur D V, Veziroglu A, Zaginaychenko S Y, Matysina Z A, Veziroglu T N, Gabdullin M T, Ramazanov T S, Zolonarenko A D and Zolonarenko A D 2019 Theoretical studies of lithium–aluminum amid and ammonium as perspective hydrogen storage *Int. J. Hydrog. Energy* **44** 24810–20
- [289] Li C, Li C, Fan M, Chen H, Shu K, Zhang Y, Gao M, Liu Y and Pan H 2019 Synthesis of a ternary amide $\text{LiK}(\text{NH}_2)$ and a novel $\text{Li}_3\text{K}(\text{NH}_2)_{4-x}\text{MgH}_2$ combination system for hydrogen storage *J. Energy Chem.* **35** 37–43

- [290] Gizer G, Puzskiel J, Cao H, Pistidda C, Le T T, Dornheim M and Klassen T 2019 Tuning the reaction mechanism and hydrogenation/dehydrogenation properties of $6\text{Mg}(\text{NH}_2)_2/29\text{LiH}$ system by adding LiBH_4 *Int. J. Hydrog. Energy* **44** 11920–9
- [291] Zhang Z, Cao H, Zhang W, Cui J, Xiong Z and Chen P 2020 Thermochemical transformation and reversible performance of $\text{Mg}(\text{NH}_2)_2\text{-NaMgH}_3$ system *Int. J. Hydrog. Energy* **45** 23069–75
- [292] White J L, Baker A A, Marcus M A, Snider J L, Wang T C, Lee J R I, Kilcoyne D A L, Allendorf M D, Stavila V and El Gabaly F 2020 The inside-outs of metal hydride dehydrogenation: imaging the phase evolution of the Li–N–H hydrogen storage system *Adv. Mater. Interfaces* **7** 1901905
- [293] Ping C, Feng B-Q, Ge J, Li G-Z, Zhu W, Teng Y-L, Zhang Y-R and Dong B-X 2020 Cyclic reaction-induced enhancement in the dehydrogenation performances of the KNH_2 -doped LiNH_2 and LiH system *Int. J. Hydrog. Energy* **45** 25927–34
- [294] Gao W, Guo J and Chen P 2019 Hydrides, amides and imides mediated ammonia synthesis and decomposition *Chin. J. Chem.* **37** 442–51
- [295] Paik B and Wolczyk A 2019 Lithium Imide (Li_2NH) as a solid-state electrolyte for electrochemical energy storage applications *J. Phys. Chem. C* **123** 1619–25
- [296] Makepeace J W, Brittain J M, Sukhwani Manghnani A, Murray C A, Wood T J and David W I F 2021 Compositional flexibility in Li–N–H materials: implications for ammonia catalysis and hydrogen storage *Phys. Chem. Chem. Phys.* **23** 15091–100
- [297] Yan H, Gao W, Wang Q, Guan Y, Feng S, Wu H, Guo Q, Cao H, Guo J and Chen P 2021 Lithium palladium hydride promotes chemical looping ammonia synthesis mediated by lithium imide and hydride *J. Phys. Chem. C* **125** 6716–22
- [298] Yu P, Wu H, Guo J, Wang P, Chang F, Gao W, Zhang W, Liu L and Chen P 2020 Effect of BaNH , CaNH , Mg_3N_2 on the activity of Co in NH_3 decomposition catalysis *J. Energy Chem.* **46** 16–21
- [299] Wang Q-R, Guan Y-Q, Gao W-B, Guo J-P and Chen P 2019 Thermodynamic properties of ammonia production from hydrogenation of alkali and alkaline earth metal amides *ChemPhysChem* **20** 1376–81
- [300] Chang F, Wu H, van der Pluijm R, Guo J, Ngene P and de Jongh P E 2019 Effect of pore confinement of NaNH_2 and KNH_2 on hydrogen generation from ammonia *J. Phys. Chem. C* **123** 21487–96
- [301] de Kort L M, Harmel J, de Jongh P E and Ngene P 2020 The effect of nanoscaffold porosity and surface chemistry on the Li-ion conductivity of $\text{LiBH}_4\text{-LiNH}_2$ /metal oxide nanocomposites *J. Mater. Chem. A* **8** 20687–97
- [302] Zettl R, de Kort L, Gombotz M, Wilkening H M R, de Jongh P E and Ngene P 2020 Combined effects of anion substitution and nanoconfinement on the ionic conductivity of Li-based complex hydrides *J. Phys. Chem. C* **124** 2806–16
- [303] Makepeace J W and David W I F 2017 Structural insights into the lithium amide-imide solid solution *J. Phys. Chem. C* **121** 12010–7
- [304] Wolczyk A, Pinatel E R, Chierotti M R, Nervi C, Gobetto R and Baricco M 2016 Solid-state NMR and thermodynamic investigations on $\text{LiBH}_4\text{LiNH}_2$ system *Int. J. Hydrog. Energy* **41** 14475–83
- [305] Wolczyk A et al 2017 $\text{Li}_5(\text{BH}_4)_3\text{NH}$: lithium-rich mixed anion complex hydride *J. Phys. Chem. C* **121** 11069–75
- [306] Wood B C et al 2017 Nanointerface-driven reversible hydrogen storage in the nanoconfined Li–N–H system *Adv. Mater. Interfaces* **4** 1600803
- [307] Li S, Reynolds J E, Dun C, Urban J J, Klebanoff L E, Wood B C, Stavila V and Allendorf M D Selective host-guest interactions lead to improved H_2 release thermodynamics of nanoconfined Li–N–H system (in preparation)
- [308] Abrahams S C, Ginsberg A P and Knox K 1964 Transition metal-hydrogen compounds. II. The crystal and molecular structure of potassium rhenium hydride, K_2ReH_9 *Inorg. Chem.* **3** 558–67
- [309] Poupin L, Humphries T D, Paskevicius M and Buckley C E 2020 An experimental high temperature thermal battery coupled to a low temperature metal hydride for solar thermal energy storage *Sustain. Energy Fuels* **4** 285–92
- [310] Jung J Y, Fadonougbo J O, Suh J-Y, Lee Y-S, Huh J-Y and Cho Y W 2018 Synthesis of Mg_2FeH_6 by hydrogenation of Mg/Fe powder mixture prepared by cold roll milling in air: effects of microstructure and oxygen distribution *Int. J. Hydrog. Energy* **43** 16758–65
- [311] Fadonougbo J O, Jung J Y, Suh J-Y, Lee Y-S, Shim J-H, Fleury E and Cho Y W 2019 The role of Fe particle size and oxide distribution on the hydrogenation properties of ball-milled nano-crystalline powder mixtures of Fe and Mg *J. Alloys Compd.* **806** 1039–46
- [312] Fadonougbo J O, Jung J-Y, Suh J-Y, Lee Y-S, Shim J-H and Cho Y W 2017 Low temperature formation of Mg_2FeH_6 by hydrogenation of ball-milled nano-crystalline powder mixture of Mg and Fe *Mater. Des.* **135** 239–45
- [313] Rzeszutarska M, Czujko T and Polański M 2020 $\text{Mg}_2(\text{Fe,Cr,Ni})\text{HX}$ complex hydride synthesis from austenitic stainless steel and magnesium hydride *Int. J. Hydrog. Energy* **45** 19440–54
- [314] Polanski M, Nawra D and Zasada D 2019 Mg_2FeH_6 synthesized from plain steel and magnesium hydride *J. Alloys Compd.* **776** 1029–40
- [315] Hardian R et al 2018 Waste Mg–Al based alloys for hydrogen storage *Int. J. Hydrog. Energy* **43** 16738–48
- [316] Pistidda C et al 2014 Hydrogen storage systems from waste Mg alloys *J. Power Sources* **270** 554–63
- [317] Huot J, Hayakawa H and Akiba E 1997 Preparation of the hydrides Mg_2FeH_6 and Mg_2CoH_5 by mechanical alloying followed by sintering *J. Alloys Compd.* **248** 164–7
- [318] Paik B, Walton A, Mann V, Book D, Jones I P and Harris I R 2010 Microstructure of ball milled MgH_2 powders upon hydrogen cycling: an electron microscopy study *Int. J. Hydrog. Energy* **35** 9012–20
- [319] Baum L A, Meyer M and Mendozazelis L 2008 Complex Mg-based hydrides obtained by mechanochemistry: characterization and formation kinetics *Int. J. Hydrog. Energy* **33** 3442–6
- [320] Deledda S and Hauback B C 2009 The formation mechanism and structural characterization of the mixed transition-metal complex hydride $\text{Mg}_2(\text{FeH}_6)_{0.5}(\text{CoH}_5)_{0.5}$ obtained by reactive milling *Nanotechnology* **20** 204010
- [321] Takagi S and Orimo S 2020 New functionalities of hydride complexes with high hydrogen coordination *J. Phys. Soc. Japan* **89** 051010
- [322] Matsuo M, Saitoh H, Machida A, Sato R, Takagi S, Miwa K, Watanuki T, Katayama Y, Aoki K and Orimo S 2013 Formation of an Fe–H complex anion in YFe_2 : adjustment of imbalanced charge by using additional Li as an electron donor *RSC Adv.* **3** 1013–6
- [323] Saitoh H, Takagi S, Matsuo M, Iijima Y, Endo N, Aoki K and Orimo S 2014 Li_4FeH_6 : iron-containing complex hydride with high gravimetric hydrogen density *APL Mater.* **2** 076103
- [324] Takagi S, Iijima Y, Sato T, Saitoh H, Ikeda K, Otomo T, Miwa K, Ikeshoji T, Aoki K and Orimo S 2015 True boundary for the formation of homoleptic transition-metal hydride complexes *Angew. Chem., Int. Ed.* **54** 5650–3
- [325] Saitoh H, Takagi S, Sato T, Iijima Y and Orimo S 2017 Synthesis of novel hydride $\text{Li}_3\text{AlFeH}_8$ at high temperature and pressure *Int. J. Hydrog. Energy* **42** 22489–95
- [326] Spektor K, Crichton W A, Filippov S, Simak S I and Häussermann U 2019 Exploring the Mg–Cr–H system at high pressure and temperature via *in situ* synchrotron diffraction *Inorg. Chem.* **58** 11043–50

- [327] Spektor K, Crichton W A, Filippov S, Simak S I, Fischer A and Häussermann U 2020 Na₃FeH₇ and Na₃CoH₆: hydrogen-rich first-row transition metal hydrides from high pressure synthesis *Inorg. Chem.* **59** 16467–73
- [328] Takagi S, Iijima Y, Sato T, Saitoh H, Ikeda K, Otomo T, Miwa K, Ikeshoji T and Orimo S 2017 Formation of novel transition metal hydride complexes with ninefold hydrogen coordination *Sci. Rep.* **7** 44253
- [329] Meng D, Sakata M, Shimizu K, Iijima Y, Saitoh H, Sato T, Takagi S and Orimo S 2019 Superconductivity of the hydrogen-rich metal hydride Li₅MoH₁₁ under high pressure *Phys. Rev. B* **99** 024508
- [330] Fukai Y and Okuma N 1993 Evidence of copious vacancy formation in Ni and Pd under a high hydrogen pressure *Jpn. J. Appl. Phys.* **32** L1256–9
- [331] Reilly J J and Wiswall R H 1967 Reaction of hydrogen with alloys of magnesium and copper *Inorg. Chem.* **6** 2220–3
- [332] Barkhordarian G, Klassen T and Bormann R 2009 Composite material storing hydrogen, and device for the reversible storage of hydrogen *U.S. Pat.* **11** 493
- [333] Vajo J J, Skeith S L and Mertens F 2005 Reversible storage of hydrogen in destabilized LiBH₄ *J. Phys. Chem. B* **109** 3719–22
- [334] Bösenberg U et al 2007 Hydrogen sorption properties of MgH₂–LiBH₄ composites *Acta Mater.* **55** 3951–8
- [335] Bonatto Minella C, Garroni S, Pistidda C, Baró M D, Gutfleisch O, Klassen T and Dornheim M 2015 Sorption properties and reversibility of Ti(IV) and Nb(V)-fluoride doped-Ca(BH₄)₂–MgH₂ system *J. Alloys Compd.* **622** 989–94
- [336] Garroni S, Pistidda C, Brunelli M, Vaughan G B M, Suriñach S and Baró M D 2009 Hydrogen desorption mechanism of 2NaBH₄+MgH₂ composite prepared by high-energy ball milling *Scr. Mater.* **60** 1129–32
- [337] Karimi F, Pranzas P K, Hoell A, Vainio U, Welter E, Raghuvanshi V S, Pistidda C, Dornheim M, Klassen T and Schreyer A 2014 Structural analysis of calcium reactive hydride composite for solid state hydrogen storage *J. Appl. Crystallogr.* **47** 67–75
- [338] Hu J, Witter R, Shao H, Felderhoff M and Fichtner M 2014 Beneficial effects of stoichiometry and nanostructure for a LiBH₄–MgH₂ hydrogen storage system *J. Mater. Chem. A* **2** 66–72
- [339] Bergemann N, Pistidda C, Milanese C, Emmeler T, Karimi F, Chaudhary A-L, Chierotti M R, Klassen T and Dornheim M 2016 Ca(BH₄)₂–Mg₂NiH₄: on the pathway to a Ca(BH₄)₂ system with a reversible hydrogen cycle *Chem. Commun.* **52** 4836–9
- [340] Karimi F et al 2015 Structural and kinetic investigation of the hydride composite Ca(BH₄)₂ + MgH₂ system doped with NbF₅ for solid-state hydrogen storage *Phys. Chem. Chem. Phys.* **17** 27328–42
- [341] Pinkerton F E, Meyer M S, Meisner G P, Balogh M P and Vajo J J 2007 Phase boundaries and reversibility of LiBH₄/MgH₂ hydrogen storage material *J. Phys. Chem. C* **111** 12881–5
- [342] Minella C B, Pistidda C, Garroni S, Nolis P, Baró M D, Gutfleisch O, Klassen T, Bormann R and Dornheim M 2013 Ca(BH₄)₂ + MgH₂: desorption reaction and role of Mg on its reversibility *J. Phys. Chem. C* **117** 3846–52
- [343] Ding Z, Li H and Shaw L 2020 New insights into the solid-state hydrogen storage of nanostructured LiBH₄–MgH₂ system *Chem. Eng. J.* **385** 123856
- [344] Kim K-B, Shim J-H, Park S-H, Choi I-S, Oh K H and Cho Y W 2015 Dehydrogenation reaction pathway of the LiBH₄–MgH₂ composite under various pressure conditions *J. Phys. Chem. C* **119** 9714–20
- [345] Neves A M, Puszkiel J, Capurso G, Bellosta von Colbe J M, Milanese C, Dornheim M, Klassen T and Jepsen J 2021 Modeling the kinetic behavior of the Li-RHC system for energy-hydrogen storage: (I) absorption *Int. J. Hydrog. Energy* **46** 32110–25
- [346] Karimi F et al 2021 Characterization of LiBH₄–MgH₂ reactive hydride composite system with scattering and imaging methods using neutron and synchrotron radiation *Adv. Eng. Mater.* **23** 2100294
- [347] Rizzi P, Pinatel E, Luetto C, Florian P, Graizzaro A, Gagliano S and Baricco M 2015 Integration of a PEM fuel cell with a metal hydride tank for stationary applications *J. Alloys Compd.* **645** S338–42
- [348] Belmonte N, Girgenti V, Florian P, Peano C, Luetto C, Rizzi P and Baricco M 2016 A comparison of energy storage from renewable sources through batteries and fuel cells: a case study in Turin, Italy *Int. J. Hydrog. Energy* **41** 21427–38
- [349] Agostini A, Belmonte N, Masala A, Hu J, Rizzi P, Fichtner M, Moretto P, Luetto C, Sgroi M and Baricco M 2018 Role of hydrogen tanks in the life cycle assessment of fuel cell-based auxiliary power units *Appl. Energy* **215** 1–12
- [350] Yartys V A et al 2019 Magnesium based materials for hydrogen based energy storage: past, present and future *Int. J. Hydrog. Energy* **44** 7809–59
- [351] Crivello J-C et al 2016 Mg-based compounds for hydrogen and energy storage *Appl. Phys. A* **122** 85
- [352] Lys A, Fadonougbo J O, Faisal M, Suh J-Y, Lee Y-S, Shim J-H, Park J and Cho Y W 2020 Enhancing the hydrogen storage properties of AxBy intermetallic compounds by partial substitution: a short review *Hydrogen* **1** 38–63
- [353] Sujan G K, Pan Z, Li H, Liang D and Alam N 2019 An overview on TiFe intermetallic for solid-state hydrogen storage: microstructure, hydrogenation and fabrication processes *Crit. Rev. Solid State Mater. Sci.* **45** 410–27
- [354] Dematteis E M, Berti N, Cuevas F, Latroche M and Baricco M 2021 Substitutional effects in TiFe for hydrogen storage: a comprehensive review *Mater. Adv.* **2** 2524–60
- [355] Marinelli M and Santarelli M 2020 Hydrogen storage alloys for stationary applications *J. Energy Storage* **32** 101864
- [356] Bellosta von Colbe J et al 2019 Application of hydrides in hydrogen storage and compression: achievements, outlook and perspectives *Int. J. Hydrog. Energy* **44** 7780–808
- [357] Bergemann N, Pistidda C, Uptmoor M, Milanese C, Santoru A, Emmeler T, Puszkiel J, Dornheim M and Klassen T 2019 A new mutually destabilized reactive hydride system: LiBH₄–Mg₂NiH₄ *J. Energy Chem.* **34** 240–54
- [358] Hu J, Fichtner M and Baricco M 2017 Preparation of Li-Mg-N-H hydrogen storage materials for an auxiliary power unit *Int. J. Hydrog. Energy* **42** 17144–8
- [359] Puszkiel J, Garroni S, Milanese C, Gennari F, Klassen T, Dornheim M and Pistidda C 2017 Tetrahydroborates: development and potential as hydrogen storage medium *Inorganics* **5** 74
- [360] He T, Cao H and Chen P 2019 Complex hydrides for energy storage, conversion, and utilization *Adv. Mater.* **31** 1902757
- [361] Milanese C, Garroni S, Gennari F, Marini A, Klassen T, Dornheim M and Pistidda C 2018 Solid state hydrogen storage in alanates and alanate-based compounds: a review *Metals* **8** 567
- [362] Sheppard D A and Buckley C E 2019 The potential of metal hydrides paired with compressed hydrogen as thermal energy storage for concentrating solar power plants *Int. J. Hydrog. Energy* **44** 9143–63
- [363] Javadian P, Sheppard D A, Jensen T R and Buckley C E 2016 Destabilization of lithium hydride and the thermodynamic assessment of the Li–Al–H system for solar thermal energy storage *RSC Adv.* **6** 94927–33
- [364] Humphries T D, Sheppard D A, Li G, Rowles M R, Paskevicius M, Matsuo M, Aguey-Zinsou K-F, Sofianos M V, Orimo S and Buckley C E 2018 Complex hydrides as thermal energy storage materials: characterisation and thermal decomposition of Na₂Mg₂NiH₆ *J. Mater. Chem. A* **6** 9099–108
- [365] Bürger I, Luetto C and Linder M 2014 Advanced reactor concept for complex hydrides: hydrogen desorption at fuel cell relevant boundary conditions *Int. J. Hydrog. Energy* **39** 7346–55

- [366] Rönnebro E, Whyatt G, Powell M, Westman M, Zheng F and Fang Z 2015 Metal hydrides for high-temperature power generation *Energies* **8** 8406–30
- [367] Paskevicius M, Sheppard D A, Williamson K and Buckley C E 2015 Metal hydride thermal heat storage prototype for concentrating solar thermal power *Energy* **88** 469–77
- [368] Manickam K et al 2019 Future perspectives of thermal energy storage with metal hydrides *Int. J. Hydrog. Energy* **44** 7738–45
- [369] Bird J E, Humphries T D, Paskevicius M, Poupin L and Buckley C E 2020 Thermal properties of thermochemical heat storage materials *Phys. Chem. Chem. Phys.* **22** 4617–25
- [370] Harries D N, Paskevicius M, Sheppard D A, Price T E C and Buckley C E 2012 Concentrating solar thermal heat storage using metal hydrides *Proc. IEEE* **100** 539–49
- [371] Reissner A et al 2015 Metal hydride hydrogen and heat storage systems as enabling technology for spacecraft applications *J. Alloys Compd.* **645** S9–S13
- [372] Nguyen T T, Sheppard D A and Buckley C E 2017 Lithium imide systems for high temperature heat storage in concentrated solar thermal systems *J. Alloys Compd.* **716** 291–8
- [373] Bachman J C et al 2016 Inorganic solid-state electrolytes for lithium batteries: mechanisms and properties governing ion conduction *Chem. Rev.* **116** 140–62
- [374] Unemoto A, Yoshida K, Ikeshoji T and Orimo S 2016 Bulk-type all-solid-state lithium batteries using complex hydrides containing cluster-anions *Mater. Trans.* **57** 1639–44
- [375] Gulino V, Wolczyk A, Golov A A, Eremin R A, Palumbo M, Nervi C, Blatov V A, Proserpio D M and Baricco M 2020 Combined DFT and geometrical–topological analysis of Li-ion conductivity in complex hydrides *Inorg. Chem. Front.* **7** 3115–25
- [376] Takahashi K, Hattori K, Yamazaki T, Takada K, Matsuo M, Orimo S, Maekawa H and Takamura H 2013 All-solid-state lithium battery with LiBH_4 solid electrolyte *J. Power Sources* **226** 61–64
- [377] Zaïdi W, Bonnet J-P, Zhang J, Cuevas F, Latroche M, Couillaud S, Bobet J-L, Sougrati M T, Jumas J-C and Aymard L 2013 Reactivity of complex hydrides Mg_2FeH_6 , Mg_2CoH_5 and Mg_2NiH_4 with lithium ion: far from equilibrium electrochemically driven conversion reactions *Int. J. Hydrog. Energy* **38** 4798–808
- [378] Matsuo M et al 2009 Complex hydrides with $(\text{BH}_4)^-$ and $(\text{NH}_2)^-$ anions as new lithium fast-ion conductors *J. Am. Chem. Soc.* **131** 16389–91
- [379] Unemoto A, Matsuo M and Orimo S 2014 Complex hydrides for electrochemical energy storage *Adv. Funct. Mater.* **24** 2267–79
- [380] Matsuo M and Orimo S 2011 Lithium fast-ionic conduction in complex hydrides: review and prospects *Adv. Energy Mater.* **1** 161–72
- [381] Jørgensen M et al 2020 Understanding superionic conductivity in lithium and sodium salts of weakly coordinating closo-hexahalocarborate anions *Chem. Mater.* **32** 1475–87
- [382] Skripov A V, Soloninin A V, Ley M B, Jensen T R and Filinchuk Y 2013 Nuclear magnetic resonance studies of BH_4 reorientations and Li diffusion in $\text{LiLa}(\text{BH}_4)_3\text{Cl}$ *J. Phys. Chem. C* **117** 14965–72
- [383] Soloninin A V, Babanova O A, Skoryunov R V, Skripov A V, Grinderslev J B and Jensen T R 2021 NMR study of the dynamical properties of $\text{LiLa}(\text{BH}_4)_3\text{Br}$ and $\text{LiLa}(\text{BH}_4)_3\text{I}$ *Appl. Magn. Reson.* **52** 595–606
- [384] Skripov A V, Majer G, Babanova O A, Skoryunov R V, Soloninin A V, Ley M B, Jensen T R, Orimo S and Udovic T J 2021 Lithium-ion diffusivity in complex hydrides: pulsed-field-gradient NMR studies of $\text{LiLa}(\text{BH}_4)_3\text{Cl}$, $\text{Li}_3(\text{NH}_2)_2\text{I}$ and $\text{Li}-1\text{-CB}_9\text{H}_{10}$ *Solid State Ion.* **362** 115585
- [385] Gradišek A, Jørgensen M, Paskevicius M, Hansen B R S and Jensen T R 2021 Molecular dynamics in $\text{Ag}_2\text{B}_{12}\text{H}_{12}$ studied by nuclear magnetic resonance *J. Phys. Chem. C* **125** 5534–41
- [386] Gradišek A, Krnel M, Paskevicius M, Hansen B R S, Jensen T R and Dolinšek J 2018 Reorientational motions and ionic conductivity in $(\text{NH}_4)_2\text{B}_{10}\text{H}_{10}$ and $(\text{NH}_4)_2\text{B}_{12}\text{H}_{12}$ *J. Phys. Chem. C* **122** 17073–9
- [387] Kato Y, Hori S, Saito T, Suzuki K, Hirayama M, Mitsui A, Yonemura M, Iba H and Kanno R 2016 High-power all-solid-state batteries using sulfide superionic conductors *Nat. Energy* **1** 16030
- [388] Takagi S, Ikeshoji T, Sato T and Orimo S 2020 Pseudorotating hydride complexes with high hydrogen coordination: a class of rotatable polyanions in solid matter *Appl. Phys. Lett.* **116** 173901
- [389] Huang Z, Gallucci J, Chen X, Yisgedu T, Lingam H K, Shore S G and Zhao J-C 2010 $\text{Li}_2\text{B}_{12}\text{H}_{12} \cdot 7\text{NH}_3$: a new ammine complex for ammonia storage or indirect hydrogen storage *J. Mater. Chem.* **20** 2743
- [390] Vitillo J G, Groppo E, Bardají E G, Baricco M and Bordiga S 2014 Fast carbon dioxide recycling by reaction with $\gamma\text{-Mg}(\text{BH}_4)_2$ *Phys. Chem. Chem. Phys.* **16** 22482–6
- [391] Vitillo J G 2015 Magnesium-based systems for carbon dioxide capture, storage and recycling: from leaves to synthetic nanostructured materials *RSC Adv.* **5** 36192–239
- [392] Sahiner N, Demir S and Yildiz S 2014 Magnetic colloidal polymeric ionic liquid synthesis and use in hydrogen production *Colloids Surf. A* **449** 87–95
- [393] Heere M, Payandeh Gharibdoust S H, Frommen C, Humphries T D, Ley M B, Sørby M H, Jensen T R and Hauback B C 2016 The influence of LiH on the rehydrogenation behavior of halide free rare earth (RE) borohydrides (RE = Pr, Er) *Phys. Chem. Chem. Phys.* **18** 24387–95
- [394] Heere M, Gharibdoust S, Brighi M, Frommen C, Sørby M, Černý R, Jensen T and Hauback B 2017 Hydrogen sorption in erbium borohydride composite mixtures with LiBH_4 and/or LiH *Inorganics* **5** 31
- [395] Lee Y, Ley M B, Jensen T R and Cho Y W 2016 Lithium ion disorder and conduction mechanism in $\text{LiCe}(\text{BH}_4)_3\text{Cl}$ *J. Phys. Chem. C* **120** 19035–42
- [396] Marks S, Heck J G, Habicht M H, Oña-Burgos P, Feldmann C and Roesky P W 2012 $[\text{Ln}(\text{BH}_4)_2(\text{THF})_2]$ (Ln = Eu, Yb)—a highly luminescent material. Synthesis, properties, reactivity, and NMR studies *J. Am. Chem. Soc.* **134** 16983–6
- [397] Paskevicius M, Jakobsen A S, Bregnhøj M, Hansen B R S, Møller K T, Ogilby P R and Jensen T R 2019 Comment on ‘Bi-functional $\text{Li}_2\text{B}_{12}\text{H}_{12}$ for energy storage and conversion applications: solid-state electrolyte and luminescent down-conversion dye’ by J A Teprovich Jr, H Colón-Mercado, A L Washington II, P A Ward, S Greenway, D M Missimer, H Hartman, J Velten, J H Christian and R Zidan *J. Mater. Chem. A* **7** 4185–7
- [398] Wegner W, van Leusen J, Majewski J, Grochala W and Kögerler P 2019 Borohydride as magnetic superexchange pathway in late lanthanide borohydrides *Eur. J. Inorg. Chem.* **2019** 1776–83
- [399] Schouwink P, Didelot E, Lee Y-S, Mazet T and Černý R 2016 Structural and magnetocaloric properties of novel gadolinium borohydrides *J. Alloys Compd.* **664** 378–84
- [400] Skibsted J, Payandeh S, Ley M B and Jensen T R 2021 11B nuclear spin–electron spin interactions in 11B MAS NMR spectra of paramagnetic metal borohydrides *J. Phys. Chem. C* **125** 1113–24

- [401] Schuy C *et al* 2018 Experimental assessment of lithium hydride's space radiation shielding performance and Monte Carlo benchmarking *Radiat. Res.* **191** 154
- [402] Wang W, Li Q, Li Q, Yang X and Le G 2016 A review of irradiation stability of lithium hydride neutron shielding material *Mater. Sci. Technol.* **0836** 1–4
- [403] Černý R, Schouwink P, Sadikin Y, Stare K, Smrčok L, Richter B and Jensen T R 2013 Trimetallic borohydride $\text{Li}_3\text{MZN}_5(\text{BH}_4)_{15}$ (M = Mg, Mn) containing two weakly interconnected frameworks *Inorg. Chem.* **52** 9941–7
- [404] Schouwink P, Ley M B, Jensen T R, Smrčok L and Černý R 2014 Borohydrides: from sheet to framework topologies *Dalt. Trans.* **43** 7726
- [405] Cao H, Santoru A, Pistidda C, Richter T M M, Chaudhary A-L, Gizer G, Niewa R, Chen P, Klassen T and Dornheim M 2016 New synthesis route for ternary transition metal amides as well as ultrafast amide–hydride hydrogen storage materials *Chem. Commun.* **52** 5100–3
- [406] Ravnsbæk D B and Jensen T R 2010 Tuning hydrogen storage properties and reactivity: investigation of the LiBH_4 – NaAlH_4 system *J. Phys. Chem. Solids* **71** 1144–9
- [407] Schneemann A *et al* 2018 Nanostructured metal hydrides for hydrogen storage *Chem. Rev.* **118** 10775–839
- [408] Palumbo M, Torres F J, Ares J R, Pisani C, Fernandez J F and Baricco M 2007 Thermodynamic and *ab initio* investigation of the Al–H–Mg system *Calphad* **31** 457–67
- [409] Witman M, Ling S, Grant D M, Walker G S, Agarwal S, Stavila V and Allendorf M D 2020 Extracting an empirical intermetallic hydride design principle from limited data via interpretable machine learning *J. Phys. Chem. Lett.* **11** 40–47
- [410] Hatrick-Simpers J R, Choudhary K and Corgnale C 2018 A simple constrained machine learning model for predicting high-pressure-hydrogen-compressor materials *Mol. Syst. Des. Eng.* **3** 509–17
- [411] Zahid T, Xu K and Li W 2017 Machine learning an alternate technique to estimate the state of charge of energy storage devices *Electron. Lett.* **53** 1665–6
- [412] Rahnama A, Zepon G and Sridhar S 2019 Machine learning based prediction of metal hydrides for hydrogen storage, part I: prediction of hydrogen weight percent *Int. J. Hydrog. Energy* **44** 7337–44
- [413] Shi R, Heo T W, Wood B C and Wang Y 2020 Critical nuclei at hetero-phase interfaces *Acta Mater.* **200** 510–25
- [414] Wan L F *et al* 2019 Edge-functionalized graphene nanoribbon encapsulation to enhance stability and control kinetics of hydrogen storage materials *Chem. Mater.* **31** 2960–70
- [415] Wood B C, Heo T W, Kang S, Wan L F and Li S 2020 Beyond idealized models of nanoscale metal hydrides for hydrogen storage *Ind. Eng. Chem. Res.* **59** 5786–96
- [416] White J L, Newhouse R J, Zhang J Z, Udovic T J and Stavila V 2016 Understanding and mitigating the effects of stable dodecahydro- closo-dodecaborate intermediates on hydrogen-storage reactions *J. Phys. Chem. C* **120** 25725–31
- [417] Pranzas P K *et al* 2011 Characterization of hydrogen storage materials and systems with photons and neutrons *Adv. Eng. Mater.* **13** 730–6
- [418] Reed D and Book D 2011 Recent applications of Raman spectroscopy to the study of complex hydrides for hydrogen storage *Curr. Opin. Solid State Mater. Sci.* **15** 62–72
- [419] Bösenberg U, Pistidda C, Tolkiehn M, Busch N, Saldan I, Suarez-Alcantara K, Arendarska A, Klassen T and Dornheim M 2014 Characterization of metal hydrides by *in-situ* XRD *Int. J. Hydrog. Energy* **39** 9899–903
- [420] Jensen T R, Nielsen T K, Filinchuk Y, Jørgensen J-E, Cerenius Y, Gray E M and Webb C J 2010 Versatile *in situ* powder x-ray diffraction cells for solid–gas investigations *J. Appl. Crystallogr.* **43** 1456–63
- [421] Soloninin A V, Babanova O A, Skripov A V, Hagemann H, Richter B, Jensen T R and Filinchuk Y 2012 NMR study of reorientational motion in alkaline-earth borohydrides: β and γ phases of $\text{Mg}(\text{BH}_4)_2$ and α and β phases of $\text{Ca}(\text{BH}_4)_2$ *J. Phys. Chem. C* **116** 4913–20
- [422] D'Anna V, Lawson Daku L M and Hagemann H 2013 Vibrational spectra and structure of borohydrides *J. Alloys Compd.* **580** S122–4
- [423] D'Anna V, Spyratou A, Sharma M and Hagemann H 2014 FT-IR spectra of inorganic borohydrides *Spectrochim. Acta A* **128** 902–6
- [424] Severa G, Hagemann H, Longhini M, Kaminski J W, Wesolowski T A and Jensen C M 2010 Thermal desorption, vibrational spectroscopic, and DFT computational studies of the complex manganese borohydrides $\text{Mn}(\text{BH}_4)_2$ and $[\text{Mn}(\text{BH}_4)_4]^{2-}$ *J. Phys. Chem. C* **114** 15516–21
- [425] Humphries T D, Munroe K T, DeWinter T M, Jensen C M and McGrady G S 2013 NMR spectroscopic and thermodynamic studies of the etherate and the α , α' , and γ phases of AlH_3 *Int. J. Hydrog. Energy* **38** 4577–86
- [426] Humphries T D, Makepeace J W, Hino S, David W I F and Hauback B C 2014 Regeneration of sodium alanate studied by powder *in situ* neutron and synchrotron x-ray diffraction *J. Mater. Chem. A* **2** 16594–600
- [427] Humphries T D, Birkmire D, Hauback B C, Sean McGrady G and Jensen C M 2013 *In situ* high pressure NMR study of the direct synthesis of NaAlH_4 *Phys. Chem. Chem. Phys.* **15** 6179